Chemical Reviews

Clusters and Surfaces

E. L. MUETTERTIES,*† T. N. RHODIN,*# ELLIOT BAND, C. F. BRUCKER, and W. R. PRETZER‡

Cornell Materials Science Center, Cornell University, Ithaca, New York 14853

Contents

I. The Cluster–Surface Analogy

A. Introduction

A proposition has been advanced that discrete, molecular metal clusters may be reasonable models of metal surfaces in the processes of chemisorption and of catalysis.[1-4] If this thesis is correct to at least a first approximation, then the ramifications become exceedingly important in the advancement of surface science because the many details of structure, of the kinetic and mechanistic features of mobility for bound molecules, atoms, or groups of atoms, and of the mechanistic features of stoichiometric or catalytic reactions are more readily established for molecular (cluster) chemistry than for surface chemistry. A comprehensive body of detailed information exists, on the other hand, on the atomistic and microscopic properties of single-crystal metal surfaces and of the surface crystallography, kinetics, and thermodynamics pertinent to the nature of the surface bonding of simple chemisorbed molecules.[5]

Qualitative assessments of the metal cluster–metal surface analogy suggest that the analogy may have some range of validity.[1-3,6-11] A more detailed, quantitative analysis necessary to set boundary conditions is the objective of this article. The analysis is limited to the chemisorption process simply because the data for the cluster catalysis process[1-3,6-20] are too sketchy in number and scope. Size and shape, coordination number, structure and stereochemistry, thermodynamics, and ligand mobility are the critical elements in this assessment of the cluster–surface analogy.

* Authors to whom inquiries should be addressed.

† Department of Chemistry, University of California, Berkeley, Calif. 94720.

School of Applied and Engineering Physics, Cornell University, Ithaca, N.Y. 14853.

‡ Gulf Research & Development Co., Chemicals and Minerals, P.O. Drawer 2038, Pittsburgh, Pa. 15230.

B. The Metal Cluster Family

Little more than a decade ago, the number of defined, molecular metal clusters was small; today, the number is in the hundreds and many have been structurally characterized through crystallographic studies.[20,21] In addition, the cluster prototypes, the dinuclear metal clusters, are also now a large and structurally well-defined group. These dinuclear metal complexes, although they are not clusters, are relevant to cluster–surface analogy since in some chemisorption and catalytic processes two metal atoms may suffice to characterize the processes. With such riches, a comprehensive review of chemical bonding in metal clusters compared to metal surfaces is neither practical nor appropriate here. For illustration and for anticipation of later discussions, exemplary metal clusters are listed in Tables I through VI. Cluster size ranges from 2 in the prototypical group to 30. Ligands are as varied in character as the molecules, molecular fragments, and atoms that have been investigated in surface chemistry for the chemisorbed state, and the ligands encompass many of the species that are or could be involved in catalytic reactions on a metal surface. The largest subgroup comprises the metal carbonyl clusters and the size range within this subgroup extends through the full, established range for clusters of 3 to 30.

The polyhedra defined by the metal atom positions in metal clusters are largely deltahedra, polyhedra with all triangular faces. Exceptions are few in number: several square-planar or nearly square-planar clusters, several trigonal prismatic six-atom clusters, and two C_{4v}-capped square antiprismatic nine-atom clusters. Thus, the metal frameworks of most clusters represent fragments of close-packed arrays. A distinctive example[20] is $Rh_{13}(CO)_{24}H_3^{2-}$, illustrated in Figure 1, which is literally a 13-atom "piece" of a hexagonal close-packed array. With this dominance of cluster polyhedra by deltahedra, we see one serious deficiency—at least at this state in the development of cluster chemistry. There are presently few cluster models of chemisorbed states on metals that have body-centered cubic packing. However, future advances in the cluster synthesis science should rectify this situation. In fact, recent advances in chemical synthesis by Chini and his co-workers[23] have demonstrated that "pieces" of body-centered cubic packing can be generated in large rhodium clusters like $Rh_{14}(CO)_{25}^{4-}$ (Figure 2). Remarkable in form is another class of platinum clusters discovered also by Chini and co-workers.[24] This class, which has the composition $[Pt_3(CO)_6]_n^{2-}$ (with $n = 2, 3, 4, 5, 6$, and 10), is based on stacked trigonal prisms.[25] The triangular faces are not eclipsed so the stacks have a helical character (Figure 3).

Metal-atom coordination or connexity numbers are uniformly higher for surface atoms in metals than for surface atoms in clusters. For example, the surface metal atoms in a close-packed array have maximally a metal atom coordination number of 9; this number drops to 7 and 6 for a small number of surface sites (steps and kinks) in a high Miller index plane. These features for a high Miller index plane are illustrated in Figure 4, and this is to be contrasted with the low Miller index planes for hexagonal

$$[Pt_3(CO)_3(\mu_2\text{-}CO)_3]_2^{2-}$$

$$[Pt_3(CO)_3(\mu_2\text{-}CO)_3]_3^{2-}$$

$$[Pt_3(CO)_3(\mu_2\text{-}CO)_3]_5^{2-}$$

Figure 3. Platinum forms an unusual class of carbonyl clusters of the chemical formula $[Pt_3(CO)_6]_n^{2-}$. It is structurally based on stacked trigonal prisms because the triangular faces are slightly staggered. The stacks have a helical character as shown above for structurally defined 6-, 9-, and 15-atom clusters.
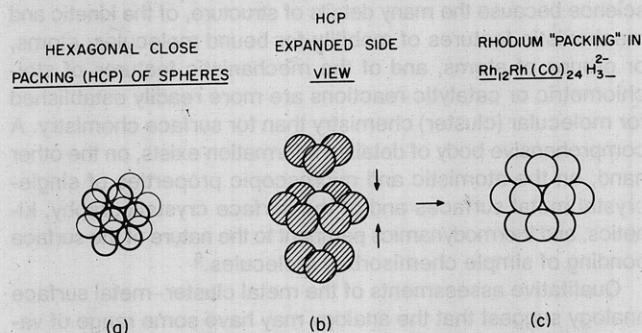
Figure 1. Illustration of the packing of the 13 rhodium atoms in $Rh_{12}Rh(CO)_{24}H_3^{2-}$. The metal framework has D_{3h} symmetry and has hexagonal close packing. About the periphery are 12 terminal carbonyl ligands (one per rhodium) and 12 bridging carbonyl ligands. The hydrogen atoms are inside the polyhedron and bridge square faces.
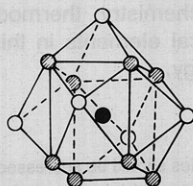
Figure 2. Representation of the metal atom framework in the rhodium cluster $Rh_{14}(CO)_{25}^{4-}$. This framework is a fragment of body-centered cubic close packing. The Rh atom in the center has eight Rh atoms bound to it in a cubic array. Five of the six faces of the cube are capped with Rh atoms.

Figure 4. A representation of a high Miller index plane for a face-centered cubic metal structure in which there are discrete areas described as (1) "terraces", which are (111) sections with surface metal atoms (unshaded circles) that have a coordination number of 9, i.e., nine nearest neighbor metal atoms; (2) "steps" where the metal atoms (light shading) have a coordination number of 7; and (3) "kinks" where the atoms (dark shading) at the leading edge have a coordination number of 6. This drawing originally was prepared by Ms. Carol E. Smith at the University of California at Berkeley.

TABLE I. Representative Examples of Cluster Prototypes and Metal Clusters Arranged by Class (Size) and Periodic Group

cluster class	transition metal group[a]						post-transition group
	4 and 5[h]	6[h]	7	8A	8B	8C	
dinuclear	$Nb_2Br_6(SC_4H_8)_3$	$Cr_2(CO)_{10}^{2-}$	$Mn_2(CO)_{10}$	$Fe_2(CO)_9$	$Co_2(CO)_8$	$Pd_2(CNR)_6^{2+}$	Hg_2^{2+}
	$Ta_2Br_6(SC_4H_8)_3$	$Mo_2(C_5H_5)_2$- $(CO)_6$	$Te_2Cl_8^-$	$Fe_2(C_5H_5)_2(CO)_4$	$Co_2(C_5H_5)_2(CO)_2^-$	$PdPt(CNR)_6^{2+}$	Cd_2^{2+}
		$Mo_2(OCOR)_4$	$Re_2Cl_8^{2-}$	$Fe_2(\eta^3\text{-}C_3H_5)_2$- $(CO)_6$	$Rh_2(PR_3)_8$	$Pt_2(CNR)_6^{2+}$	Te_2^{2+}
		$Mo_2Cl_8^{2-}$	$Re_2Cl_2(OCOR)_4$	$Ru_2(OCOR)_4^{0,+1}$	$Rh_2(OCOR)_4$	$Pd_2(C_5H_5)_2(C_4H_7)$- $(PR_3)_2$	
		$W_2(NR_2)_6$	$Re_2(CO)_{10}$		$Rh_2H_2[P(OR)_3]_2$	$Pt_2(PR_2)_2(PR_3)_2$	
trinuclear triangles, maximally 6 framework electrons framework electrons	$[C_6(CH_3)_6]_3Ta_3$- Cl_2^+		$Mn_3H_3(CO)_{12}$	$Fe_3(CO)_{12}$	$Co_2Os(CO)_{11}$	$Ni_3(C_5H_5)_3(CO)_2$	
			$Mn_3(C_5H_5)_3$- $(NO)_4$	$Ru_3(CO)_{12}$	$Co_3(CO)_{11}$	$Pd_3(CNR)_6$	
			$Re_3Cl_{12}^{3-}$	$Os_3(CO)_{12}$	$Rh_3(C_5H_5)_3(CO)_3$	$Pt_3(CNR)_6$	
			$Re_3Br_{11}^{2-}$	$Os_3H_2(CO)_{11}$	$Rh_3H_3[P(OR)_3]_6$	$Pt_3(PR_2)_3(PR_3)_3$	
			$Re_3H_2(CO)_{12}^-$	$FeRu_2(CO)_{12}$			
			$Re_3(CH_3)_6Cl_3$	$Fe_2Mn(CO)_{12}$			
tetranuclear tetrahedra, maximally 12 framework electrons			$Re_4H_6(CO)_{12}^{2-}$	$Fe_4(CO)_{13}^{2-}$	$Co_4(CO)_{12}$	$Ni_4(CNR)_7$	Pb_4^{4-}
			$Re_4H_4(CO)_{12}$	$Ru_4H_4(CO)_{12}$	$Co_4H_4(C_5H_5)_4$	$Ni_4(CO)_6(PR_3)_4$	
				$Ru_4H_2(CO)_{13}$	$Rh_4(CO)_{12}$	$Ni_4(C_5H_5)_4H_3(45e)$	
				$Os_4H_4(CO)_{12}$	$Ir_4(CO)_{12}$	$Pt_4(CO)_5(PR_3)_4$[b]	
				$FeRu_3H_2(CO)_{13}$	$Co_3Rh(CO)_{12}$		
				$Fe_4(C_5H_5)_4(CO)_4$	$Rh_2Fe_2(C_5H_5)_2$- $(CO)_8$		
					$Co_2Os_2(CO)_{12}H_2$		
heteronuclear tetrahedra		$SMo_3S_2(C_5H_5)_3$		$SFeCo_2(CO)_9$	$RCCo_3(CO)_9$	$RCNi_3(C_5H_5)_3$	
				$SFe_2Co(CO)_9$	$SCo_3(CO)_9$		
				$SRu_3H_2(CO)_9$	$RGeCo_3(CO)_9$		
				$SOs_3H_2(CO)_9$			
tetranuclear polygon, 14 framework electrons			$Re_4(CO)_{12}^{2-}$	$Fe_4(CO)_{13}H^-$			Te_4^{2+}
							Se_4^{2+}
							Hg_4^{6-}
							Bi_4^{2-}
pentanuclear trigonal bipyramid, 12 framework electrons[c]				$Os_5(CO)_{16}$		$Ni_3W_2(CO)_{16}^{2-}$	Bi_5^{3+}
				$Ru_5Cl_{12}^{2-}(?)$		$Ni_3Mo_2(CO)_{16}^{2-}$	Sn_5^{2-}
						$Pt_3Sn_2Cl_6(COD)_2$	Pb_5^{2-}
						$Ni_5(CO)_{12}^{2-}$	
hexanuclear octahedra,	$Nb_6Cl_{12}X_6^{2-}$	$Mo_6Cl_{14}^{2-}$		$Fe_6C(CO)_{16}^{2-}$	$Co_6(CO)_{16}$	$Ni_2Co_4(CO)_{14}^{2-}$	$Au_6(PR_3)_6^{2+}$
	$Ta_6Cl_{12}L_6^{2-}$	$Mo_6X_8Y_6^{2-}$		$Ru_6C(CO)_{17}$	$Co_6(CO)_{15}^{2-}$	$Ni_6(CO)_{12}^{2-}$	$Cu_6(R_2N\text{-}C_6H_4)_4$- Br_2
14 framework electrons	$Ta_5MoCl_{12}L_6^{3-}$	$Mo_6Cl_{12}(PR_3)_2$		$Ru_6C(C_6H_6)(CO)_{14}$	$Co_6(CO)_{14}^{4-}$		$Cu_6H_6(PR_3)_6$[g]
	Zr_6I_{12}			$Ru_6H_2(CO)_{18}$	$Rh_6(CO)_{16}$		
	$Zr_6Cl_{12}^{3+}$			$Os_6(CO)_{18}^{2-}$	$(OC)_{15}Rh_6Rh_6$- $(CO)_{15}^{2-}$		
				$Os_6H(CO)_{18}^-$	$Ir_6(CO)_{15}^{2-}$		
					$Ir_2Cu_4(C\equiv CR)_8$- $(PR_3)_2$		
					$Co_6C(CO)_{15}$		
heteronuclear octahedra				$Fe_5C(CO)_{15}$	$Co_4(PR)_2(CO)_{10}$		
hexanuclear trigonal prisms, 18 framework electrons					$Co_6C(CO)_{15}^{2-}$	$Pt_6(CO)_{12}^{2-}$[d]	Te_6^{6+}
					$Rh_6C(CO)_{15}^{2-}$		
hexanuclear capped polyhedra				$Os_6(CO)_{18}$[e]			
				$Os_6H_2(CO)_{18}$[f]			

[a] Italicized elements in heteronuclear polyhedra represent vertex defining elements, and italicized elements for polyhedra represent centered "carbide" atoms in octahedra and trigonal prisms. [b] One edge nonbonded. [c] The nickel group examples do not have 12 framework electrons; this set of clusters can be considered as a basic 3-atom triangle capped above and below the triangular faces with a 2-electron donor. [d] $Pt_6(CO)_{12}^{2-}$ has 14 framework electrons; the analogous $Ni_6(CO)_{12}^{2-}$ cluster is an octahedron. [e] Bicapped tetrahedron or capped trigonal bipyramid. [f] Capped (triangular) square pyramid. [g] 12 framework electrons. [h] The group 4, 5, and 6 hexanuclear halide clusters are electronically distinct from the other M_6 clusters.

close-packed, face-centered cubic and body-centered cubic structures (Figures 5–11). For body-centered cubic metals, the surface connexity number is minimally 4. Connexity of peripheral metal atoms with respect to other metal atoms is relatively low in clusters: 3 in tetrahedra, 4 in octahedra, 5 in some of the very large polyhedra like $Rh_{13}(CO)_{24}H_3^{2-}$ (Figure 1) and maximally 7 in $Rh_{14}(CO)_{25}^{4-}$ (Figure 2) and $Rh_{15}(CO)_{27}^{3-}$. For connexity numbers that enumerate the metal atom to ligand interactions, there is an inversion: the connexities for metal atoms in clusters are large, 3 to 5, and for surface metal atoms, the connexities

TABLE II. Large Metal Clusters

polyhedral size	cluster[a,b]	no. of framework electrons	polyhedron defined by the metal framework	ref
7	$Rh_7(CO)_{16}^{3-}$	14	C_{3v}-capped octahedron	c
	$Rh_7(CO)_{15}I^{2-}$	14	C_{3v}-capped octahedron	d
	$Os_7(CO)_{21}$	14	C_{3v}-capped octahedron	e
	Sb_7^{3-}	18	C_{3v}-capped trigonal prism	f
	Pb_7^{3-}	18	C_{3v}-capped trigonal prism	g
8	$Os_8(CO)_{23}$	14		h
	$Rh_8C(CO)_{19}$	18	edge capped-C_{2v} capped trigonal prism	i
	$Co_8C(CO)_{18}^{2-}$	18	tetragonal antiprism	j
	$Au_6Au(PR_3)_8^{3+}$	16	D_{2h}	k
	Bi_8^{2+}	22	square antiprism	l
9	Bi_9^{5+}	22	D_{3h}-tricapped trigonal prism	m
	Pb_9^{4-}	22	C_{4v}-capped square antiprism	n
	Sn_9^{4-}	22	C_{4v}-capped square antiprism	n
	$Ni_9(CO)_{18}^{2-}$	20	stacked trigonal prisms	o
	$Pt_9(CO)_{18}^{2-}$	20	stacked trigonal prisms	p
10	$Au_{10}Au(PR_3)_7(SCN)_3$	18	defect icosahedron	q, r
12	$Rh_{12}RhH_3(C)_{24}^{2-}$	26	D_{3h}-hexagonal close-packed	s
	$Pt_{12}(CO)_{24}^{2-}$	26	stacked trigonal prisms	p
13	$Rh_{13}Rh(CO)_{25}^{4-}$	24	body centered cubic packing	t
14	$Ni_8(PR)_6(CO)_8$	24	O_h-hexacapped cube	u
	$Rh_{14}RhC_2(CO)_{28}^{-}$	32	tetracapped pentagonal prism	v
	$Rh_{14}Rh(CO)_{27}^{3-}$	24	intermediate between hcp and bcc	t
15	$Pt_{15}(CO)_{30}^{2-}$	32	stacked trigonal prisms	p
16	$Rh_{16}RhS_2(CO)_{32}^{3-}$	40	four staggered squares	w
17	$Pt_{17}Pt_2(CO)_{12}^{4-}$	14	three staggered pentagons capped at each end	t
18	$Pt_{18}(CO)_{36}^{2-}$	38	stacked trigonal prism	p
30	$Pt_{30}(CO)_{60}^{2-}$	62	stacked trigonal prism	p

[a] Boldface elements lie within the polyhedron. [b] Italic elements define the polyhedral vertices. [c] V. G. Albano, P. L. Bellon, and G. Ciani, *Chem. Commun.*, 1024 (1969). [d] V. G. Albano, G. Ciani, S. Martinego, P. Chini, and G. Giordano, *J. Organomet. Chem.*, **88**, 381 (1975). [e] C. R. Eady, B. F. G. Johnson, J. Lewis, R. Manson, P. B. Hitchcock, and K. M. Thomas, *J. Chem. Soc., Chem. Commun.*, 385 (1977). [f] D. G. Adolphson, J. D. Corbett, and D. J. Merryman, *J. Am. Chem. Soc.*, **98**, 7234 (1976). [g] W. Dahlmann and H. G. V. Schnering, *Naturwissenschaften*, **59**, 420 (1972); **60**, 429 (1973). [h] C. R. Eady, B. F. G. Johnson, and J. Lewis, *J. Chem. Soc., Dalton Trans.*, 2606 (1975). [i] V. G. Albano, M. Sansoni, P. Chini, S. Martinego, and D. Strumolo, *ibid.*, 305 (1975). [j] V. C. Albano, P. Chini, G. Ciani, M. Sansoni, D. Strumolo, B. T. Heaton, and S. Martinego, *J. Am. Chem. Soc.*, **98**, 5027 (1976). [k] P. L. Bellon, F. Cariati, M. Manaserro, L. Naldini, and M. Sansoni, *Chem. Commun.*, 1423 (1971). [l] J. D. Corbett, *Inorg. Chem.*, **7**, 198 (1968). [m] R. M. Friedman and J. D. Corbett, *ibid.*, **12**, 1134 (1973). [n] J. D. Corbett and P. A. Edwards, *J. Am. Chem. Soc.*, **99**, 3313 (1977). [o] J. C. Calabresi, L. F. Dahl, A. Cavalieri, P. Chini, G. Longoni, and S. Martinego, *ibid.*, **96**, 2616 (1974). [p] J. C. Calabrese, L. F. Dahl, P. Chini, G. Longoni, and S. Martinego, *ibid.*, **96**, 2614 (1974). [q] M. McPartlin, R. Mason, and L. Malatesta, *Chem. Commun.*, 334 (1969). [r] V. G. Albano, P. L. Bellon, M. Manassero, and M. Sansoni, *ibid.*, 1210 (1970). [s] V. G. Albano, A. Ceriotto, P. Chini, G. Ciani, S. Martinego, and W. M. Anker, *J. Chem. Soc., Chem. Commun.*, 859 (1975). [t] Reference 23. [u] L. D. Lower and L. F. Dahl, *J. Am. Chem. Soc.*, **98**, 5046 (1976). [v] V. G. Albano, M. Sansoni, P. Chini, S. Martinego, and D. Strumolo, *J. Chem. Soc., Dalton Trans.*, 970 (1976). [w] Reference 13; J. L. Vidal, R. A. Fiato, L. A. Cosby, and R. L. Pruett, *Inorg. Chem.*, **17**, 2574 (1978).

TABLE III. Polyhedral Borane Clusters[a]

size	borane[b]	heteroborane[b]	no. of framework electrons	polyhedron
4	B_4Cl_4		8	tetrahedron
5	$[B_5H_5^{2-}]$	$\underline{B}_3C_2H_5$	12	trigonal bipyramid
5	$[B_5H_5^{4-}]$		14	square pyramid
6	$B_6H_6^{2-}$	$\underline{B}_4C_2H_6$	14	octahedron
6	$B_6H_6^{6-}$		18	trigonal prism
7	$B_7H_7^{2-}$	$\underline{B}_5C_2H_7$	16	pentagonal bipyramid
7	$[B_7H_7^{2-}]$		16	capped octahedron
8	$B_8H_8^{2-}$	$\underline{B}_6C_2H_8$	18	D_{2d} dodecahedron[c]
8	$B_8H_8^{2-}$		18	square antiprism[d]
8	$B_8H_8^{2-}$		18	C_{2v}-bicapped trigonal prism[e]
9	$B_9H_9^{2-}$	$\underline{B}_7C_2H_9$	20	D_{3h}-tricapped trigonal prism
9	$[B_9H_9^{2-}]$		20	C_{4v}-capped square antiprism[f]
9	$[B_9H_9^{4-}]$		22	C_{4v}-capped square antiprism
10	$B_{10}H_{10}^{2-}$	$\underline{B}_8C_2H_{10}, \underline{B}_9H_9\underline{S}$	22	D_{4d}-bicapped square antiprism
11	$B_{11}H_{11}^{2-}$	$\underline{B}_9C_2H_{11}$	24	C_{2v}-octadecahedron
12	$B_{12}H_{12}^{2-}$	$\underline{B}_{10}\underline{C}_2H_{10}, \underline{B}_{11}\underline{P}H_{12}$	26	icosahedron
12	$[B_{12}H_{12}^{2-}]$		26	cuboctahedron

[a] For a discussion of borane cluster chemistry see "Boron Hydride Chemistry", E. L. Muetterties, Ed., Academic Press, New York, 1975. [b] Hypothetical boranes are enclosed by brackets; polyhedral vertex elements are underlined. [c] Solid state. [d] Solution state (H_2O). [e] Solution state (ethers). [f] Electronically degenerate.

are small, 1 or less on average. Even very large clusters like $Pt_{18}(CO)_{36}^{2-}$ and $Rh_{13}(CO)_{24}H_3^{2-}$ have individual metal atom connexities of 3 and 2, respectively. Only in $Pt_{19}(CO)_{12}^{4-}$ do the metal to ligand connexities drop below 1. For flat metal surfaces, the connexities may be 1 or less for ligands larger than hydrogen for a full coverage chemisorption state but the connexities could

TABLE IV. Polyhedral Metalloboranes[a]

size	metalloborane[b]	no. of framework electrons	polyhedron
6	$(OC)_3FeB_5H_3(CO)_2$	14	octahedron
	$(C_5H_5)_3Co_3B_3H_5$	14	octahedron
7	$(C_5H_5)_2Co_2B_4H_6$	14	capped octahedron
	$(OC)_3FeB_4C_2H_6$	16	pentagonal bipyramid
	$(OC)_3MnB_3C_3H_5CH_3$	16	pentagonal bipyramid
8	$(C_5H_5)_4Co_4B_4H_4$	16	dodecahedron (?)
9	$(OC)_3MnB_6C_2H_8^-$	20	tricapped trigonal prism
	$(C_5H_5)_3Ni_3B_5CH_6$	22	capped square antiprism
10	$Co(B_7C_2H_9)_2^-$	22	bicapped square antiprism
	$(C_5H_5)_2Co_2B_6C_2H_8$	22	bicapped square antiprism
11	$(C_5H_5)CoB_8C_2H_{10}$	24	octadecahedron
12	$Fe(B_9C_2H_{11})_2^{2-}$	26	icosahedron
	$(C_5H_5)_2Co_2B_8C_2H_{10}$	26	icosahedron
13	$Fe(B_{10}C_2H_{12})^{2-}$	28	capped icosahedron
	$Co(C_5H_5)B_{10}C_2H_{12}$	28	capped icosahedron

[a] For a discussion of metalloborane chemistry see "Boron Hydride Chemistry", E. L. Muetterties, Ed., Academic Press, New York, 1975. [b] Polyhedral vertex elements are italicized.

be higher for small, highly dispersed metal particles. These variances in connexities for the two limiting cases *represent a breakdown in the analogy* for the smaller clusters (3–12) but not for some of the large clusters, especially $Rh_{15}(CO)_{27}^{3-}$ and $Pt_{19}(CO)_{12}^{4-}$. Another way to express this disjoint feature is that a flat or nearly flat metal surface cannot be modeled by a polyhedral metal cluster. However, the highly dispersed metal particle–metal cluster analogy would not be so seriously flawed. It is difficult to assess the significance of these variances in connexities for the two limiting cases in the context of the
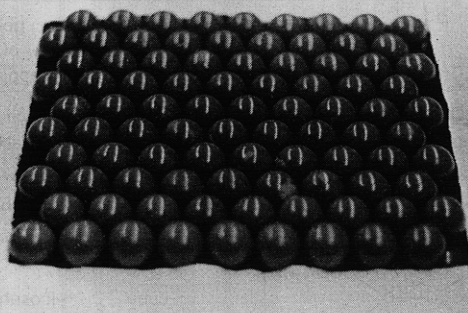

Figure 5. View looking down of the close-packed array in the face-centered cubic (cubic close-packed) (111) plane. The orientation here is specified by a set of Miller indices (*hkl*). The coordination number of all surface atoms is 9 (the bulk atoms have a coordination number of 12).

analogy for the chemisorption process. Are such variances likely to lead to substantive differences in the structural features of the bound molecule (ligand) in the surface and cluster cases? Are large differences to be found between the binding energies for the molecule on the metal cluster and on the metal surface? These three critical aspects of cluster–surface analogy, structure, thermochemistry, and surface mobility are discussed separately below.

Variances in the two types of connexity could lead to some differences in chemistry. All steps in some catalytic cycles, in principle, could occur at a single metal center in a molecular metal cluster but usually could not occur at a single surface metal atom. Nevertheless, catalytic reactions on clusters may involve more than one metal center in the course of the typically many-stepped cycles. Presently, there is no definitive mecha-

TABLE V. Examples of M_4S_4 and M_4X_4 Cubane-Like Clusters

complex	total electron count	M_4S_4 or M_4X_4 symmetry	M–M dist. Å	av M–M[a] bond order	ref
$Fe_4S_4(NO)_4$	60	T_d	2.634	1	c
$Fe_4S_2(NR)_2(NO)_4$	60	D_{2d}	4 at 2.731	1	c
$Re_4S_4(CN)_{12}^{4-}$	60	$\sim T_d$	2.76	1	d
$Co_4(NR)_4(NO)_4$	64	$\sim D_2$	2 at 2.460	$2/3$	e
			2 at 2.544		
			2 at 2.717		
$Fe_4S_4(C_5H_5)_4^{2+}$	66	D_{2d}	4 at 2.834	$1/2$	f
			2 at 3.254		
$Fe_4S_4[S_2C_2(CF_3)_2]_4^{2-}$	66	D_{2d}	4 at 2.73 (av)	$1/2$	g
			2 at 3.23 (av)		
$Fe_4S_4(C_5H_5)_4^+$	67	D_2	2 at 2.65	$7/12$	f
$Fe_4S_4(C_5H_5)_4$	68	D_{2d}	2 at 2.65	$1/3$	h
$Co_4P_4(C_5H_5)_4$	68	D_{2d}		$1/3$	i
$Co_4S_4(C_5H_5)_4$	72	T_d	3.295	0	j
$Cu_4Cl_4(PR_3)_4$	72	T_d	3.21	0	k
$W_4(OH)_4(H)_4(CO)_{12}$	72		3.48	0	l
$Ni_4(OH)_4[C_6H_9(NH_2)_3]_4^{2+}$	72	T_d	3.16–3.20	0	m
$Fe_4S_4(SC_6H_5)_4^{2-}$	54	D_{2d}	2 at 2.730	?	n
			4 at 2.739		
$Fe_4S_4(SCH_2C_6H_5)_4^{2-}$	54	D_{2d}	2 at 2.776	?	o
			4 at 2.732		
$Mo_4Hg_4(Mo(CO)_3C_5H_5)_4$[b]		$\sim T_d$	6 at 4.2 to 4.4 (HgHg)		p
			6 at 3.9 to 4.1 (MoMo)		
			12 at 2.6 to 3.2 (HgMo)		

[a] Based on the gross general assumption that there are six M–M bonding and six M–M antibonding molecular orbitals. [b] The $C_5H_5Mo(CO)_3$ groups are bound to mercury. [c] R. S. Gall, C. Tang-Wah Chu, and L. F. Dahl, *J. Am. Chem. Soc.*, **96**, 4019 (1974). [d] M. Laing, P. M. Kiernan, and W. P. Griffeth, *J. Chem. Soc., Chem. Commun.*, 221 (1977). [e] R. S. Gall, N. G. Connelly, and L. F. Dahl, *J. Am. Chem. Soc.*, **96**, 4017 (1974). [f] Trinh-Tuan, B. K. Teo, J. A. Ferguson, T. J. Meyer, and L. F. Dahl, *ibid.*, **99**, 408 (1977). [g] I. Bernal, B. R. Davis, M. L. Good, and S. Chandra, *J. Coord. Chem.*, **2**, 61 (1972). [h] C. H. Wei, G. R. Wilkes, P. N. Treichel, and L. F. Dahl, *Inorg. Chem.*, **5**, 900 (1966). [i] G. L. Simon and L. F. Dahl, *J. Am. Chem. Soc.*, **95**, 2175 (1973). [j] G. L. Simon and L. F. Dahl, *ibid.*, **95**, 2164 (1973). [k] M. R. Churchill, B. G. DeBoer, and S. J. Mendak, *Inorg. Chem.*, **14**, 2041 (1975). [l] U. Sartorelli, L. Garlaschelli, G. Ciani, and G. Bonora, *Inorg. Chim., Acta* **5**, (1971); V. G. Albano, G. Ciani, M. Manassero, and M. Sansoni, *J. Organomet. Chem.*, **34**, 353 (1972). [m] B. Aurivillus, *Acta Chem. Scand.*, **A31**, 501 (1977). [n] L. Que, Jr., M. A. Bobrik, J. A. Ibers, and R. H. Holm, *J. Am. Chem. Soc.*, **96**, 4168 (1974). [o] B. A. Averill, T. Herskovitz, R. H. Holm, and J. A. Ibers, *ibid.*, **95**, 3523 (1973). [p] M. L. Ziegler, *Angew. Chem., Int. Ed. Engl.*, **16**, 704 (1977).

TABLE VI. Eight Atom Clusters. The Cube and Fully Capped Cube

complex	geometry of Mg core	geometry of ligand capping sphere	symmetry	av M–M dist Å	electron count	av[a] M–M bond order	ref
$Cu_{14}[SC(CH_3)_2CH_2NH_2]_{12}Cl^{7+}$ [b]	~cube	~icosahedron (12 S)	~$T_h(Cu_8S_{12}Cl)$	3.3	134	5/12	c
$Cu_{14}(\text{D-penicillaminato})_{12}Cl^{5-}$ [b]	~cube	~icosahedron (12 S)	~$I_h(Cu_8S_{12}Cl)$	3.3	134	5/12	d
$Cu_8\left[\begin{matrix}S\\ \\ S\end{matrix}C=C\begin{matrix}CN\\ \\ CN\end{matrix}\right]_6^{4-}$	~cube	~icosahedron (12 S)	~$T_h(Cu_8S_{12})$	2.83	128	2/3	e
$Cu_8\left[\begin{matrix}S\\ \\ S\end{matrix}C-C\begin{matrix}COOC_2H_5\\ \\ COOC_2H_5\end{matrix}\right]_6^{4-}$	~cube	~icosahedron (12 S)	~$T_h(Cu_8S_{12})$	2.84	128	2/3	f
$Cu_8\left[\begin{matrix}S\\ \\ S\end{matrix}\begin{matrix}C-C\\ \\ C-C\end{matrix}\begin{matrix}O\\ \\ O\end{matrix}\right]_6^{4-}$	~cube	~icosahedron (12 S)	~$T_h(Cu_8S_{12})$	2.79	128	2/3	f
$Ni_8(PC_6H_5)_6(CO)_8$	~cube	octahedron (6 S)	$O_h(M_8P_6)$	2.6	120	1	g

[a] Based on the assumption that there are 12 M–M bonding and 12 antibonding molecular orbitals. [b] $ClCu^I_8L_{12}(Cu^{II})_6^{7+}$; the chlorine atom is in the center. [c] H. J. Schugar, C. Ou, J. A. Thich, J. A. Potenza, R. A. LaLancette, and W. Furey, Jr., *J. Am. Chem. Soc.*, **98**, 3047 (1976). [d] P. J. M. W. L. Birker and H. C. Freeman, *ibid.*, **99**, 6890 (1977). [e] L. E. McCandlish, E. C. Bissell, D. Coucouvanis, J. P. Fackler, and K. Knox, *ibid.*, **90**, 7357 (1968). [f] F. J. Hollander and D. Coucouvanis, *ibid.*, **99**, 6268 (1977). [g] L. D. Lower and L. F. Dahl, *ibid.*, **98**, 5046 (1976).

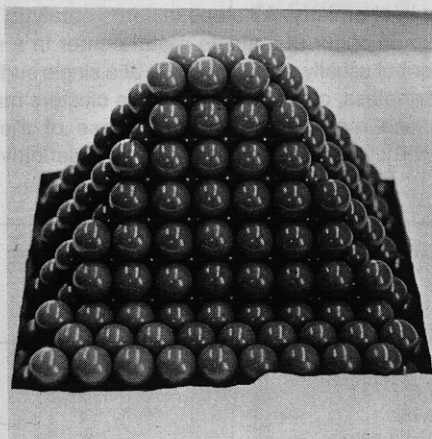nistic information for cluster catalytic reactions bearing on the issue of multimetal site chemistry.

Figure 6. A ball model of the face-centered cubic (100) crystallographic plane. This model is based on (111) layers. In this "slice", the α_1 and β_1 angles are 0 and 54.74°, respectively. The coordination number of the surface atom is 8.
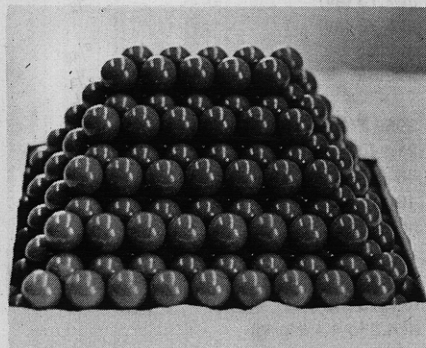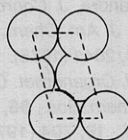

Figure 7. A "corrugated" surface which is the face-centered cubic plane (311) generated from a model based on (111) layers with α_1 and β_1 equal to 0 and 29.50°, respectively. The projecting atoms have coordination numbers of 7 and those in the troughs have coordination numbers of 11. The unit cell is:

C. The Extended Metal Surface Family

The surface bonding and atomic geometry for clean single crystal metal surfaces strongly reflects the bonding and structure on a two-dimensional scale of the bulk crystal.[26–28] In that sense,
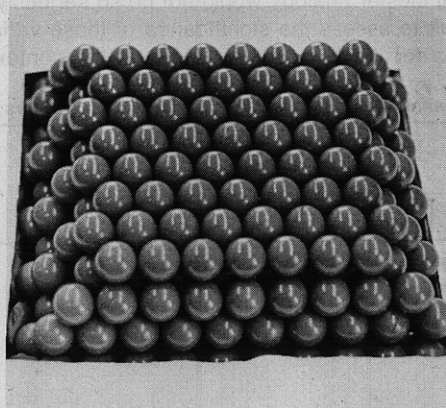

Figure 8. The close-packed (001) plane for the hexagonal close-packed structure with $\beta_2 = 0°$ ($\frac{1}{2} \leq \delta < 1$). Surface atoms have a coordination number of 9.
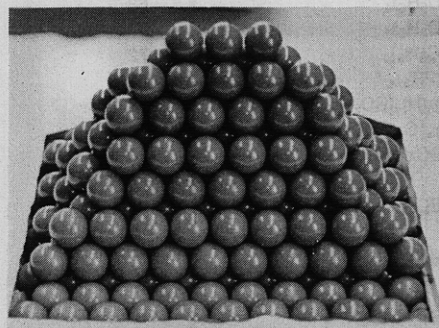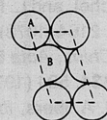

Figure 9. The (101) plane for the hexagonal close-packed structure ($0 \leq \delta < \frac{5}{6}$). Coordination numbers for the surface atoms are 8 and 9 for the surface atoms A and B in the unit cell:
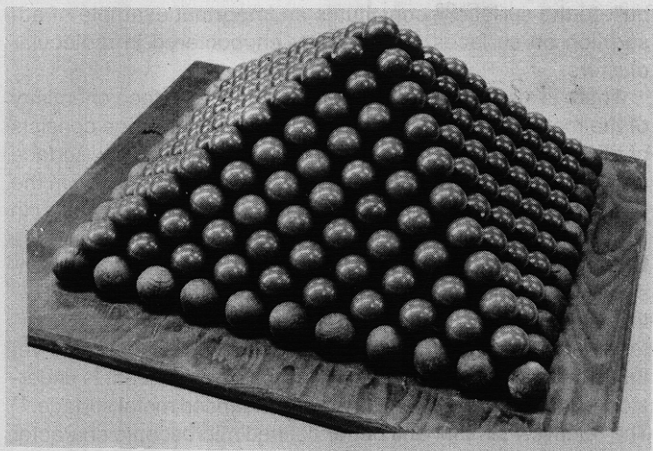
Figure 10. View of the (110) face of a body-centered cubic structure. The model is based on (100) layers and is cleaved to generate the (110) face. In this model, α is 0° and β is 45°. The coordination number for the surface atoms is 6.

Figure 11. A view looking down on the (100) face of a body-centered cubic lattice. This model is based on a buildup from (100) layers. The α angle is undefined and β is 0°, and the coordination number for the topmost spheres which have a square unit cell (the next layer forms the centered position for the square cell) is only four.

to a very rough approximation, the bonding, reactivity, and crystallography of any planar orientation in the bulk crystal may be simulated by cutting the crystal in any desired direction by a plane and discarding all the atoms on one side of the plane. This approximation is probably best with reference to defining the surface crystallography since surface atom relaxation is a relatively minor effect. It is probably poorest for estimating the residual surface energy or valency since rearrangement of the free electrons at the surface usually plays a major role in surface bonding.[29]

In Table VII are listed the kinds of packing observed for the stable, room-temperature phases of the transition metals.[30,31] The surface features for the three dominant structures, body-centered cubic, face-centered cubic (cubic close-packed), and hexagonal close-packed are illustrated in Figures 5–11 for the (100), (110), and (111) faces. Metal–metal distances observed for the bulk metals at ~20 °C and calculated distances for the bulk metals based on uniform 12-coordination for the metal

atoms are given in Table VIII.

The physical and chemical properties of single crystal metal surfaces obtained from sectioning the corresponding pure metal single crystal encompass a large range depending on the nature and strength of bonding in the crystal, the behavior of the free electrons unique to a specific class of metallic electrons as well as the atomic arrangement, characteristic of a given section through the crystal.[32,33] The bonding properties vary from the low-melting metals (such as aluminum) with relatively low cohesive energies to the refractory ones with extremely high cohesive energies (such as tungsten). The electron properties range all the way from those of the free- and nearly free-electron metals (such as lithium and aluminum), to the noble metals (such as silver, copper, and gold), to the transition metals of the first, second, and third series and finally to the rare earth metals. The surface crystallography[34] ranges from the almost atomically flat high density planes associated with low Miller indices to the

TABLE VII. Stable Structures[a] (20 °C) for the Transition Metals

Ti	V	Cr	Mn	Fe	Co	Ni	Cu	Zn
HCP	BCC	BCC	[b]	BCC	Cp[c]	FCC	FCC	HCP
Zr	Nb	Mo	Tc	Ru	Rh	Pd	Ag	Cd
HCP	BCC	BCC	HCP	HCP	FCC	FCC	FCC	HCP
Hf	Ta	W	Re	Os	Ir	Pt	Au	
HCP	BCC	BCC	HCP	HCP	FCC	FCC	FCC	

[a] HCP = hexagonal close packed, BCC = body-centered cubic, FCC = face-centered cubic = cubic close packed. [b] A complex structure with 8- and 12-coordinate metal atoms. [c] A hybrid of HCP and FCC.

TABLE VIII. Bond Distances[a,b] in Transition Metals, Observed and Calculated[c] for Coordination Number 12

Ti	V	Cr	Mn	Fe	Co[e]	Ni	Cu	Zn
2.8956 (H)[25]	2.6224 (B)[25]	2.4980 (B)[25]	2.3–2.9[d]	2.4823 (B) 18	2.5061 (C)[18]	2.4916 (C)[18]	2.5560 (C)[20]	2.6694 (H)[25]
2.94	2.70	2.58	2.74	2.52	2.50	2.50	2.56	2.74
Zr	Nb	Mo	Tc	Ru	Rh	Pd	Ag	Cd
3.179 (H)[20]	2.8584 (B)[20]	2.7251 (B)[20]	2.703 (H)[20]	2.6502 (H)[25]	2.6901 (C)[20]	2.7511 (C)[25]	2.8894 (C)[25]	2.9788 (H)[21]
3.20	2.94	2.80	2.70	2.68	2.68	2.74	2.88	3.02
Hf	Ta	W	Re	Os	Ir	Pt	Au	
3.1273 (H)[24]	2.86 (B)[20]	2.7409 (B)[25]	2.741 (H)[20]	2.6754 (H)[20]	2.714 (C)[20]	2.746 (C)[20]	2.8841 (C)[25]	
3.18	2.94	2.82	2.74	2.70	2.72	2.78	2.88	

[a] First entry is the observed value for the room-temperature stable phase. Second entry is the calculated distance for a 12-coordinate metal atom structure. Distances are in angstroms. (H) is hexagonal close-packed with the temperature in °C given as the superscript, (B) is body-centered cubic, and (C) is face-centered cubic or cubic close packed. [b] "Handbook of Chemistry and Physics", 55th ed., CRC Press, Cleveland Ohio, 1973. [c] A. F. Wells, "Structural Inorganic Chemistry", 4th ed., Clarendon Press, Oxford, 1975, p 1022. [d] Data given for α-Mn, a complex structure, which has metal atom coordination numbers from 12 to 16. [e] Actually a hybrid hexagonal and cubic close-packed structure.
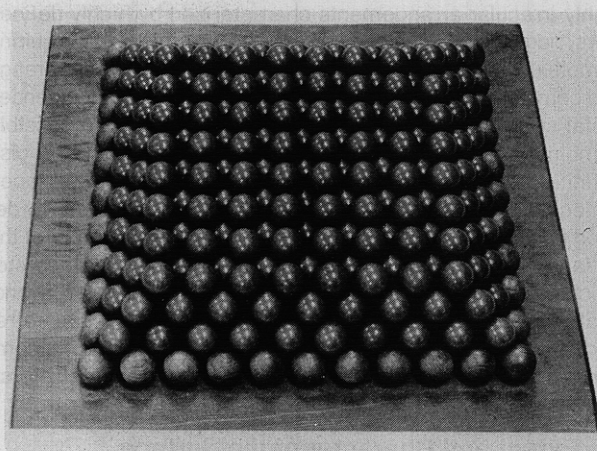
highly irregular arrangements characterized by highly defined rows, ridges, steps, kinks, and jogs on an atomic scale requiring complex Miller indices for their exact depiction. The large range and complexity of electron and atomistic structures of extended metal surfaces are a natural consequence of these possible combinations. It is not surprising, therefore, that the precise definition of only a few of the corresponding metal surface–molecule combinations have just begun to be satisfactorily defined in terms of the atomistic and microscopic character of the surface-chemical bond.[5] The specific factors of surface stereochemistry, of surface energetics and thermodynamics,[35] and, finally, of surface bonding and mobility are all an intimate reflection of these considerations and will be discussed in comparison to the surface chemistry of metal molecular clusters.

D. Extent and Character of the Surface

It is useful to depict the limiting case of the single-crystal surface as composed of more or less close-packed arrays of hard spheres in a planar configuration extending with a perfect periodicity infinitely in two dimensions. It is clear that, even in the limiting case when the molecular interaction is essentially localized onto a single atom, both the local atomic and electronic structure will be influenced by the more distant atoms in both the surface and the half-space of the bulk.[36] It is also apparent that the location of the surface boundary is not too precisely defined since the free electrons can extend out about a lattice parameter in depth into the vacuum, and the interacting atom or molecule can often penetrate below the mathematical external plane of the crystal. A long-range surface periodicity also exists in the surface potential field corresponding to regular fluctuations in both the electron density and atomic forces at the surface. This periodicity of surface forces extends into the vacuum with highly defined orientation and symmetry as well as with well-defined directionality in the plane of the surface. Since this periodicity and directionality is always anisotropic, particularly in the surface plane, it will have a correspondingly significant influence on both bonding and mobility at the surface.[36] The possibility of long-range interactions among the chemisorbed molecules is a possible consequence of the extended atomic and electronic periodicity of the metal surface. Even in the highly localized case of surface bonding involving a single adatom–surface atom theoretical complex imbedded in a planar sea of surface electrons and atoms, the latter will always play a role in the behavior of the adatom; this has no direct analogy in molecular clusters. Nevertheless, the close analogy of the imbedded theoretical complex to the molecular cluster[37] provides a useful point from which to initiate our analysis of bonding and structure.

It will be important to consider extension of this analogy even further in terms of composition, structure, and environment from the simple consideration of an approximately planar, single component, single phase surface in contact with a vacuum. The nature of chemical bonding on the single-crystal surface will approach more closely that in a molecular cluster as the curvature increases and the surface atomic density decreases such as in a very small crystal aggregate or metal whisker.[38] It is significant that the surface chemistry of both of these configurations is becoming increasingly better defined with the rapidly advancing effectiveness of surface experimental techniques.[39,40] Furthermore, there is no reason why the comparison of multicomponent surfaces cannot be usefully carried over to molecular clusters containing more than one kind of metal atom. This opens up a variety of intriguing opportunities to investigate effects of short- and long-range order, of dilution factors, and of mutual bonding perturbations in surfaces and clusters. Some examples of these possibilities will be discussed later. In the context of other variations from the pure metal surface, the occurrence of surface segregation of impurity atoms from the

bulk to the surface[35] constitutes an important example of adsorption on surfaces not normally encountered in molecular clusters.

There is also a useful analogy between the surface chemistry of the metal and that of the cluster when the interface consists of a juncture with a liquid or another solid. The mobility, surface energy, and surface bonding can be significantly altered in the extrapolation of our considerations to these environments. In the latter case, especially, considerations of the role of surface stress, as distinct from surface energy, may be usefully considered from the viewpoint of the surface–cluster approach.[35] Interpetative applications to solid–liquid and solid–solid interfaces are very important from the applied viewpoint, and yet these are the very classes of systems for which least is understood in terms of the chemistry of the extended metal surface.[41] The relatively simpler and better defined microscopic character of molecular cluster chemistry makes this an interesting aspect of the analogy. It is clear in terms of the extended consideration of the surface–cluster comparison that in each case the simplest example can probably be best understood, but that the closeness and perhaps the ultimate benefit of the approach will be most productive when more complicated examples from each class can be effectively analyzed and compared. It appears that the connection between the two classes becomes closer, at least in some types of bonding phenomena, when coupling is achievable between a polycomponent atomically rough metal surface and a complex molecular cluster. We shall initiate our efforts most effectively with the simpler examples now available from both groups. It will probably be some time before the more complex examples from both systems in the analogy may be effectively defined and compared.

E. The Importance of Cluster Size

Discrete molecular clusters seem large to an inorganic chemist but even the largest of them, the 19- and 30-atom species, are only submicroscopic fragments of a metal surface. Then, can the most commonly studied clusters, the three-, four-, and six-atom clusters, be plausible models of surfaces? Unfortunately, ab initio theory usually cannot provide an unequivocal answer—there are too many electrons for calculations to be made without qualifying assumptions. On the other hand, approximate theory is beginning to provide some qualitative answers.

A hypothetical cluster of metal atoms must be large, probably hundreds of metal atoms, for the cluster to truly possess the properties of a metal. Calculations based on σ molecular orbital theory, extended Hückel, and CNDO or INDO indicate that a hypothetical cluster of metal becomes *metal-like* at numbers that range from 13 to 19 for nickel and palladium, 30 to 51 for silver (with chains slightly favored over clusters in this size range), 30 for lithium, and ~28 for cadmium.[42] Similar calculations have been carried out with the $X\alpha$-SW approximation with similar results although the transition to metal-like properties generally appears for clusters smaller than those found from molecular orbital calculations. For example, the principal features of the band structure of crystalline nickel appear to be determined by short-range order as nominally represented by a cubo-octahedral cluster of 13 atoms. Convergence to bulk properties would seem to be attainable with clusters of 25 to 50 atoms. This $X\alpha$-type of calculation has been reviewed recently by Rösch.[43]

The larger clusters with metal-like properties exhibit energy gaps (between HOMO and LUMO) ~ten times larger than bulk metal, a larger work function, and a lower cohesive energy. Results from molecular orbital calculations for palladium are summarized in Table IX.[42] The calculations do show that small, four- to six-atom clusters are not metal-like in properties. Hence these small molecular clusters are not models of a metal. But

TABLE IX. Calculated (Extended Hückel) Electronic Properties of Palladium Clusters[a]

size	geometry[b]	r_{eq}, Å	d holes per atom	BE/n, eV	HOMO, eV	LUMO, eV
2	linear	1.75	1.00	0.60	8.20	7.25
3	triangle	2.30	0.67	0.80	8.03	7.85
4	pyramid	2.10	0.52	0.74	8.01	8.02
5	bipyramid	2.30	0.41	0.67	8.11	8.11
6	square bipyramid	2.30	0.35	0.55	8.08	8.04
8	cube	2.40	0.35	0.56	8.14	8.14
9	BCC cube	2.75	0.40	0.47	8.25	8.25
13	FCC	2.50	0.62	1.19	8.19	8.19
19	FCC	2.75	0.42	1.29	8.27	8.26
2[c]	linear	2.57		1.08 ± 0.2		
bulk[d]	FCC	2.75	~0.5	3.9		

[a] R. C. Baetzold, *Adv. Catal.*, **25**, 1 (1976). [b] BCC = body-centered cubic, FCC = face-centered cubic. [c] Experimental values for gaseous Pd_2. [d] Experimental values.

TABLE X. Generalized Valence Bond Calculations of Chemisorbed Species by Goddard et al.[a]

species	D_0, kcal/mol	ΔH_f, kcal/mol	d, Å
NiH	64	−12	1.45
NiCO	27	−53	1.90
Ni_2CO	34	−60	1.94
Ni=CH_2	65	27	1.78
Ni_2CH_2	122	−30	1.91
$NiCH_3$	60	−25	1.87
NiC(H)=OH	57	−47	
NiCHOH	56	−4	
Ni=O	91	−31	1.60
Ni_2O	101	−41	1.79
NiOH	50	−41	1.72

[a] W. A. Goddard III, S. P. Walch, A. K. Rappe, T. H. Upson, and C. F. Melius, *J. Vac. Sci. Technol.*, **14**, 416 (1977).

TABLE XI. Borane Structures ($2n + 2$)

borane	framework electrons	geometry
$[B_5H_5{}^{2-}]$	12	D_{3h}–trigonal bipyramid
$B_6H_6{}^{2-}$	14	O_h–octahedron
$B_7H_7{}^{2-}$	16	D_{5h}–pentagonal bipyramid or C_{2v}–capped trigonal prism
$B_8H_8{}^{2-}$	18	D_{2d}–dodecahedron, D_{4d}–square antiprism, or C_{2v}–bicapped trigonal prism
$B_9H_9{}^{2-}$	20	D_{3h}–tricapped trigonal prism
$B_{10}H_{10}{}^{2-}$	22	D_{4d}–bicapped square antiprism
$B_{11}H_{11}{}^{2-}$	24	C_{2v}–octadecahedron
$B_{12}H_{12}{}^{2-}$	26	I_h–icosahedron
$[B_{12}H_{12}{}^{2-}]$	26	O_h–cube octahedron

the putative cluster–surface model is not structured on this comparison but rather on a comparison between *a discrete or molecular metal cluster which has a polyhedral metal core and, in most cases, a periphery of ligand atoms, groups of atoms or molecules and a metal surface with a similar set of ligands chemisorbed at the surface.*

There have been a number of attempts to analyze the chemisorbed state with approximate valence bond, molecular orbital and Xα theory. As a necessary simplification, a "surface molecule" concept has been employed; this concept assumes that adsorbed molecules or groups of atoms interact strongly with a limited set of metal atoms. This assumption appears to be a reasonable approximation although contributions from nonlocalized surface states seem to be significant. For example, in the adsorption of carbon monoxide on nickel, it was found that the size of a planar net of nickel atoms did not substantially affect the chemisorption energy. Extended Hückel calculations[44] for CO on eight-atom nickel indicated
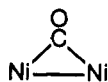
bridging bonding to be slightly more stable than single-site NiCO bonding, 2.53 vs. 2.39 eV as compared with the experimental value of 1.98 eV. Recently, Goddard has been applying a generalized valence bond (GVB) method to the binding of molecules like CO to one nickel atom, two, three, etc.[45] For the NiCO molecules, the NiC distance was calculated to be 1.90 Å and the CO binding energy to be 1.15 eV. In Table X are listed some of the results of the early Goddard calculations. The Xα modeling of CO chemisorption in M_5CO clusters and of O_2 chemisorption on Ni, Cu, and Ag in M_4O clusters is discussed by Rösch.[43] Theoretical results obtained for these small cluster molecule interactions will be of interest to compare with the surface chemisorption data and with molecular clusters.

Of special note here are the molecules obtained through matrix isolation techniques. Ozin and co-workers[46] have developed procedures for the isolation of molecules like $Ni(C_2H_4)_x$ ($x = 1-4$), $Ni_2(C_2H_4)_x$, and $Ni_3(C_2H_4)_x$[46] and similar ones for the copper–ethylene system.[47] Mixed-metal clusters of the type Cr_mMo_n ($m = 0$ to 3 and $n = 3$ to 0) have also been reported[48] to be formed by a photoaggregation process. Provided that accurate interpretations of spectroscopic data for these metastable species can be achieved, the molecules will provide excellent checks for the calculational results of Goddard and others. In summary, there is progress in the theory of the chemisorbed state, and the surface state or semilocalized model of the chemisorbed state appears to be valid in the first approximation. Thus, the proposed metal cluster–metal surface analogy, with

respect to the chemisorbed state, is not inconsistent with the preliminary results from approximate quantum theory.

F. Molecular Clusters

Theoretical analysis of the known molecular clusters has been attempted by extended Hückel methods[49,50] and by the non-parameterized Fenske–Hall[51,52] method. Any individual cluster can be approximately analyzed by such procedures, but the chemist's need is in systematics and generalizations. Recently Lauher[53] has formulated a useful, generalized molecular orbital treatment of the metal cluster structures that has the virtues of systematization and simplicity. Most of the three-dimensional clusters can be approximated by a model in which it is assumed that each cluster atom utilizes three orbitals, of a and e symmetry, for framework binding. On this basis, the boron clusters (polyhedral boranes, heteroatom–polyhedral boranes, and the metalloboranes), which are listed in Tables III and IV, can serve as models[54] for the smaller and medium-sized metal clusters (up through ~12 to 14 atoms). LCAO–MO calculations for the polyhedral boranes show closed-shell configurations and relatively large HOMO–LUMO energy gaps to result for the $B_nH_n{}^{2-}$ clusters with $2n + 2$ framework electron in the geometries shown in Table XI.[57] The hypothetical B_4H_4 (eight framework electrons) should have T_d geometry and the known B_4Cl_4 molecule has tetrahedral geometry. Closed-shell configurations for hypothetical boranes which do not have the $2n + 2$ framework electrons are given in Table XII. These guidelines, set in terms of the number of framework electrons per given polyhedron, are remarkably accurate in the rationalization and prediction of geometry for small three-dimensional molecular metal clusters:

1. In the small three-atom clusters, triangles prevail. Those with six framework electrons are electron precise. Those with only four framework electrons usually have one very short M—M distance that may be considered as an M—M double bond.

TABLE XII. Borane Structures (non-2n + 2)

borane	framework electrons	geometry
B_4H_4	8	T_d-tetrahedron
$B_4H_4^{4-}$	12	T_d-tetrahedron
$B_4H_4^{6-}$	14	C_{2v}-butterfly
$B_4H_4^{8-}$	16	D_{4h}-plane
$B_5H_5^{4-}$	14	C_{4v}-square pyramid
B_6H_6	12	C_{2v}-capped trigonal bipyramid
$B_6H_6^{6-}$	18	D_{3h}-trigonal prism
B_7H_7	14	C_{3v}-capped octahedron
$B_7H_7^{4-}$	18	C_{3v}-capped octahedron
$B_8H_8^{8-}$	24	O_h-cube
$B_9H_9^{4-}$	20	C_{4v}-capped square antiprism
$B_{14}H_{14}^{2+}$	26	O_h-face-capped cube

2. Nearly all tetranuclear clusters have 12 framework electrons and tetrahedral geometry. This pervasive class is electron precise; formally there are six two-electron M—M bonds. A few clusters have only 8 or 10 framework electrons; these are formally electron deficient and also are tetrahedral. A few are "electron-rich", 16-framework electron clusters, and have planar or near-planar geometry. Thus, four-atom clusters with 8 to 12 framework electrons are regular or nearly regular tetrahedra, and those with 13 to 14 electrons are butterfly or bat-winged structures. With 16 framework electrons, the structure should be square planar.

3. Five-atom clusters with 12 and 14 framework electrons have trigonal-bipyramidal and square-pyramidal geometry, respectively. The subgroup of post-transition metal cluster ions[58] like Bi_5^{3+} and Sn_5^{2-} are assumed, by analogy to the boranes, to have a pair of nonbonding valence electrons associated with each metal atom. Thus trigonal-bipyramidal Bi_5^{3+} has $[5(5) - 5(2) - 3]$ or 12 framework electrons and a hypothetical square pyramidal Sn_5^{4-} would have $[5(4) - 5(2) + 4]$ or 14 framework electrons.

4. Six-atom clusters almost invariably have 14 framework electrons and octahedral geometry. Those with 18 framework electrons have trigonal-prismatic geometry. The notable exception to these generalizations is $Pt_6(CO)_{12}^{2-}$, which formally has 14 framework electrons and adopts trigonal prismatic geometry[25] although the analog $Ni_6(CO)_{12}^{2-}$ has octahedral geometry. Clusters with only 12 framework electrons may adopt the capped trigonal-bipyramidal (bicapped tetrahedron) geometry.

5. Seven atom clusters have 14 framework electrons and all these have capped octahedral geometry.

6. An important subclass of tetranuclear metal clusters have cubane-like M_4S_4 or M_4X_4 cores which may be considered as S or X capped tetrahedra (Table V). For the electron-precise tetrahedron in which the M—M bond order is one, there presumably are 12 electrons in a set (e + a + t) of framework bonding orbitals.[50] Lying above are a set of six antibonding orbitals ($t_1 + t_2$); thus those clusters that have 24 framework electrons, e.g., the $[LCuX]_4$ set, have a formal M—M bond order of zero. Included in this set of clusters (Table IV) are the ferridoxin models[59] $[RSFeS]_4^{2-}$ which are not electronically analogous to the $[C_5H_5FeS]_4$ and $[ONFeS]_4$ sets where there are strong field ligands. In the borane analogy, the ferridoxin models appear as substantially electron-deficient clusters with only six framework (Fe_4) electrons.

7. There is a class of eight-atom clusters that have a cubic array of copper atoms enveloped by a near icosahedral set of sulfur atoms—and often have an internal chloride ion. These clusters, which are of biological significance, have a surfeit of framework electrons that can exceed the electron precise count of 24 for a cube (Table VI). These excess electrons presumably go into largely M—M antibonding orbitals so as to reduce the M—M bond order.

8. Nine-atom naked clusters[58] like Bi_9^{5+}, Sn_9^{4-}, and Pb_9^{4-} have 22 framework electrons and either D_{3h}-tricapped trigonal prismatic or C_{4v}-monocapped square antiprismatic geometry. Overall charge on these clusters has a major effect upon the ordering of the top bonding orbitals.

The borane analogy for the metal clusters has utility primarily for systematizing and for rational, designed synthesis purposes. It is most accurate for clusters in which (1) the formal oxidation state of the metal atom is low, (2) the ligands are strong field ligands, and (3) the nd, $(n + 1)$s, and $(n + 1)$p levels (transition metals) are close in energy. Exceptions should be anticipated in early transition metal clusters, metal halide clusters (higher oxidation state and weak field ligands as in $Mo_6Cl_{14}^{2-}$) and highly charged clusters. Individual MO calculations have been performed[60,61] for the "aberrant" metal halide clusters like $[Mo_6Br_8]Br_4 2H_2O$. The borane analogy is not a substitute for approximate calculations where questions of electronic spectra, magnetism, or chemistry are involved. In addition, the analogy has proven to be quite inadequate in predictive capability and even in the rationalization of the very large molecular clusters like the rhodium series, Rh_{13} through Rh_{17} where close-packed arrays may or may not be present.

II. Structural Comparisons between the Chemisorbed State and Metal Clusters

A. Introduction

Unless there is a close correspondence in the structure and bonding features of ligands—i.e., of molecules, atoms, or groups of atoms bound to metal atoms both in the molecular cluster and metal surface regimes—then the putative analogy between the two for the processes of chemisorption and catalysis is not applicable. Such comparisons ideally are made only when the correspondence in (i) the metal, (ii) the ligand, (iii) the coverage by the ligand on the cluster or on the metal surface, and (iv) the crystallography is precisely one-to-one. The first constraint presents no tactical problem. The second does for some ligands in that it is not feasible presently to synthesize isolable molecular clusters where the only ligand is, say, ethylene, acetylene, or hydrogen although clusters with such ligands in combination with other ligands, e.g., carbon monoxide, either are known or could be prepared by established synthesis principles. The equivalent coverage requirement has a constraint dictated by the molecular clusters. Most molecular clusters are coordinately saturated. We assume that this state has as its analog in metal surfaces the monolayer chemisorbed state because we believe that the localized bonding model for the chemisorbed state is in its approximation optimal for the case of monolayer or near-monolayer coverage. It is in the fourth requirement—equivalent crystallography for the metal atoms—that the major theoretical and experimental problems arise. For the chemisorbed metal surface, reasonably definitive structural and electronic analysis through a range of surface studies can be made for a pure metal crystal in which there is a "flat" surface of well-defined crystallography, on which a molecule is then chemisorbed. Molecular clusters, however, are polyhedra with triangular faces or with a mixture of triangular and square faces; this is true even for very large molecular clusters. This disjoint crystallographic feature will be ever present for the two regimes. Nevertheless, these are experimental variables in metal surface studies that if systematically followed can begin to redress this crystallographic deficiency. Structural as well as chemical studies of single crystal metal surfaces with chemisorbed molecules can be systematically examined as a function of crystallography by varying the crystal face of low Miller index planes where there may be close packing, to higher planes where not only may the metal–metal coordination number for surface atoms decrease dramatically but also where irregular features, namely steps and kinks, may develop (the reader is referred to Figures 4–11 and

to an excellent atlas[34] of bcc, fcc, and hcp planes). In all these cases, ultrahigh-vacuum conditions and all the key surface physics techniques are applicable. Correspondence in crystallography between the two regimes becomes much closer as the chemisorbed metal surface is changed from a single crystal to a film or better to small (still large with respect to a cluster) particles or spherulites. However, in this sequence the number of applicable surface physics techniques decreases and *definitive* structural analysis of the chemisorbed state is significantly less feasible with present day spectroscopic and diffraction techniques. Chemical studies, however, may assist, at least in qualitative comparisons involving metal films and small particles. There remains the technologically important class of supported metal and alloy particles which introduces a new unknown interaction between the support and the metal particles.

In this structure section, the primary comparison between clusters and surface will be limited to metal-surface information derived from studies of single crystal metal surfaces. Accordingly, the reader must keep in mind at all times the discrepancy in crystallography for the comparison of these "flat" surfaces that have chemisorbed molecules with molecular cluster polyhedra. In the two following sections, the primary structural techniques are briefly described and limitations in these techniques are duly noted.

B. Structural Analysis of Molecular Clusters

Structure, stereochemistry, and precise structural parameters for molecular clusters can and have been established by single-crystal X-ray crystallographic studies.[62,63] The single-crystal requirement is the only major limiting factor in these diffraction studies. Occasionally, the production of a single crystal of adequate size has proven to be experimentally difficult. For clusters that have hydride ligands, precise location of the hydride hydrogen atoms generally requires a complementary neutron diffraction[64] study; Bau[65] has recently reviewed this area of cluster structural studies. The potential precision in these determinations is very high, but this potential has not been realized in a number of cluster crystallographic studies because of disorder problems, small or poor quality crystals, or limited data sets. Some of the reported crystal studies should be updated because the clusters are literally key structural reference points. A case in point is $Ir_4(CO)_{12}$ which is extremely difficult to obtain in single-crystal form free of disorder.

For the solution state, the most generally effective structural technique is the nuclear magnetic resonance measurement. Prime magnetic nuclei for high-resolution studies are ^1H, ^{13}C, ^{31}P, ^{11}B, and ^{19}F. The high-resolution experiment can in the ideal case define structure and stereochemistry but not structural parameters. With modification of the spectrometer probe to allow sample spinning, structural features can be established for the solid state if the nucleus under study is magnetically dilute. Excellent treatises dealing with the theory and practice of nuclear magnetic resonance are available.[66,67] In section IV, the use of the nuclear magnetic resonance technique for the study of dynamic processes in clusters is discussed.

Infrared analysis is employed largely as a diagnostic technique, e.g., in distinguishing between terminal and bridging ligand positions. Occasionally, vibrational data can be more structurally informative as in the definition of molecular symmetry if the cluster molecule has relatively high symmetry and if isotopic substitution is employed.

The above four techniques are the most generally applicable to cluster structural studies.

C. Structural Analysis of the Chemisorbed State

Structural definition of the chemisorbed state with respect to stereochemistry and to precise quantitative measures of bond distances and angles is, in principle, possible for the specific case of simple chemisorbed species on an ordered surface of well-defined crystallography. In fact, this has been done for the specific case of atoms (O, S, Se, and Te) on low Miller index faces of transition metals, e.g., nickel.[68,69] These analyses were the result of very careful experimental and theoretical analyses based on the diffraction characteristics of low energy electrons from these surfaces.[70] Extension of this type of study—commonly referred to as low-energy electron diffraction, or simply as LEED, studies—to the chemisorption of molecules on ordered metal surfaces is feasible and has been done, but the analyses are far more difficult. The LEED study is complementary to another surface science technique, angle-resolved photoemission.[71] The combination of the two techniques is preferred for the more complex problem of chemisorbed polyatomic species. A third spectroscopic technique that is somewhat in the developmental stage provides vibrational information about chemisorbed species and is based on the energy loss spectrum of electrons inelastically scattered from the surface.[72] There are alternative means to obtain such information, but the energy-loss spectroscopy has the virtues of high sensitivity and adaptability to the ultrahigh-vacuum system in which clean and well-defined metal surfaces can be examined in the chemisorption process. A brief discussion of these techniques in terms of applicability (specifically citing limitations) is presented in the following paragraphs because many of the readers may not be familiar with the techniques (reference is given to authoritative presentations of theory and practice).[39,72,74,84]

The geometrical arrangement of atoms at a crystal surface is clearly basic to the understanding of many surface properties and processes, in particular, surface chemical bonding. Information about surface structure obtained from low-energy electron diffraction is essentially the same as that derived by standard X-ray analysis for bulk crystals, e.g., the geometry of the diffraction patterns, the features of various diffraction patterns, and the intensities of various diffraction beams with electron energy and geometry. The main difference is that allowance must be made for the two-dimensional character of the sample and the scattering properties peculiar to low-energy electrons. The experimental devices fall into two basic classes, instruments which provide the diffraction geometry directly and the intensities indirectly and those where the intensities are measured explicitly and the spectra calculated directly. Most systems currently in use are "display-type" where the patterns are indicated directly and the intensity spectra indirectly.[34] Although the theory of LEED intensity analysis[74] is not sufficiently advanced to allow the routine interpretation of structure achievable by X-ray methods, pattern studies provide a great deal of useful information on the geometry and symmetry of surface structure whereas structure analysis based on intensity studies has been limited to a much smaller number of simple atomic chemisorbed states. The essential features of a LEED apparatus consist of a source of collimated monoenergetic electrons with energies in the 20–500-eV range, a manipulator for proper positioning of the single-crystal target, and an electronic or visual detection system for measuring the position and intensity of the electrons which are elastically back-scattered. Careful effort must be made in terms of sample environment to maintain the structure and composition of the surface constant during the measurements. The design and operation of the method is well described.[34] Most surface geometrical information has been obtained by the comparison of experimental and theoretical LEED intensity vs. voltage (I–V) curves, whether by the "dynamical",[74] "data averaging",[75] or "Fourier transform[76,77] methods. Following rather intense activity after the first successful LEED structural determinations from the calculational analysis of the intensity–voltage relationship in 1971, various trends have become apparent concerning atomic, and, to a lesser extent, molecular bonding at surfaces. Known structures
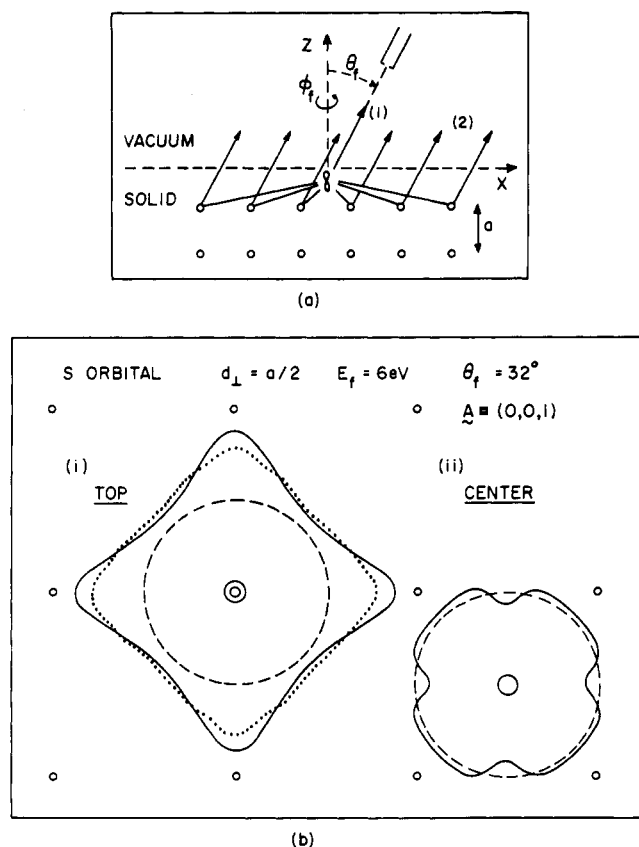
Figure 12. (a) Angle resolved photoemission from molecule on surface showing both initial electron scattering and multiple electron scattering contributions from final state. (b) Contours of angle resolved azimuthal intensity plots corresponding to (i) terminal bridging, and (ii) fourfold face bridging (after Liebsch, ref 71a).

for clean and chemisorbed metal surfaces are reviewed in the next section; comprehensive summaries are those of Van Hove[73] and Tong.[78]

It is important to recognize that the determination of surface crystallography by LEED is never as straightforward as the analysis of bulk crystal structure by X-ray diffraction. This is due to several complicating factors, including (i) multiple scattering of electrons within and between surface layers, (ii) energy-dependent electron-scattering cross sections from surface atoms, (iii) diffraction of electrons at the surface potential discontinuity, (iv) electron–phonon scattering, and (v) strong inelastic damping of the incident flux by surface plasmon and single particle excitations. To provide an effective theoretical interpretation of LEED data, a rather sophisticated description is thus required, containing some form of provision to treat each of the above five physical processes.[79] Recent emphasis has been toward a more effective treatment of these processes. A by-product of the difficulties faced in LEED has been the development of very efficient theoretical tools for treating electron scattering at solid surfaces. These techniques,[78] which include the layer KKR, T-matrix, layer-doubling, and other perturbation methods, are useful not only for LEED but also for other surface probes that involve the passage of electrons through atomic layers.

A host of surface structures on a wide variety of clean and chemisorbed metal surfaces have been reported during the past several years.[73] Calculations including the proper ingredients are now able to obtain excellent agreement with measured intensity–voltage data on many of these surfaces. Attempts are being made to lessen the dependence on necessarily qualitative visual comparisons of experimental and theoretical intensity–voltage curves, mainly through the use of numerical reliability

factors.[80] Such efforts are aimed at developing more quantitative and less subjective measures of the correctness of a reported structure, in addition to providing the nonpractitioner of LEED with a firmer basis for critical comparison.

Concerning the reliability of LEED structural results, early discrepancies that had cast doubt on the value of LEED as a tool for extracting accurate surface bond lengths have been resolved.[81] It can now be said that results are, for the most part, reproducible and consistent with each other. Furthermore, preliminary information from other complementary surface analysis techniques, such as high-resolution energy loss spectroscopy[72] and angle-resolved UV photoemission spectroscopy,[71a] is beginning to show agreement with LEED results. Also, some small-cluster calculations[82,83] have characterized surface structures that partially agree with LEED results. Unfortunately there is simply too little information presently available from these techniques to make meaningful comparisons, although this will certainly be possible in the near future. For completeness, it must be pointed out that some LEED structural determinations have been unable to discriminate between two or three different geometries, and some failures to agree on a structure have occurred.

A second method of electron spectroscopy which can provide information on surface structure is based on the photoemission of electrons from solids.[84] The kinetic energies of photoemitted electrons from molecules on or in surfaces of solids are related to the binding energies of the electrons. The level of binding being explored is defined by the energy range of the photoexcitation. Structural information can be inferred in two ways. Since the photoelectron spectra probes the electronic structure of the surface molecules, it is a particularly sensitive reflection of perturbations of molecular orbitals of the molecules by the surface metal atoms. In this sense, variations of intensity and position of spectral peaks corresponding to these orbitals can provide, in principle, information on the bending and stretching of bonds for certain molecular systems in the surface region.

The second type of structural information relates to the multiple scattering of the photoemitted electrons which originate at an effective point source in the surface molecules within an electron mean free path distance of the emitting surface.[71a] Where such final state photoemission effects dominate, information may be obtained on the coordination and spacing of surface atoms through appropriate analysis of the momentum- and energy-dependence of the photoemitted electrons corresponding to specific electron transitions in the molecule (Figure 12). In both cases, the intensity of the photoemitted electrons is measured as a function of their energy for specific photoexcitation energies and directional features of the incident and emitted beams. Synchrotron radiation sources in addition have the advantage of providing intense, polarized photon beams over a wide energy range.[85] Photoemission consists of a series of complicated processes,[71] and interpretation of surface structural information from photoemission spectra is presently at a preliminary stage of development. The theory and instrumental methods of angle resolved photoemission for these purposes are discussed in detail.[84,85]

It is instructive to compare the LEED technique with angle-resolved ultraviolet photoemission spectroscopy (ARUPS).[87] Whereas LEED probes the long-range order of surface atoms, ARUPS probes primarily the local symmetry and direction of surface bonds. LEED is sensitive to changes in the interlayer spacing of order 0.1 Å, whereas ARUPS is more sensitive to interatomic spacings in the plane of the surface. In general, ARUPS is better suited for determining the orientation and bond angles of adsorbed molecules containing hydrogen (e.g., C_2H_2, NH_3, H_2O) as well as discerning structural differences in adsorbed molecules with similar atomic electron scattering factors. Furthermore, small changes in molecular bond order may be discernible using photoemission by observation of changes in

relative orbital ionization potentials. These are often extremely sensitive to small changes in bond lengths.[88a]

A third method of current significance for determining surface atomic structure is based on vibrational spectroscopies which explore the symmetry and strength of localized bonding modes of chemisorbed molecules.[89] Important from the viewpoint of our discussion are studies of adsorption on surfaces of well-defined composition and structure. Development of reflection-adsorption infrared spectroscopy has been applied to the measurement of spectra for adsorbates on well-defined single crystal surfaces.[90] The sensitivity limits this application to systems involving strongly bound adsorbates such as CO and some hydrocarbons. Vibrational information associated with bonding on well-defined surfaces has recently become more available through the use of high-resolution electron energy loss spectroscopy, as developed by Ibach and others.[89] The type of information provided by electron energy loss spectroscopy is identical with that obtained by infrared spectroscopy but with an extended energy range and higher sensitivity. These features make this method highly adaptable to exploration of bonding on surfaces which can also be well defined by other types of surface probes. The potential of this approach, first demonstrated by the work of Propst and Piper,[91] has recently been greatly extended by others (Ibach[89] and Andersson[92]). The precise measurement of small electron losses is associated with phonon interactions of a very low energy monochromatic beam of electrons with surface molecules. The high level of electron spectroscopic technique required to obtain significant results by this approach has been described.[72] Development has progressed to the level now where the site geometry and the nature of chemical bonding can be identified in surface atomic and molecular complexes formed upon chemisorption of gases on a variety of single-crystal metal surfaces. This method involves electron measurements at a solid–vacuum surface under ultrahigh vacuum. A variation of this method involving electron-loss measurements is associated with inelastic electron tunneling in the solid state through structures where adsorbed molecules are positioned on very thin oxide films sandwiched between two metals.[93-95] This method has promise for a limited set of adsorbed molecules but has not as yet been extensively applied to surface structural studies. In addition, there is a variety of other promising spectroscopic techniques now being developed which are capable in principle of providing detailed information on the atomic structure of molecules at surfaces, for example, such as extended X-ray adsorption fine structure (EXAFS). These fledgling techniques have not as yet provided sufficient new data to warrant discussion here.

D. Surface Structure in Chemisorbed Systems

1. Atomic Adsorption—LEED Studies

To date, the exploration of metal surface structures has been limited, with a few exceptions, to low-index surfaces of single-crystal metals, either clean or with an ordered atomic overlayer. Within these limits a few conclusions of general validity have begun to emerge concerning several aspects of surface crystallography relevant to surface bonding, viz., adsorption registry, bond lengths and directions, and implied charge transfers.[73] Registry is a term used by surface scientists to denote the geometric periodicity of an upper two-dimensional surface lattice relative to a lower one.[97,98] The latter may have the same or related sequence of translational vectors. Pseudomorphism is an extreme state of registry when the symmetry and spacing of one ordered phase are continued across the compositional interface into a second phase.[99] The clean metal surfaces whose structures have been determined exhibit the atomic arrangement of the bulk up to and including the topmost atomic layer within a few percent except for certain cases where a top layer may undergo inward relaxation perpendicular to the surface. The
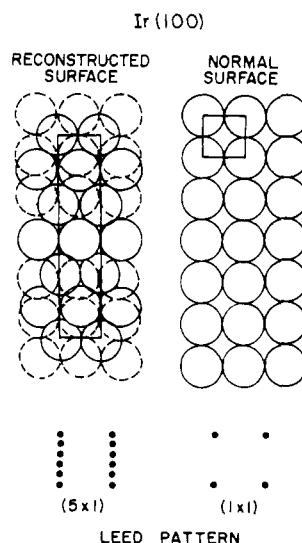

Ir (100)

RECONSTRUCTED SURFACE   NORMAL SURFACE

(5 x 1)   (1 x 1)

LEED PATTERN

Figure 13. Schematic representation of the outermost atomic layer for a clean Ir(100) surface in its (a) reconstruction (5 × 1) and (b) normal (1 × 1) states. Unit cells indicated by rectangle and square (after Ignatiev, Jones, and Rhodin[127a] and Rhodin and Broden[127b]).

results of LEED analysis indicate, despite a few exceptions, a clear correlation between surface bond-length contraction and surface "roughness" on an atomic scale. Surfaces which may be considered smooth, i.e., hcp(0001) and fcc(111), exhibit little or no contraction (<1%). The bcc(110) and fcc(001) faces are less smooth, while the fcc(110), bcc(001), and bcc(111) faces are considered "rough". On rough faces, a small but definite contraction of the topmost interlayer spacing is observed, ranging from ~4 to 15%. One possible explanation for this behavior invokes the notion of reduced surface coordination; i.e., presumably the reduced number of nearest neighbors in rough surfaces increases the bonding electron density in the fewer available bonds, thereby decreasing their length. This is consistent with the observation that adsorbed atoms tend to counter the bond-length contraction observed on rough surfaces (cf. below).

There is a separate and exceptional class of clean metal surfaces characterized by the spontaneous formation of a surface superlattice, observed primarily for the (100) and (110) surfaces of Ir, Pt, and Au. The structure of these so-called "reconstructed" surfaces has not been determined by LEED calculations, but for the reconstructed (100) surfaces it is believed to involve rearrangement of the outermost atomic layer into a quasi-hexagonal close-packed array, even though the underlying lattice has quadratic symmetry[125,127a,b] (Figure 13). This would indicate a tendency to maximize the number of nearest neighbors but to pucker the surface on an atomic scale.

Recently a less severe form of reconstruction has been observed in LEED studies of carefully cleaned and annealed surfaces of Mo(100) and W(100).[126a] The reconstruction, which is thought to involve periodic displacements of the surface atoms along (110) directions in the plane of the surface,[126b] can be induced by lowering the temperature below ~200 K and is completely reversible.

Atomic adsorption on clean metal surfaces generally takes place in the "expected" sites of high symmetry and coordination, i.e., sites that continue the metal lattice structure into the overlayer (Figure 14, Table XIII). No exception to this registry on an atomic scale is known for the (100) surfaces of either bcc or fcc materials, although in the Fe(100)p(1×1)–O[289] structure the oxygen atom may actually lie closer to the underlying Fe atom than the four nearest top-layer Fe (100) atoms (see Figure 11 for a representation of the bcc-(100) face). This deep penetration is accompanied by an outward relaxation of the top metal layer to a value ~7.5% greater than the bulk spacing. Similarly,

TABLE XIII. Surface Structures Formed by Chalcogen Adsorption on Nickel[a]

plane	coverage (monolayers)	oxygen	sulfur	selenium	tellurium
(100)	1/4	p(2×2)	p(2×2)	p(2×2)	p(2×2)
	1/2	c(2×2)	c(2×2)	c(2×2)	c(2×2)
	>1	NiO(100)			
(111)	1/4	p(2×2)	p(2×2)	p(2×2)	
	1/3	($\sqrt{3}$×$\sqrt{3}$)R30°	($\sqrt{3}$×$\sqrt{3}$)R30°	($\sqrt{3}$×$\sqrt{3}$)R30°	
	1/2		complex structures on heating		
	>1	NiO(111)			
(110)	1/3	p(3×1)			
	1/2	p(2×1)	c(2×2)	c(2×2)	
	2/3	p(3×1)	p(3×2)		
	10/9	p(9×4)			
	>1	NiO(100)			

[a] T. N. Rhodin and S. Adams, "Treatise on Solid State Chemistry", Vol. 6A, N. B. Hannay, Ed., Pergamon Press, New York, 1976.

TABLE XIV. Model Structures for Chalcogens on Ni(100)[a]

covalent radius	Demuth et al.		Van Hove and Tong	
	d	r	d	r
O 0.73	0.9	0.73	0.9	0.73
S 1.02	1.3	0.94	1.3	0.94
Se 1.16	1.45	1.04	1.53	1.10
Te 1.35	1.90	1.36	1.80	1.27

[a] Interlayer spacing, d and oxygen atom radius, r for c(2×2) structures. All models have oxygen atom in site of four-coordination on Ni(100) plane. Van Hove and Tong's analysis pertains to the p(2×2) structures. See footnote a, Table XIII.

(a) TOP VIEW

(110)   (001)   (111)

(b) SIDE VIEW

(110)   (001)   (111)
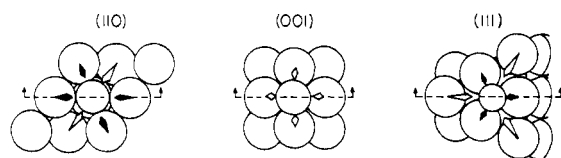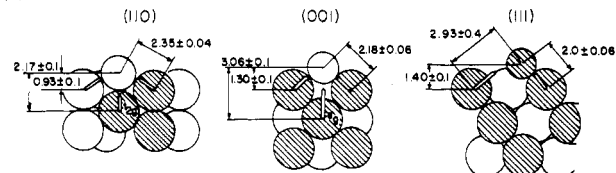
Figure 14. Schematic bonding configurations for sulfur atoms in the Ni(100)-c(2×2), Ni(001)-c(2×2), and Ni(111)-p(2×2) structures. The filled and empty arrows represent Ni e_g and t_{2g} orbitals, respectively (note: orbital notation refers to bulk phase configuration) (after Demuth, Jepsen, and Marcus,[127c,d]).

In the Ni(100)p(2×2)–C structure, the presence of carbon causes an expansion of the top metal interlayer spacing by ~8.5% with respect to the bulk. Indeed, it is a general observation that adsorption tends to elongate underlying metal–metal bonds, expecially in the case of surfaces which are "rough" on an atomic scale, i.e., bcc(111), bcc(100), and fcc(110).[73]

On close-packed atomic planes, such as fcc(111) or hcp(0001), two cases are known in which chemisorption does *not* occur on the "expected" locations: Ti(0001)p(1×1)–Cd, where the registry of the Cd atoms corresponds to a stacking fault in the normal ABAB ... stacking sequence [102] and Ti(0001)p(1×1)–N, where the small N atoms penetrate into the octahedral holes between the first and second substrate layers to form an "underlayer" of nitrogen atoms.[103] Only one example each of a chemisorbed structure is known for fcc(110) and bcc(110) surfaces, and in both cases the adsorbate atoms are *not* found in "expected" locations. In the Ni(110)p(2×1)–O structure, the oxygen atoms reside on the twofold bridge sites
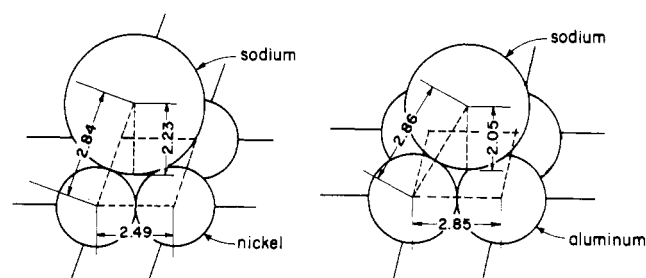
Figure 15. Hard-sphere models showing the local geometry and bond lengths for sodium on Ni(001) (left) and Al(100) (right) surfaces. The measured bond lengths are in good agreement with the single bond covalent radii for Ni (1.35 Å), and Na (1.49 Å). (After Hutchins, Rhodin, and Demuth,[127g] Andersson and Pendry,[127f] and Van Vechten and Phillips[127e]).

between two adjacent metal atoms.[104] Similarly, it is likely that the oxygen atoms in W(110)p(2×1)–O prefer the quasi-threefold site that maximizes the number of nearest metal neighbors, although the possibility that they choose the "expected" twofold site cannot be excluded.[105,106] These limited data raise the possibility that atomic registry of the bulk atoms by adatoms does not always occur on close-packed surfaces. In addition, bond elongation of metal atoms in the underlying surface also appears to be less likely in this case.

Among known structures it appears that the adsorption site in contrast to the known surface structures is largely independent of adatom density. This is illustrated (Table XIV) by results for chalcogen adsorption on Ni(100) in quarter-monolayer p(2×2) and half-monolayer c(2×2) structures, where the long-range order of the absorbate tends to be coverage-dependent.[127c] On the other hand, we also note that the adsorption sites themselves are only slightly influenced by the adatom valency. This is surprising when one considers such chemically different adatoms as N, O, N, Na, Si, Cl, and related elements in these groups.[290]

Another conclusion from the results obtained for adsorption of atoms is that the hard-sphere picture, an effective approximation in bulk crystallography, seems to be a useful concept in describing surface structures. Observed metal–adatom separations are close in magnitude to the sum of the covalent radii of the adatom and the metal atom (bulk) (see Figure 15, also Table XV) but the variances exceed the uncertainties in measured LEED bond lengths, which typically range from 0.04 to 0.09 Å.[73] Hence these structural data may provide a measure of bond-order effects which often induce bond-length variations in excess of 0.1 Å (Table XV). The variation of effective radius with coordination number for a variety of adsorbates on transition metal surfaces is indicated in Table XV containing data for chemisorbed oxygen, sulfur, selenium, and chlorine selected

TABLE XV. Effective Radii of Adsorbates[a]

adatom species	situation	coord. no.	bond dist, Å	effective radius of adatom, Å
Cl	Pauling radius			0.99
	Ag(001) + c(2×2)Cl	4	2.67 ± 0.06	1.23 ± 0.06
O	Ni(111) + p(2×2)O	3	1.88 ± 0.06	0.64 ± 0.06
	Pauling radius			0.66
	Ni(110) + p(2×1)O	2	1.92 ± 0.04	0.68 ± 0.04
	W(110) + p(2×1)O	3	2.08 ± 0.07	0.72 ± 0.07
	Ni(001) + c(2×2)O	4	1.98 ± 0.05	0.74 ± 0.05
	Ni(001) + p(2×2)O	4	1.98 ± 0.05	0.74 ± 0.05
	Fe(001) + p(1×1)O	1 + 4[b]	2.07 ± 0.06	0.84 ± 0.06
S	Ni(111) + p(2×2)S	3	2.02 ± 0.06	0.78 ± 0.06
	Ni(110) + c(2×2)S	1 + 4[c]	2.17 ± 0.10	0.93 ± 0.10
	Ni(001) + c(2×2)S	4	2.19 ± 0.06	0.95 ± 0.06
	Ni(001) + p(2×2)S	4	2.19 ± 0.06	0.95 ± 0.06
	Pauling radius			1.04
	Fe(001) + c(2×2)S	4	2.30 ± 0.06	1.06 ± 0.06
Se	Ni(001) + c(2×2)Se	4	2.28 ± 0.06	1.04 ± 0.06
	Ni(001) + p(2×2)Se	4	2.34 ± 0.07	1.10 ± 0.07
	Pauling radius			1.13
	Ag(001) + c(2×2)Se		2.80 ± 0.07	

[a] After Van Hove, ref 73. [b] 1 nearest neighbor + 4 next-nearest neighbors 0.02 Å farther away. [c] 1 nearest neighbor + 4 next-nearest neighbors 0.18 Å farther away.

from the work of Van Hove.[73] With few exceptions it is found that the bond lengths appear to increase with increasing coordination number, a familiar trend in coordination chemistry. Much more detailed and systematic studies are required before the apparent variations in adatom variations can be attributed to meaningful factors involving the bonding mechanism itself rather than to the limited accuracy of the LEED determinations.

A third conclusion is that charge transfer is small and shows in general a complicated behavior as a function of crystal face and coverage (Table XVI). The amount of charge transfer can be inferred from observed adsorption bond lengths, which in general do not exhibit strong ionic effects, and from direct work function measurements. One finds in this way that charge transfer per adatom does not exceed about a tenth of an electron charge even for alkali metal adsorbates.[73] Charge transfer shows a complicated dependence on coverage, especially in the case of the chalcogen series where in one case (Se on Ni) the work function change actually changes sign between quarter- and half-monolayer coverage. There is no obvious explanation on a step-free flat surface for such seemingly aberrant behavior but at least the generally small magnitude of the effect is consistent with other evidence that lateral adatom–adatom interactions are weak in comparison to the metal–adatom bond in full analogy to the cluster case.

2. Molecular Adsorption—LEED Studies

Molecular chemisorption has been structurally investigated by LEED intensity analysis for only two systems up to 1978: Ni(100)c(2×2)–CO[108] and acetylene on Pt(100).[109] In the case of carbon monoxide, the carbon atoms were located 1.8 Å directly above the top-layer nickel atoms and the oxygen atoms 0.95 Å above the plane of the carbon atoms. Because of the relative insensitivity of the analysis to lateral registry, with reference to the oxygen atom, a direct calculation of the C–O bond distance was precluded. A C–O bond distance equal to that in Ni(CO)₄ was assumed in the LEED study with the justifications that (i) high-resolution energy loss studies of CO chemisorbed on nickel showed vibrational losses associated with the adsorbed carbon monoxide that correlated well with Ni–C and C–O stretching vibrations of Ni(CO)₄, and (ii) the Ni–C distance was essentially identical with the value 1.84 (4) Å observed for Ni(CO)₄. This assumption then implied a registry difference

TABLE XVI. Charge Transfer $\Delta e/e$[a]

adsorbate	substrate	coverage	d, Å	$\Delta\phi$, eV	$\Delta e/e$, %
I	Ag(111)	0.33	2.25	0.5	2.6
N	Mo(001)	0.5	1.02	1.05	11[b]
Na	Al(001)	0.5	2.07	1.45	6.3
Na	Ni(001)	0.5	2.23	2.5	−7.7
O	Ni(111)	0.25	1.20	−0.7	−7.0
O	Ni(001)	0.25	0.90	0.22	3.3
O	Ni(001)	0.5	0.90	0.36	2.7
O	Ni(110)	0.5	1.46	0.46	3.1
O	W(110)	0.5	1.25	0.7	4.4
S	Ni(111)	0.25	1.40	1.0	3.4
S	Ni(001)	0.25	1.30	0.24	2.5
S	Ni(001)	0.5	1.30	0.38	2.0
Se	Ni(001)	0.25	1.55	0.08	0.7
Se	Ni(001)	0.5	1.45	−0.07	−0.3
Te	Ni(001)	0.25	1.80	0.29	−2.2
Te	Ni(001)	0.5	1.90	0.43	−1.5

[a] After Van Hove.[73] Implied charge transfers, $\Delta e/e$. Coverage is normalized to 1 for an overlayer that has one adatom per substrate unit cell: d is the overlayer spacing, i.e., the component of the bond length perpendicular to the surface. [b] This surface presents difficulties in the comparison of LEED theory and experiment.

between carbon and oxygen of ~0.65 Å or a rather large tilt, 34°, of the carbon monoxide with respect to the surface normal. Some tilt of the adsorbed ligand is not unexpected, but the magnitude of this tilt is much larger than those generally observed for mononuclear metal carbonyls.[291] However, the body of data indicates the orientation of chemisorbed CO is typically normal to the surface for the Ni(100) system.[110] This is not always the case for other related admolecules as indicated for chemisorbed NO on Ni(100) and Ir(111) where the adsorbed molecule may be bent as much as 30° away from the normal to the surface;[111,112] here, however, substantially bent M–NO bonds are not unexpected based on the established coordination chemistry of nitric oxide.

Acetylene on Pt(100) has been the subject of intensive study by Somorjai,[109] Ibach,[89] and by Demuth.[122] Experimental and calculational studies are continuing. Complementary studies of this system through high-resolution energy-loss spectroscopy suggest that the surface species may not have the elementary composition C_2H_2 but C_2H_4 (CH_3CH) due to hydrogen (a ubiquitous impurity in most ultrahigh-vacuum studies of hydrocarbon reactions) reaction with the chemisorbed C_2H_2 species. This illustrates the significant chemical complications that can arise in the studies of chemisorbed species derived from polyatomic molecules, especially hydrocarbons; the Auger analysis for the determination of surface composition is inapplicable to hydrogen —where facile scission of carbon–hydrogen and carbon–carbon bonds may occur in the chemisorption process. Further interpretational remarks on the structure of chemisorbed molecules on metals are premature in light of the available data.

3. Atomic and Molecular Adsorption—ARUPS

Angle-resolved photoemission can be used to investigate adsorption geometries and the electronic properties of chemical bonding at surfaces of both molecules and chemisorbed layers.[71a,b] It is complementary to LEED with regard to atomic structure although the analysis of the photoemission process is more complicated. The stage of development is correspondingly in a more preliminary state of interpretative application than for LEED. Information sensitive to the adsorption geometry results from the interference of contributions both from electron waves emitted directly from excited stages of adatom core levels and those emitted indirectly by repeated scattering of the photoemitted electrons through the surface layer. Theoretical results have been compared with experiments for ordered overlayers of c(2×2)S + c(2×2)O structures on Ni(001).[114] From

the dependence of emission intensity on polar angle of emission, plane of emission, photon emission, photon incidence, and polarization, conclusions can be made on the symmetry and strength of the various orbitals. That oxygen and sulfur systems have very different emission properties is of particular significance in this structural interpretation.

The coordination number of the adsorption sites and the vertical "d" spacing between the adsorbate–metal layer have been determined for the sulfur overlayer.[115] It was established that the sulfur atom sits at the fourfold site at an interlayer distance of 1.37 ± 0.6 Å, in agreement with the calculated LEED value. However, structural changes that preserve bond symmetries and directions such as interlayer spacings are less easily followed by angle-resolved photoemission studies than by LEED analysis. LEED analyses are sensitive to bond-length changes of less than 0.1 Å, whereas angle-resolved photoemission is not. On the other hand, the adsorption orientation of molecules on surfaces is generally more sensitive to angle-resolved photoemission especially in those cases in which adsorbed molecules with small differences in scattering cross sections are involved.

The site location as well as the orientation of the chemisorbed CO molecule on Ni(001) surfaces has also been studied in some detail by angle-resolved photoemission. Surface structural information has been obtained by dynamical analysis of the photoionization resonance curves and the polar angle electron emission plots.[115] These established that the CO molecule is located over a nickel atom with a coordination number of 1 and not in bridge-bonded sites with a coordination number of 2 or 4. The angle-resolved data were not, however, sufficiently sensitive to provide a value for the interlayer spacing in this case. These structural conclusions apply only to a saturated CO coverage. Since effects of lateral interactions are sensitive to adsorbate density, other coordination geometries may prevail at lower coverages. The effect of ligand surface density on orientation is a general one which is applicable in principle in a parallel manner to molecular metal clusters.

Angle-resolved photoemission can also be applied to the orientation determination of a molecule chemisorbed on a metal surface through the intensity dependence of a "shaped resonance" emission from a molecular orbital which does not participate itself in surface bonding but which presents a fixed and well-defined orientation of the molecule with reference to the electric field vector normal to the surface. This technique was initially used by Allyn and others[116] to determine that the CO molecule is chemisorbed on the Ni(001) and Ni(111) surfaces at saturated coverage and room temperature in an orientation normal to the surface. Similar results have been obtained for CO on Pt(111)[117] and for CO on Ir(111).[118] The same approach can be used to determine the orientation of a molecule that is not placed normal to the surface by using a photon excitation where the electric field vector is oriented parallel to the surface (e.g., s polarization). In this case, enhanced photoemission can only occur with a tilted orientation. Such is the case for NO on Ni(100)[111] and for NO on Ir(111).[112] Since ligand orientations in metal molecular clusters may depart from the surface normal of the cluster, similar variations from the orientation normal to the metal surface resulting from electronic bonding effects in chemisorbed systems is not unexpected.

4. Atomic and Molecular Adsorption—Electron Loss Spectroscopy

The vibrational modes of adsorbed gases on metals are a direct reflection of the orientation of the molecule on the surface, of its state of dissociation, and of its coordination geometry with reference to the underlying metal crystal face. Hence, vibrational spectra are inherently sensitive to structure in the localized region of the molecule–surface complex. As previously discussed, the high-resolution energy loss (EELS) measurements of very low-energy electrons reflected from metal surfaces can provide

vibrational information on well-defined chemisorbed surfaces.[72,89] This type of approach is particularly valid when the results are combined and interpreted in conjunction with other surface probes of electron structure and composition such as LEED, Auger, and photoemission. The EELS approach is finding increasing application to the surface structural characterization of a variety of adsorption systems involving both chemisorbed inorganic gases and hydrocarbons on metals and semiconductors. Since the effects of hydrogen atoms are not seen by most other surface techniques, EELS is especially important for studies of hydrocarbons chemisorbed on metals as discussed by Ibach.[89] Diagnostic applications for detection of specific molecular subunits can be achieved. For example, the CH-bending modes of CH_2 and CH_3 can be identified in electron loss spectroscopy because the frequencies are fairly independent of the remainder of the molecule and therefore likely to be approximately the same in various adsorption complexes.[89] A study of the vibrational character of a series of simple olefins on platinum in the temperature range 300–500 K indicated that the CH_3CH radical must be a relevant surface species for the catalytic hydrogenation of ethylene over platinum.[89] More definitive characterization of the bending and stretching modes of chemisorbed hydrocarbons on transition metal surfaces are now in progress. Information on the principal stretching and bending modes of chemisorbed hydrocarbon molecules obtained for vibrational spectroscopy of this kind is providing insight into the connection between molecular structure and the chemistry operational at surfaces.

A series of electron loss studies combined with LEED analysis have also demonstrated the influence of chemisorbed layers on the structure of chemical bonds of CO on clean and chemisorbed Ni(001).[92] Stretching vibrations of linearly bonded CO corresponding to the Ni–C and C–O bonds were observed for the Ni(001)c(2×2)CO structure to establish the coordination of the carbon atoms to the surface (Figure 38). Whereas a combination of both terminal and bridge-bonded CO molecules prevail on the clean surface, preadsorption of hydrogen causes the bridge-bonding to become dominant. Similarly, chemisorption on oxygenated nickel (Ni(001)p(2×2)O and Ni(001)c(2×2)O) also shows principally bridge-bonded CO molecules to be present.[92] Evidence for the existence of two different adsorption sites for CO on Pt(111) have also been obtained using double-beam infrared reflection spectroscopy[119] in agreement with earlier work[120] using electron loss spectroscopy and LEED structures.[121] Two stretching vibrations for Pt–C and C–O were observed at low coverages corresponding to a terminal adsorption structure with a coordination number of 1 for carbon. Two stretching vibrations observed at higher coverages corresponded to CO adsorption on a bridge position with a carbon coordination number of 2. Combination of LEED and EELS studies of CO adsorption on the (100) faces of nickel and platinum as a function of surface coverage suggests that the adsorption tends to occur in general on top for low coverages ($\theta = 0.3$) and becomes a mixture of about 1:1 of terminal and bridge-bonded molecules with a coordination number of 2, at higher coverages ($\theta = 0.5$). Preadsorption of oxygen or hydrogen on nickel appears to promote the latter type of binding at lower coverages of CO. Dependence of vibrational modes and surface lattice structure on surface coverage is essential to understanding the contribution of lateral interactions of chemisorbed ligands on metals. Similar combinations of vibrational studies with angle-resolved photoemission for olefin adsorption on transition metals such as nickel and platinum are now in progress. It is, however, premature to comment further at this time on the correlation of these data in providing essential details connecting electronic and surface coordination of chemisorbed molecules.

5. Electron Spectroscopy Approach to Metal Surfaces

Interpretations of chemical bonding clearly can be achieved through the application of spectroscopic methods (particularly

LEED, UPS-XPS, and EELS) to define the surface crystallography of chemisorbed atoms and molecules on extended metal surfaces. A complete definition of the surface structure eventually will be obtained from data derived from a combination of two or more of these techniques. They all involve indirect theoretical analysis which provides insight into selected aspects of the surface structure such as bond angles, bond distances, orbital symmetries, etc. Interpretative theory is all in a rather preliminary state of development particularly with applications to the analysis of the precise surface configuration and location of chemisorbed molecules. Furthermore, the very nature of the measurements limits their application primarily to the solid–vacuum interface whereas many interesting systems are characterized by gases at higher pressures and by liquids. Nevertheless, the most important underlying feature is that these methods have the potential for providing unique information on bonding and charge transfer in terms of specific atomic configurations. These basic concepts have a broad application to the understanding of the nature of chemical bonding in general and of the similarities and differences in bonding in metal clusters and chemisorbed metals in particular. These preliminary considerations of the surface crystallography of adsorption on extended metal surfaces compared to the stereochemistry of metal clusters show that much can be learned through appropriate comparisons in this rapidly growing field. The importance of this analogy is based on the fact that the principles of chemical bonding involving localized groupings of atoms are basically independent, to a first approximation, of the more generalized configurational effects of the larger matrix in which the local grouping may be included.

E. Molecular Metal Clusters—Structural Details and Generalizations

1. Classes of Molecular Metal Clusters

There are only three classes of molecular clusters in which the ligands are all the same—the formal analogs of traditionally studied chemisorbed states derived from a single type of molecule and a pure metal surface. These are the halide cluster class, the carbonyl cluster class 20, and the presently diminutive isocyanide cluster class; finally, there is the nonligand class[21] of naked metal cluster ions, e.g., Pb_9^{4-} and Bi_9^{5+}. All three of the binary classes are discussed in separate sections below. For the remaining ligands such as hydride and alkyl that are of substantial scientific and even technological importance, there is no simple binary class of isolable complexes. These ligand cluster classes are necessarily referenced to mixed ligand cluster complexes. Strict comparison of these ligands in the two regimes will require study of mixed ligand chemisorption states—a type of surface study that is feasible and is now being attempted by some investigators.

2. Halide Metal Clusters

This potentially large class of binary clusters is dominated by three major subclasses, the triangular $M_3X_{12}^{3-}$, octahedral $M_6X_{14}^{2-}$, and octahedral $M_6X_{12}^{2+}$ structures. Halide binding in these clusters encompasses two-center terminal, three-center edge-bridging and four-center face-bridging interactions. For the M_3 triangular structures, the rhenium halides comprise the paradigmatic set.[128] The formal rhenium–rhenium bond order is 2 and the X-ray diffraction studies consistently show short Re–Re bond distances of 2.47 to 2.49 Å as compared with an Re–Re distance of 2.74 Å for bulk rhenium metal.[128] The $Re_3Cl_{12}^{3-}$ structure[129] has three types of chloride ligands: axial, equatorial, and bridging, 1. In every Re_3 complex, the bridging chloride ligands are substantially longer, ~2.5 Å, than the terminal ligands, 2.36–2.4 Å, as in $Re_3Cl_{12}^{3-}$, $Re_3Cl_{11}^{2-}$, $Re_3Cl_{10}^{-}$, and Re_3Cl_9.[129,130] The Re–Cl–Re angle for the bridging inter-

1
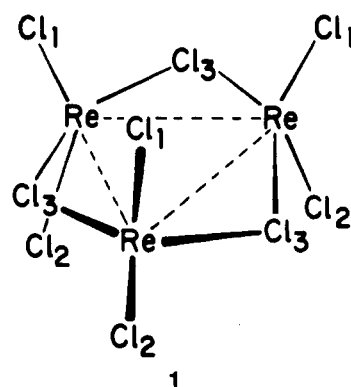
action is about 61°. In 2 the basic repeating unit for crystalline Re_3Cl_{12} is presented.

2
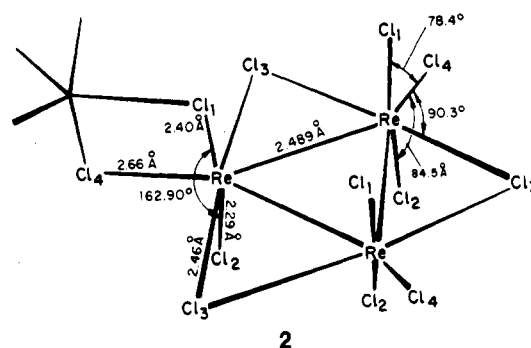
In the classic $Mo_6X_{14}^{2-}$ structure, the molybdenum atoms form the vertices of an octahedron. The Mo–Mo distances in $Mo_6Cl_{14}^{2-}$ are ~2.65 Å, a value lower than the bulk molybdenum metal separation of 2.725 Å.[131] Eight of the halide ligands bridge the octahedral faces and the other six are terminally bound, one to each molybdenum atom, 3. In $(Mo_6Cl_{12})Cl_2$, the Mo–Mo dis-

3
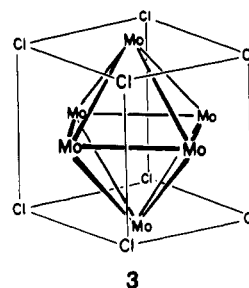
tances are 2.61 Å.[132] A precisely determined structure,[133] $Mo_6Br_{12}\cdot2H_2O$, has a similar structure with Mo–Mo separations of 2.64 and 2.63 Å. Again, the terminal MoBr separations are shorter than the bridging MoBr separations, but only slightly, ~2.59 Å as compared to 2.61 Å. The Br–Mo–Br angles for the bridging ligands are about 61°; the Mo_3Br tetrahedra have near regular tetrahedral angles. There is also an analogous octahedral Nb_6I_8 cluster unit in Nb_6I_{11}. The average niobium–niobium distance is 2.85 Å, virtually identical with the separation in bulk niobium metal and the mean Nb–I distance for the triply bridging (Nb_3I) interactions is 2.93 Å.[134] Despite the disparate I and Nb radii, the Nb_3I tetrahedra formed by the triply bridging iodine atoms again have near regular tetrahedral angles.

The M_6X_{12} octahedral structures are rarely O_h in symmetry; typically there is a tetragonal elongation. In the niobium and tantalum clusters the metal–metal separations are about 2.9 Å, a value close to the bulk metal values of 2.86 Å. The 12 halide atoms bridge the octahedral edges, 4, and the M–X–M angles are about 69°.[135] For the $Ta_6Cl_{12}(OH_2)_6^{2+}$ clusters, the bridging Ta–Cl distances are about 2.58 Å; the corresponding iodide distances are about 2.7 to 2.8 Å. Analogous scandium and zirconium M_6X_{12} clusters have also been reported.[136a]
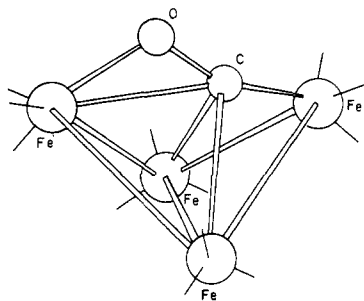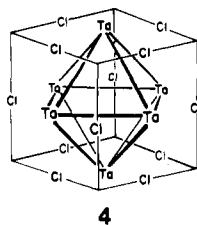
Figure 16. Depiction of the skeletal structure of $[Fe_4(CO)_{13}H]^-$ with $\bigcirc$ = Fe, O = C and O. Other CO ligands are shown as solid lines emanating from Fe atoms.

4

If the analogy between clusters and surfaces is valid for halogen ligands, we would expect that at least for chlorine the M-Cl-M angles for M_2Cl and M_3Cl bridging positions will be 60-70° and the M-Cl separations will be ~2.5 to 2.6 Å for second- or third-row transition metal clusters. Angles should decrease slightly and M-X distances increase slightly (0.1 to 0.2 Å) in passing from Cl to Br to I. Generally, the M-X distance for a terminal two-center site should not be substantially (<0.05 Å) shorter than for a bridging three-center site. For face-bridging halides in clusters, the M_3X tetrahedra will have near regular tetrahedral angles.

3. Carbonyl Clusters

The largest known class of binary molecular clusters is the carbonyl cluster class.[20,21] Carbonyl clusters with terminal and with edge- or face-briding carbonyls are well established; in fact, there is a number of clusters in which all three types of ligand interactions are present. The range of cluster size is quite large—from the 3-atom set to at least 19 (a 30-atom cluster has been tentatively reported but is not as yet well-defined).

The three common forms of carbonyl bonding in metal carbonyls [(a) two-center or terminal MCO, (b) three-center or edge-bridging M_2CO, and (c) four-center or triangular face-bridging, M_3CO] are all implicated for the CO chemisorbed state on metal surfaces. Multiple CO ligand binding at a single metal site is the rule for molecular metal clusters—only one cluster has less than one CO per metal atom; all others have more than one. In contrast, multiple ligand bonding at a single metal site is the exception for the chemisorbed state on metal surfaces, at least for flat metal surfaces. Clusters that have carbonyl ligands with greater than four-center interactions are unknown to this point in time, but five- and six-center interactions are established or feasible for chemisorbed carbon monoxide on a metal surface. Multiple ligand binding on metal surfaces may occur for "protruding" metal atoms on irregular metal surfaces, e.g., the metal atoms at corner, step, kink, or atop a terrace position. One of the few apparent examples of multiple ligand bonding to a single atom in a crystal surface has been reported for two and three CO ligands on a single rhodium metal atom in the close-packed Rh(111) surface of a small rhodium metal cluster in a planar configuration on a metal oxide support.[124]

While terminal and edge-bridging CO ligands are found in mononuclear and binuclear complexes, respectively, the face-bridging mode is geometrically unique to metal cluster complexes and is only rarely found in the smallest, the trinuclear

clusters. Bridging CO ligands are commonly observed for the first- and second-row transition metal cluster complexes but are only seen infrequently among neutral third-row metal cluster complexes. Among those neutral cluster complexes consisting only of metal atoms and CO ligands, no bridging carbonyl groups have been observed for third-row metal clusters; only as the electron density on the metal atoms is increased through substitution of CO by better donor ligands, e.g., phosphines, or by development of formal negative charge, are bridging CO interactions generated. This may represent a possible breakdown in the metal cluster–metal surface analogy since it has generally been observed that ligands bond to metal surfaces in a manner such as to obtain maximum coordination to the surface metal atoms. However, the relative degree of coordination saturation in the metal cluster complex vs. the extent of ligand coverage on the metal surface must also be considered when making such comparisons. In the case of the CO chemisorbed state on metals, there is the interesting effect of systematic and well-defined variations in the degree of surface roughness on an atomistic scale. Bonding is generally strongest on the open, less dense crystal faces where the metal coordination number is lowest. An important factor contributing to the stronger bonding is the greater degree of unsaturation characteristic of the atomically less dense faces. In addition, the free electrons that are so characteristic of a metal surface play an important role in maintaining distinctions in bonding among the different crystal faces.

A unique mode of CO bonding which cannot be classified into the three groups described above is found in the $[Fe_4(CO)_{13}H]^-$ anion[136b] (Figure 16). One of the carbon monoxide ligands is coordinated to all four iron atoms which are arrayed in a butterfly configuration. Two distinct Fe-C distances are observed: Fe-C = 1.81 (2) and Fe-C = 2.10-2.17 (2) Å. Another intriguing aspect of this cluster complex is the bonding of the oxygen atom of this CO ligand to one of the iron atoms (Fe-O = 2.00 Å). The C-O distance of this ligand, behaving as a four-electron donor, is also exceptionally long, 1.26 (3) Å. This complex is an excellent model for the coordination and activation of carbon monoxide on a metal surface, particularly at a step or kink site.

The range of average metal–metal distances found in metal carbonyl cluster complexes is illustrated in Table XVII, and, for comparison, metal–metal distances in bulk metals, adjusted for coordination 12, are also included. Not surprisingly, the cluster complexes show slightly longer metal–metal separations largely due to the relatively large number of ligands bound to each metal cluster atom. Quantitatively, several generalizations regarding carbon monoxide bonding to metal clusters are possible. The metal–metal distance is generally found to be from 0.03 to 0.10 Å shorter when bridged by a carbonyl ligand than when bridge bonding is absent. For a metal surface, the metal–metal bond distances, in principle, could decrease slightly with CO chemisorption at bridging sites, but, in fact, there is no evidence of surface contraction in the chemisorption process. It is expected that the favored adsorption sites leading to good geometric registry and spatial matching depend upon the matching of the periodic potential of the adsorbing molecule with the metal surface crystallography. For clusters, the difference between carbonyl bridged and nonbridged metal–metal distances appears to diminish as the number of metal atoms in the cluster complex increases. Indeed, for some of the larger cluster complexes, factors other than the presence or absence of a bridging carbonyl ligand apparently dictate metal–metal distances. In $(Rh_{13}(CO)_{24}H_3)^{2-}$, the average unbridged metal–metal distance is 2.82 Å compared with 2.79 Å for a bridged separation, yet several bridged values are 2.82 Å and several unbridged values, $\leq$2.79 Å.[22] Generally, the molecular clusters become more metal-like as the cluster size increases, as would be expected on an intuitive basis for larger arrays of electrons.

TABLE XVII. Metal–Metal Distances in Clusters

range of av M–M distance in cluster, Å	M	M–M distances (Å) in bulk metals from metallic radii for 12-coordinate metals[a]
2.58–2.71	Fe	2.52
2.78–2.90	Ru	2.68
2.75–2.91	Os	2.70
2.49–2.52	Co	2.50
2.73–2.90	Rh	2.68
2.68–2.98	Ir	2.72
2.34–2.77	Ni	2.50
2.66–2.75	Pt	2.78
2.99–3.18	Re	2.74

[a] A. F. Wells, "Structural Inorganic Chemistry", 3rd ed, Oxford University Press, London, 1962, p 84.

TABLE XVIII. Metal–Carbon Distances in Cluster Carbonyl Complexes

M	terminal, Å	bridge, Å
Fe	1.70–1.75	1.82–2.28
Ru	1.82–2.05	1.94–2.30
Os	1.86–1.96	
Co	1.70–1.87	1.90–2.06
Rh	1.70–1.96	1.97–2.20
Ir	1.85	2.10
Ni	1.75–1.89	1.82–1.91
Pt	1.77–1.80	2.00–2.03
Mn	1.79–1.85	
Re	1.84–1.91	

TABLE XIX. Predicted M–C Distances in Cluster Carbonyl Complexes

metal	dist, Å	metal	dist, Å
Fe	2.03	Co	2.04
Ru	2.11	Rh	2.11
Os	2.12	Ir	2.13
Ni	2.04	Mn	2.14
Pt	2.16	Re	2.14

For the carbonyl ligands, the metal–carbon bond distances vary with the mode of the carbonyl bonding to the cluster core. Symmetrically bridging carbonyls have metal–carbon distances 0.1–0.2 Å longer than the corresponding terminal carbonyl bond distances. The difference is even greater for face-bridging carbonyl metal–carbon distances which are 0.25–0.35 Å longer than the terminal carbonyl bond distances. Table XVIII summarizes the range of metal–carbon distances observed in cluster complexes.

With respect to CO chemisorbed on metal surfaces, few metal–carbon distances are known and even the specific type of CO bonding, e.g., terminal or bridging, has rarely been precisely determined. However, from studies of strongly chemisorbed atomic adsorbates, e.g., O, S, Se, Te, and Na on various Ni surfaces, Se, Cl and I on Ag, Na on Al, N on Mo, and O on W, several generalizations have appeared as discussed in the previous section (see Tables XIV and XV). The chemisorbed atoms seek maximum coordination to the metal surface, i.e., bridging modes, and the adsorbate–metal distance is closely approximated by the sum of the metallic radius[137,138] and the single bond covalent radius[138] of the adsorbate. Extrapolating such a predictive scheme to metal–carbon distances in carbonyl clusters affords the values listed in Table XIX. Comparison of Tables XVIII and XIX shows that the predicted values fall within the range of metal–carbon distances in metal–carbon bridge bonds in cluster complexes. The essential point is that the preference of adsorbates for maximum coordination to the metal surface can only be mimicked in the realm of coordination chemistry by cluster complexes.

The carbon–oxygen bond distances reported in cluster carbonyl complexes vary considerably, and their accuracy is highly sensitive to the quality of the diffraction data. Thus, a separation of 1.15 Å may (appear to) represent a terminal carbon–oxygen distance in one cluster and a face-bridging distance in another complex. Basically, the carbon–oxygen bond distance range is 1.10–1.20 Å. Despite variances from one cluster to another, a trend of carbon–oxygen bond length as a function of carbonyl bonding mode within a given complex is apparent. Thus, bond-order reduction is observed as the type of metal carbon bonding changes from terminal to edge-bridging to face-bridging. In general, the carbon–oxygen bond distance is about 0.02 Å longer for an edge-bridging carbonyl ligand and 0.04 Å longer for a face-bridging carbonyl ligand than the value found for a terminal carbonyl ligand in a specific complex. The carbon–oxygen distance of chemisorbed CO on transition metal surfaces is assumed to increase several hundredths of an angstrom over the CO gas-phase distance. This has been attributed to a weakening of the π orbital centered on carbon and oxygen caused by the backbonding of electrons from the metal to the 2π orbital. Trends in photoemission data[88a–e] show a correlation between the displacement of the 1π orbital relative to the 4σ orbital and the lengthening of the C–O bond on chemisorption. An energy shift in the photoemission spectra as much as 0.5 eV occurs on chemisorption corresponding to a theoretical displacement of 0.05 Å.

The spatial distribution of carbonyl ligands about metal cluster cores depend on several factors. With respect to M–C–O angles, the terminal M–C–O angle is generally greater than 170°. Crystal packing and nearest-neighbor considerations are the dominant factors causing deviation from linearity. The M–C–O angle for symmetrically edge-bridging carbonyl groups is about 134–142°, with the M–C–M angle ranging between 71 and 90° and the M–C–O angle for symmetrically face-bridging carbonyl ligands ranging between 132 and 134°. For face-bridging carbonyls, the M_3C tetrahedra have near regular tetrahedral angles.

Two factors apparently influence the distribution of the carbonyl ligands between terminal and bridging modes. These are the dissipation of electronic charge and the metal atom coordination number. The former is the dominant influence. Bridging carbonyl ligands, particularly face-bridging, are better π acids than terminally bonded carbonyl ligands and are effective in removing electron density from the cluster core. Thus, as negative charge increase on the metal framework, the number of bridging carbonyl ligands increases. These trends suggest some rather important metal surface studies: partial surface coverage with strong acceptor ligands may shift favored CO chemisorption sites to terminal, or atop a single metal surface atom. For hydrogen the effect has been observed in the preadsorption of hydrogen on Ni(001) which then favors bridge-bonding over terminal bonding of CO.[92]

Metal atom coordination number is a second consideration. For a specific metal atom in a cluster complex, the number of ligands and their mode of bonding will be influenced by the relative size of the solid angle described by that metal atom and its nearest metal atom neighbors. When this solid angle is small, the metal ligand coordination number can be expected to be higher than when the angle is large. Thus, tetranuclear clusters generally show ligand coordination numbers of 4, while as cluster size grows, this coordination progressively diminishes to 3 or 2. This is entirely reasonable for as cluster size increases, the metal core will begin to resemble a metal surface. the solid angle will increase, and the ligand to metal ratio will approach 1 or even $1/2$, i.e., monolayer coverage. Furthermore, small angles permit, but do not require, a higher relative percent of terminally bound carbonyl ligands than observed for larger clusters. Thus, in a large cluster such as $[Rh_{13}(CO)_{24}H_3]^{2-}$, one-half of the carbonyl ligands are observed in bridge bonding,[22] while in $Rh_4(CO)_{12}$,

TABLE XX. Number of Ligand Types in Carbonyl Clusters

cluster	terminal	edge-bridging	face-bridging	ref
$Co_6(CO)_{16}$	12		4	142
$[Co_6(CO)_{15}]^{2-}$	9	3	3	143
$[Co_6(CO)_{14}]^{4-}$	6		8	144
$Rh_4(CO)_{12}$	9	3		139
$[Rh_4(CO)_{11}]^{2-}$	4	7		140
$[Rh_7(CO)_{16}I]^{2-}$	10	2	4	145
$[Rh_7(CO)_{16}]^{3-}$	7	6	3	146
$Rh_6(CO)_{16}$	12		4	147
$[Rh_6(CO)_{15}I]^{-}$	11		4	148

only $^3/_{12}$ of the ligands are bridge bonded.[139] However, small clusters as stated above can also possess a high percentage of bridge-bonded ligands if electron density on the metal core is high as exemplified by $[Rh_4(CO)_{11}]^{2-}$ in which $^7/_{11}$ of the carbonyl groups are edge bonded.[140] The effect of increased bridge bonding with increased cluster size is not as pronounced for clusters based on third-row transition metals; e.g., the neutral binary osmium carbonyl clusters Os_3 through Os_8 have no carbonyl bridge bonds.[141] One final generalization relating to metal atom coordination is based on the ratio of carbonyl ligands to metal atoms. With the metal cluster size constant, the number of bridging ligands increases as the total number of ligands decreases, a rather expected result since the metal atoms can accordingly retain the same level of coordination number.

The effects of electronic charge dissipation and metal atom coordination number are illustrated in Table XX for various cluster series. The last pair presents an interesting case in which a terminal CO ligand is formally replaced by I^-. In terms of charge dissipation, the increased charge on $[Rh_6(CO)_{15}I]^-$ must be balanced by the greater electronegativity of iodine, and thus no ligand rearrangement is observed. In the series cited above, the key point is that the order of ligand-site effectiveness in charge removal from the metal sites is face-bridging > edge-bridging > terminal.

The nitrosyl ligand also exhibits bonding types similar to that shown by carbon monoxide. Only a few cluster complexes containing nitrosyl ligands have been structurally characterized; however, both edge- and face-bridging modes have been established. Indeed, $(C_5H_5)_3Mn_3(NO)_4$ contains three edge-bridging NO groups and one face-bridging nitrosyl ligand.[149] A high degree of disorder in the crystal unfortunately prevented accurate determination of molecular dimensions. Quantitative data are available for $Ru_3(CO)_{10}(NO)_2$, in which a Ru–Ru vector is symmetrically bridged by two NO groups.[150] The average Ru–NO distance is 2.03 Å and the N–O distance is 1.22 Å. Both distances are somewhat longer than that typically observed for terminal nitrosyl ligands, an observation analogous to the pattern seen in C–O distances for carbonyl ligands. The Ru–Ru distance bridged by the two NO groups is rather large, 3.15 Å, while the other Ru–Ru distances in the complex are 2.85 and 2.87 Å comparable to that seen in $Ru_3(CO)_{12}$ (2.85 Å).

4. Binary Isocyanide Clusters

Isocyanides, RNC, are electronically similar to carbon monoxide as ligands in transition metal complexes. The strength of the two-center metal–isocyanide bond appears to be generally somewhat greater than the analogous carbonyl bond; this may largely reflect the better σ donor properties of the isocyanide ligand.

Potentially, the binary class of metal isocyanide clusters is very large; however, the class presently numbers only several structurally defined clusters, all derived from nickel group metals. Platinum and palladium form zerovalent trinuclear clusters of the form $[M(CNR)_2]_3$.[152,153] In the platinum cluster, there are terminal and three-center, edge-bridging isocyanides with a near
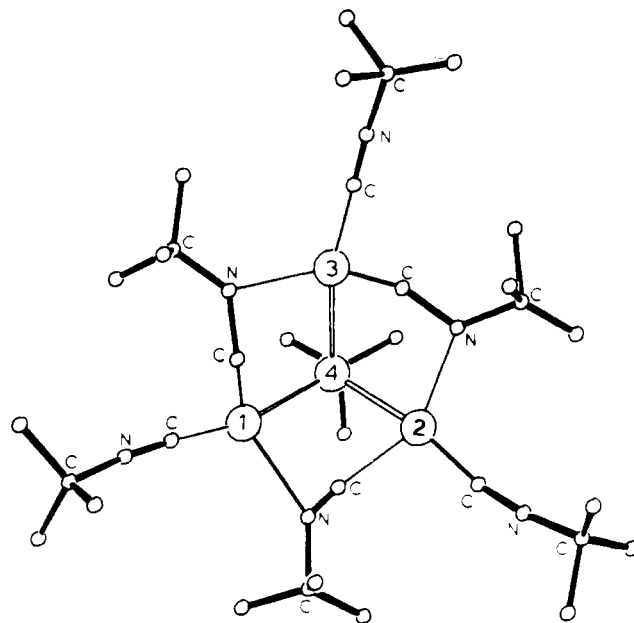

Figure 17. A representation of the structure of $Ni_4[CNC(CH_3)_3]_7$ looking down the threefold axis of the compressed tetrahedron. The unique apical nickel atoms is labeled 4, and the basal nickel atoms are numbered 1 through 3. Hydrogen atoms of the *tert*-butyl groups are not depicted. The three isocyanide ligands that bridge the basal edges of the tetrahedron are effectively four-electron donors whereas the four terminally bound isocyanide ligands are two-electron donors. Because there was a disorder in the crystal used in the crystallographic study, a precise characterization of the unique bridging isocyanide ligand atom positions was not feasible.[51] The apical to basal nickel–nickel distances are very short, ~2.34 Å.

linear (176°) CNC and a bent CNC (133°) array for the terminal and bridging isocyanides, respectively. In the platinum derivative, the average platinum–platinum separation is 2.63 Å as compared to 2.746 Å in bulk platinum metal.[153] The metal–carbon distances are 1.90 and 2.08 Å for the terminal and bridging isocyanides, respectively, and the metal–carbon–metal angle for the bridging isocyanides is 77°.[153] Bond order reduction in the isocyanide ligand is evident in going from a terminal to a bridging interaction; the average carbon–nitrogen bond distances are 1.15 and 1.21 Å, respectively. Oxidized palladium isocyanide clusters of linear form are $(CH_3NC)_8Pd_3^{2+}$ and $(CH_3NC)_6$-$[(C_6H_5)_3P]_2Pd_3^{2+}$; all isocyanides are two-center terminal ligands with approximately 1.99 Å Pd–C bond distances.[154]

Nickel forms a series of clusters with isocyanides.[9,152] In one set, the stoichiometry is $Ni_4(CNR)_7$ where R is a bulky substituent like *tert*-butyl or cyclohexyl. With isopropyl isocyanide, the cluster has the stoichiometry $Ni_2(CNR)_3$ but the structure is not established.[9] Cluster molecularity is neither established for the isopropyl derivative nor for the essentially insoluble methyl and benzyl isocyanide nickel clusters. In $Ni_4[CNC(CH_3)_3]_7$, the Ni_4 core is a flattened tetrahedron (Figure 17). Terminally bonded to each nickel atom is one isocyanide ligand and then an isocyanide molecule bridges the basal edges with the carbon and the nitrogen atoms within bonding distance of the basal and apical nickel atoms; the NiC, NiN, and CN distances for these unique bridging isocyanides (rehybridized so that the ligand is effectively a four-electron donor) are 1.64, 2.24, and 1.23 Å, respectively. For terminal isocyanides, the NiC and CN distances are 1.81 Å (2.15 Å apical) and 1.17 Å, respectively.[152] Thus, there is again some C–N bond order reduction in passing from a terminal to a multicenter bridging bond.

For metal surfaces, there is evidence that isocyanides interact in a multicenter fashion, including the carbon and nitrogen atoms, with the surface metal atoms.[155] On a nickel(111) surface, methyl isocyanide is irreversibly chemisorbed and is bound much more strongly than either carbon monoxide or the isomeric

TABLE XXI. Metal Hydride Parameters

complex	method[a]	mode[b]	M–H, Å	∠M–H–M, deg	dihedral M₃–M₂H, deg
HFe₃(CO)₉(S-i-C₃H₇)[c]	X	e	1.81 (13)	96	60
HFeCo₃(CO)₉[P(OCH₃)₃]₃[d,e]	X	f	1.63 (15)		
	N	f	1.734 (4)		
H₄Co₄(C₅H₅)₄[f]	X	f	1.67 (7)		
H₃Ni₄(C₅H₅)₄[e]	N	f	1.691 (8)		
H₄Re₄(CO)₁₂[g]	X	f	1.77 (3)		
H₃Mn₃(CO)₁₂[h]	X	e	1.72 (3)	131	
HRu₃(CO)₉(C₆H₉)[i]	X	e	1.68 av	125	0
HRu₃(CO)₁₀[C=N(CH₃)₂][j]	X	e	1.85 (3)	98	63
HRu₃(CO)₉[C≡C(t-C₄H₉)][k]	N	e	1.789 (5)	102.3	115
			1.796 (5)		
H₃Ru₃(CO)₉(CCH₃)[l]	X	e	1.72 (7)	103.3	
HOs₃(CO)₁₀[CHCH₂P(CH₃)₂(C₆H₅)][m]	X	e	1.88 av	97	110
H₂Os₃(CO)₁₀P(C₆H₅)₃[n]	X	t	1.52 (7)		
		e	1.74 (6)	107.5	
			2.00 (6)		
H₄Ru₄(CO)₁₀[(C₆H₅)₂PCH₂CH₂P(C₆H₅)₂][o]	X	e	1.64–1.81	110–120	

[a] X = X-ray diffraction, N = neutron diffraction. [b] t = terminal, e = edge, f = face. [c] R. Bau, B. Don, R. Greatrex, R. J. Haines, R. A. Love, and R. D. Wilson, *Inorg. Chem.*, **14**, 3021 (1975). [d] B. T. Huie, C. B. Knobler, and H. D. Kaesz, *J. Chem. Soc., Chem. Commun.*, 684 (1975). [e] T. F. Koetzle, R. K. McMullan, R. Bau, D. W. Hart, R. G. Teller, D. L. Tipton, and R. D. Wilson, Report 1977, Brookhaven National Laboratory, BNL 22982. From *Chem. Abstr.*, **88**, 129333g (1978). [f] G. Huttner and H. Lorenz, *Chem. Ber.*, **108**, 973 (1975). [g] R. D. Wilson and R. Bau, *J. Am. Chem. Soc.*, **98**, 4687 (1976). [h] S. W. Kirtley, J. P. Olsen, and R. Bau, *ibid.*, **95**, 4532 (1973). [i] G. Gervasio, D. Osella, and M. Valle, *Inorg. Chem.*, **15**, 1221 (1976). [j] M. R. Churchill, B. G. DeBoer, and F. J. Rotella, *ibid.*, **15**, 1843 (1976). [k] M. Catti, G. Gervasio, and S. A. Mason, *J. Chem. Soc., Dalton Trans.*, 2260 (1977). [l] G. M. Sheldrick and J. P. Yesinowski, *ibid.*, 873 (1975). [m] M. R. Churchill and B. G. DeBoer, *Inorg. Chem.*, **16**, 114 (1977). [n] M. R. Churchill and B. G. DeBoer, *ibid.*, **16**, 2397 (1977). [o] J. R. Shapley, S. I. Richter, M. R. Churchill, and R. A. Lashewycz, *J. Am. Chem. Soc.*, **99**, 7384 (1977).

acetonitrile, CH₃CN, both of which can be thermally desorbed.[155]

5. Sulfur Clusters

Strictly interpreted there is no binary metal sulfur cluster class. However, as noted in the Introduction there is a large class of M₄S₄ cubane clusters in which sulfur atoms cap all the faces of an M₄ tetrahedron and in which the terminal metal ligands range from RS to C₅H₅ radicals. The cubane M₄S₄ framework formally has metal–metal bonds of bond order 1 when the framework electron count (Table V) is 60 as in (ON)₄-Fe₄S₄,[156] (ON)₄Fe₄S₂(NR)₂,[156] and (NC)₄Re₄S₄⁴⁻.[157] In these three molecular species, the two iron–iron distance sets[156] and the rhenium–rhenium distances,[157] respectively, are 2.634, 2.731, and 2.76 Å as compared with the bulk iron and rhenium distances of 2.482 and 2.741 Å, respectively. The metal–sulfur distances are 2.22 Å, (ON)₄Fe₄S₄; 2.22 Å, (ON)₄Fe₄S₂(NR)₂; and 2.34 Å, (NC)₄Re₄S₄⁴⁻. Metal sulfur tetrahedra, the M₃S units, have angles that depart significantly from regular tetrahedral values; the M–S–M angles for the above three complexes are 73.4, 71.6, and 55°, respectively. A selenium cubane cluster, (NC)₄Re₄Se₄⁴⁻, has M–Se–M angles of 45°.[157]

These sulfur clusters are to be compared with the atomic sulfur chemisorption state on low index metal surfaces of Ni(110), Ni (100), and Ni(111) where the nickel–sulfur distances of 2.35 ± 0.04, 2.18 ± 0.06, and 2.00 ± 0.05 Å, respectively, decrease as the atomic density, ρ(hkl), of the metal surface increases, e.g., ρ(111) > ρ(100) > ρ(110). The tighter the atomic packing on the metal surface, the shorter the sulfur–nickel bond. Note, however, that the coordination of the sulfur atom is 4 for the Ni(100)c(2×2)S surface compared to three for the Ni(111)-p(2×2)S surface. The total binding energy for sulfur on the former surface is thus greater than the latter despite the fact that the Ni–S distances are slightly longer in the (100) surface.

6. The Hydride Ligand in Clusters

Hydrogen is another ligand of considerable interest since it, like carbon monoxide, is intimately associated with Fischer–Tropsch processes. Terminal, edge-bridging, and face-bridging

hydride ligands have been definitively established by X-ray and neutron diffraction studies for cluster complexes. Hydrogen adsorption on transition metals has been widely studied because it represents, in principle, the simplest model of an adsorbate. It is, in addition, involved as a primary reactant in the important processes of Fischer–Tropsch, ammonia, and methane synthesis. The occurrence of both terminal and bridge bonding has been established on single-crystal surfaces. Transitions from the former to the latter states have been observed to be induced by the presence of other adsorbates such as oxygen although the mechanism of this interaction is not understood. The very small size of the adsorbate when ionization occurs makes particularly difficult the identification of the specific adsorption site for the extremely small hydrogen atom. For those cluster complexes for which hydrogen positions have been determined, terminally bound hydrogen is the exception and the edge-bridging interaction is the rule. There are only two cluster hydrides—for which the hydride position has been defined—where there is a terminal hydride ligand. In H₂Os₃(CO)₁₀P(C₆H₅)₃, one of the hydride ligands is terminal and the other is symmetric edge-bridging.[158] The terminal hydrogen distance is 1.52 Å, substantially shorter than the sum (1.67 Å) of the metallic radius and the covalent hydrogen radius; however, M–H distances are often underestimated in the X-ray diffraction analyses. Hydrogen atom positions in H₂Ir₄(CO)₁₀²⁻ have not been defined, but the positions of the carbonyl ligands suggest that the two hydride ligand atoms occupy terminal positions in this tetrahedral hydride cluster.[159]

Four examples of face-bridging hydrides in metal clusters have now been established. These four clusters are H₄Re₄(CO)₁₂, which has all terminal CO ligands and near-T_d symmetry,[160] HCo₃Fe(CO)₉[P(OCH₃)₃]₃,[161,162] H₄Co₄(η⁵-C₅H₅)₄,[163] and H₃Ni₄(η⁵-C₅H₅)₄.[161] The metal–hydrogen bond lengths and the average metal–metal distances in hydride bridged faces are 1.75 to 1.79 Å and 2.91 Å (Re–Re); 1.73 Å (neutron), 1.63 Å (X-ray) and 2.49 Å (Co–Co in the Co₃ face); 1.67 and 2.47 Å (Co–Co); and 1.69 Å and 2.46 Å (Ni–Ni). For the HM₃ tetrahedra in these clusters, the M–H–M angles are then ~110° (Re), 94° (Co₃Fe), 96° (Co)₄, and 94° (Ni). Face-bridging hydride ligands are suspected in several other clusters, e.g., H₂Ru₆(CO)₁₈.

All other cluster hydrides in which hydride hydrogen atom positions have been established have the hydride ligands in edge-bridging positions (Table XXI). These distances are about 0.2 Å longer than the sum of the metallic radii and the covalent radius of hydrogen. Generally, the metal–hydrogen distance in edge-bridging hydrides will be 1.6 to 1.7 Å for first-row transition metals and from 1.8 to 1.9 Å for second- and third-row metals. The M–H–M angles will be from 110 to 135° for the latter metals and generally smaller (as low as 95°) for the first-row metals (however, see discussion below).

Unlike bridging carbon monoxide ligands, a bridging hydrogen atom generally yields metal–metal distances 0.03 to 0.2 Å longer than the unbridged metal–metal lengths, an observation which has been used to deduce hydrogen ligand positions in many structure determinations in which data refinement failed to resolve hydride positions, e.g., tetrahedral $H_4Ru_4(CO)_{12}$ where there are two short edges (Ru–Ru = 2.786 Å) trans to each other and which presumably bear no bridging hydride ligands and four long edges (2.95 Å) which presumably are bridged by hydride ligands.[164] The effect, however, is highly sensitive to the presence of other bridging groups, and the distance between the two metal atoms bridged by both the hydrogen atom and the other group can be the shorter M–M separation in the cluster; e.g., in $HRu_3(CO)_{10}CN(CH_3)_2$, the bridged Ru–Ru distance is about 0.03 Å shorter than the nonbridged lengths.[165] On the other hand, in the hydride edge-bridged and electron-deficient $H_3Rh_3[P(OCH_3)_3]_6$ cluster, the Rh–Rh distances are substantially longer (~0.14 Å) than the Rh–Rh distance in the bulk metal.[166] Such effects, either M–M lengthening or shortening, should prove less pronounced as cluster size increases (similar to the diminished effect of bridging CO ligands on M–M distances for large clusters). Nevertheless, more extensive and more accurate data from neutron diffraction studies are required before more extensive generalizations can be advanced.

Edge-bridging hydrogen atoms have been observed to orient in two distinct modes with respect to the metal triangle in trinuclear clusters. In the more common mode, the M–H–M angle ranges from 96 to 103°, and the dihedral angle between the metal triangle and the plane defined by the hydrogen atom and the two metal atoms spanned ranges from about 60 to 70°. The second mode which has been observed in $HRu_3(CO)_9(C_6H_9)$ (isomer "A") has an M–H–M angle of 125° and is distinguished by the inclusion of the hydrogen ligand in the plane of the three ruthenium atoms.[167] While the first mode commonly occurs for hydrogen chemisorbed on a flat metal surface, the latter is not possible.

Hydride ligand placement in a cluster may be quite sensitive to the other substituents. For example, it appears that $H_4Ru_4(CO)_{12}$ has edge-bridging hydride ligands with the two "open" edges trans to each other. Similarly, the derivatives $H_4Ru_4(CO)_{11}P(OCH_3)_3$ and $H_4Ru_4(CO)_{10}[P(C_6H_5)_3]_2$ are presumed to have analogous hydride placements (based on the X-ray data which show that there are two unique short Ru–Ru edges trans to each other).[164] However, $H_4Ru(CO)_{10}[(C_6H_5)_2-PCH_2CH_2P(C_6H_5)_2]$ has edge-bridging hydride ligands (located in the X-ray study) with three of these hydrides sharing in common a single ruthenium atom, the same ruthenium atom that is bonded to both phosphorus atoms of the chelate ligand.[162,168] The nonbridged edges are about 0.18 Å shorter than the four bridged edges. The stereochemistry may reflect the relatively high electron density on the unique ruthenium atom (note that in $H_4Ru_4(CO)_{10}[P(C_6H_5)_3]_2$ the phosphine ligands are on different ruthenium atoms). Such (apparent) substituent effects on hydride stereochemistry may prove common in cluster chemistry; substituent effects may even shift hydrides from terminal to edge-bridging to face-bridging positions.

An exciting new structural development arising from cluster hydride structural studies but of far-ranging structural and chemical implications is the disclosed but not published report that the hydrogen atoms in the $Rh_{13}(CO)_{24}H_3^{2-}$ cluster are inside the cluster and are associated with square faces.[23,169] Full structural (neutron diffraction) details will be anxiously awaited since the chemical implications of such internal hydrides for clusters and for metal surfaces are profound. Neutron diffraction studies of HNb_6I_{11}, $HNi_{12}(CO)_{21}^{3-}$, and $H_2Ni_{12}(CO)_{21}^{2-}$ also show a hydrogen inside a polyhedron, an octahedron.[169] An analogy does exist with hydrogen chemisorption on transition metal surface where chemisorbed atomic hydrogen can reside in the superficial layer and also below the plane of the surface metal atoms. Hydride formation occurs readily for hydrogen adsorption on palladium which is an extreme example of this phenomenon. The very small relative atomic size of the hydrogen atom plays an important role in this effect.

7. Hydrocarbon Ligands in Clusters

a. Classes of Hydrocarbon Ligands

Hydrocarbon ligands in clusters range from molecular species like alkynes, olefins, dienes and aromatic hydrocarbons to radicals such as simple alkyl groups to biradicals like alkylidenes and benzynes. This large and diverse family of ligands may be critical in the assessment of the cluster–surface analogy in that these ligands are potential models of hydrocarbon interactions with metal surfaces, processes of great importance in the chemical and petrochemical industries.[2-4] These hydrocarbon complexes could provide a molecular understanding of hydrogenation, dehydrogenation, isomerization, oligomerization, polymerization, and re-forming processes. The fragmentation of chemisorbed hydrocarbons on metal surfaces can be followed in some detail by both UPS photoemission[88c] and electron-loss spectroscopy.[89]

b. Alkynes

Alkynes interact with mononuclear metal complexes in the classic σ–π bonding interaction described by Chatt, Duncanson, and Dewar.[170,171] This type of interaction probably arises in the reaction of an alkyne with a metal cluster but typically the stable and isolable alkyne–cluster reaction products are not based on the interaction of one metal atom with acetylenic carbon atoms. Rather, there is an extensive rehybridization at the acetylenic carbon centers, and these carbon atoms interact or bond to three or four metal atoms. The acetylenic carbon–carbon center is substantially lengthened, in some cases, to lengths that clearly approach the normal C–C single bond distance. None of the established alkyne–cluster complexes are based on acetylene or a monosubstituted acetylene. [In the relatively large class of dinuclear metal alkyne complexes there is one example of an acetylene complex, $(C_5H_5)_2Mo_2(CO)_4(C_2H_2)$.[172]] The absence of such isolated complexes may reflect several factors: (i) the preference of synthesis chemists for the easier-to-handle and -purify disubstituted acetylenes, (ii) the facile trimerization of acetylene and monoalkyl or -aryl acetylenes, and (iii) the relatively high reactivity of acetylenic C–H bonds toward (oxidative addition) the low-valent metal atoms in a cluster. It is, however, essential that acetylene and propyne (and 2-butyne) cluster chemistry be extensively probed and compared with the analogous metal surface chemistry.

Three basic structural forms of alkyne cluster complexes have been established. One involves an interaction with four metal atoms and the other two, isomeric in form, an interaction with three metal atoms in a trinuclear cluster or an M_3 triangular face in a large cluster. In the four-metal-atom type of structure, the four metal atoms have a butterfly structure and the acetylenic carbon atoms complete an octahedral M_4C_2 framework (Figure 18) as established for $Co_4(CO)_{10}(C_2H_5C\equiv CC_2H_5)$,[173] $Ru_4(CO)_{12}(C_6H_5C\equiv CC_6H_5)$,[174] and $Ru_4(CO)_{11}(C_8H_{10})$.[175] If this alkyne cluster complex is literally interpreted as a six-atom di-

TABLE XXII. Alkyne Cluster Complex Parameters

	bonding	bonding distances, Å			
complex	mode	C–C	M–C	M–C	ref
$Ru_4(CO)_{11}(C_8H_{10})$	M_4C_2	1.43	2.16[a]	2.21[b]	g
$Ru_4(CO)_{12}(C_6H_5CCC_6H_5)$	M_4C_2	1.46	2.16[a]	2.25[b]	h
$Co_4(CO)_{10}(C_2H_5CCC_2H_5)$	M_4C_2	1.44	2.01[a]	2.10[b]	i
$Ir_7(CO)_{12}(C_8H_{12})(C_8H_{11})(C_8H_{10})$[g]	△	1.32	2.06[c]	2.20[d]	j
$Fe_3(CO)_8(C_6H_5CCC_6H_5)_2$	△	1.38	2.03[c]	1.97[d]	k
$Ni_3(CO)_3(CF_3CCCF_3)(C_8H_8)$	△	1.38	1.90[c]	2.00[d]	l
$Os_3(CO)_{10}(C_6H_5C\equiv CC_6H_5)$	△	1.44	2.19–2.29[c]	2.07–2.18[d]	m
$Fe_3(CO)_9(C_6H_5CCC_6H_5)$	△	1.41	2.06[e]	1.95[f]	n
$Ni_4(CO)_4(CF_3CCCF_3)_3$	△	1.31	1.98–2.02[e]	1.96[f]	o
$Ni_4[CNC(CH_3)_3]_4(C_6H_5CCC_6H_5)_3$	△	1.34	1.97–1.98[e]	2.20[f]	p

[a] For the two metal atoms trans to each other. [b] For the two metal atoms cis to each other. [c] For the two metal atoms parallel to the C_2 vector. [d] For the unique metal atom. [e] For the two metal atoms bridged by the C–C bond. [f] For the unique metal atom. [g] R. Mason and K. M. Thomas, *J. Organomet. Chem.*, **43**, C39 (1972). [h] B. F. G. Johnson, J. Lewis, B. E. Reichert, K. T. Schropp, and G. Sheldrick, *J. Chem. Soc., Dalton Trans.*, 1417 (1977). [i] L. F. Dahl and D. L. Smith, *J. Am. Chem. Soc.*, **84**, 2450 (1962). [j] C. G. Piermont, G. F. Stuntz, and J. R. Shapley, *ibid.*, **100**, 616 (1978). [k] R. P. Dodge and V. Schomaker, *J. Organomet. Chem.*, **3**, 274 (1965). [l] J. L. Davidson, M. Green, F. G. A. Stone, and A. J. Welch, *J. Am. Chem. Soc.*, **97**, 7490 (1975). [m] C. G. Pierpont, *Inorg. Chem.*, **16**, 636 (1977). [n] J. F. Blount, L. F. Dahl, C. Hoogzand, and W. Hubel, *J. Am. Chem. Soc.*, **88**, 292 (1966). [o] J. L. Davidson, M. Green, F. G. A. Stone, and A. J. Welch, *ibid.*, **97**, 7490 (1975). [p] M. G. Thomas, E. L. Muetterties, R. O. Day, and V. W. Day, *ibid.*, **98**, 4645 (1976).
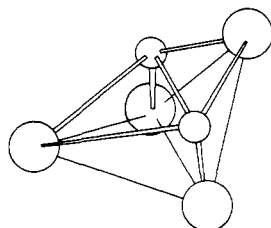
Figure 18. Framework M_4C_2 structure for an alkyne bonded to a butterfly array of four metal atoms: $\bigcirc$ = M, O = C (acetylenic carbon atom).

Figure 19. The two common M_3C_2 framework arrangements for an alkyne bonded to an M_3 triangle. $\bigcirc$ = M, O = C (acetylenic carbon atom).

carbametal cluster, the formal electron count for the framework interaction is 14, the prevailing count number for all octahedral six-atom clusters (see Introduction). The acetylenic C–C bond distances in these clusters are between 1.4 and 1.5 Å as compared to a typical C–C separation in a multicenter cluster, e.g., the small carboranes, of 1.43 to 1.54 Å (in the icosahedral carboranes, the C–C distances are in the range 1.64 to 1.70 Å).

For the alkyne–three metal atom type of interaction, the two isomeric forms are pictorially denoted as △ and △ in Figure 19. In the △ form, the acetylenic carbon atoms symmetrically bridge over two of the metal atoms. The carbon atom that lies above the M_3 center is within bonding distance of all three metal centers. The isomeric form △ has the acetylenic C_2 vector above the M_3 plane and nearly parallel to an M_2 vector and with the acetylenic carbon atoms each within bonding distance of two metal atoms, a C(MM′)C(MM′) isomer. Both the isomeric △ and △ forms have enhanced acetylenic C–C distances but not as marked as in the M_4C_2 alkyne clusters. The C_2 distances are within a range of 0.1 Å of each other and the values for the two isomeric forms overlap. In $Os_3(CO)_{10}(C_6H_5C\equiv CC_6H_5)$ there is some departure from the △-isomeric form because the C_2 and M_2 vectors are not parallel.[176]

Established alkyne clusters are listed along with structural parameters in Table XXII. From a structural view, all three models of acetylene coordination observed in cluster complexes could conceivably occur on metal surfaces.[2–4,9] The modes involving the metal triangles could occur on a flat close-packed metal surface while the butterfly array might be generated at a step or kink site. It is interesting to note that the butterfly–acetylene arrangement is not radically different from the △ mode considering spatial orientation only: removal of one "wing" metal atom from the butterfly yields a metal triangle with the acetylene bonded in the △ mode. An essential need for evaluation of the
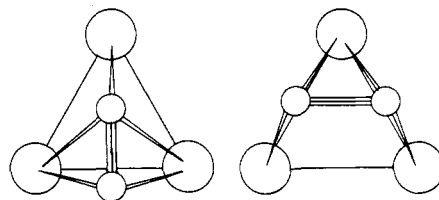
cluster surface analogy in the alkyne area is a systematic study of alkyne (ideally acetylene, propyne and 2-butyne) interactions with metal surfaces using the combined techniques of LEED, photoemission, electron loss spectroscopy, and displacement reactions.[4]

c. Olefins, Diene, and Polyene Ligands

A variety of olefinic hydrocarbons have been structurally characterized as ligands bonded to metal clusters. These include linear dienes, as in cis- and trans-$Os_3(CO)_{10}(C_4H_6)$;[177] cyclic dienes, in $Ir_7(CO)_{12}(C_8H_{12})(C_8H_{11})(C_8H_{10})$;[178] cyclic tetraenes, in $Ni_3(CO)_3(CF_3C\equiv CCF_3)(C_9H_8)$[179] and $(C_6H_5)CCo_3(CO)_6$-(C_8H_8);[180a] and olefins, in $Ru_4(CO)_{11}(C_8H_{10})$.[175]

Interaction of ethylene or any simple olefin with a clean transition metal surface is unlikely to yield a conventional σ–π olefin complex at individual metal sites. In fact, a simple σ–π ethylene complex is unknown, though feasible, for metal clusters. One of the more important recent observations in cluster chemistry is that ethylene reacts with $Os_6(CO)_{18}$ to form a $Os_6(CO)_{16}(CCH_3)_2$ cluster (as well as a $Os_6C(CO)_{16}(CH_3CCCH_3)$ butyne cluster) wherein the CH_3C groups derived from the ethylene are triangular face- and square face-bridging units; this Os_6 cluster has a framework based on a triangular face-capped square pyramid. Other examples of carbyne ligands in clusters are discussed in a later section.

Of the two isomers of $Os_3(CO)_{10}(C_4H_6)$,[177] the complex $Os_3(CO)_{10}(s$-trans-$C_4H_6)$ may more closely represent a possible model of the interaction of a conjugated diene with a metal surface (Figure 20). The C_4H_6 unit is coordinated to two osmium centers in the trans complex, but only one osmium atom coordinates the C_4H_6 units in $Os_3(CO)_{10}(s$-cis-$C_4H_6)$.[177] Similarly, only one metal atom is required for coordination of a 1,5-cyclooctadiene molecule to the Ir_7 framework of $Ir_7(CO)_{12}$-

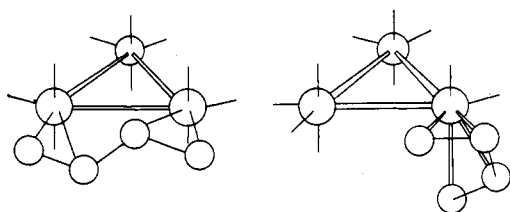**Figure 20.** Representation of the structure and stereochemistry of the trans (left) and cis (right) isomers of $Os_3(CO)_{10}(C_4H_6)$ where the butadiene ligand, trans and cis, is bound to two and one metal atoms, respectively. $\bigcirc$ = Os and O = C. The CO ligands are represented simply by solid lines.

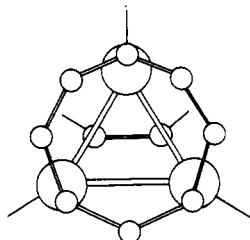**Figure 21.** Binding of the cyclooctatetraene ring shown in the skeletal structure of $Ni_3(CO)_3(CF_3C\equiv CCF_3)(C_8H_8)$ with $\bigcirc$ = Ni and O = C. The CO ligands and CF_3 groups are represented by solid lines emanating from Ni and alkyne carbon atoms, respectively. In this representation, the alkyne is below the Ni_3 triangle and the cyclooctatetraene (C_8H_8) ligand is above.
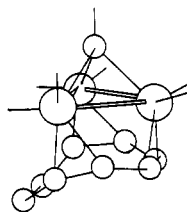
Figure 22. Another type of cyclooctatetraene binding in a cluster shown in a representation of the skeletal structure of $(C_6H_5)CCo_3(CO)_6(C_8H_8)$ with $\bigcirc$ = Co and O = C. The CO ligands and phenyl group are represented by solid lines emanating from Co atoms and the methylidyne carbon atom, respectively. The cyclooctatetraene (C_8H_8) ligand is below the Co_3 triangle.

$(C_8H_{12})(C_8H_{11})(C_8H_{10})$.[178] Such cluster complexes may represent inadequate models of diene or polyene interactions with metal surfaces although the presence of other chemisorbed species on the surface could shift the interaction of polyenes at a metal surface to the single metal atom–diene form.

A rather interesting example of an unsaturated cyclic hydrocarbon interacting simultaneously with three metal centers is seen in $Ni_3(CO)_3(CF_3C\equiv CCF_3)(C_8H_8)$[179] (Figure 21). The cyclooctatetraene ring is planar to within 0.08 Å and is parallel to the plane of the three Ni atoms to within 3°. Three sets of Ni–C distances are observed: short 2.01–2.19 Å, medium 2.32–2.37 Å, and long 2.55–2.60 Å. The C–C distances within the ring average 1.43 Å. Another interesting aspect of this complex is that the ^1H NMR shows only a singlet for the ring protons even down to −90 °C, suggesting rapid ring rotation above the metal plane. This cluster complex is thus both a potential model for coordination of a molecule with a delocalized ring system to a metal surface and a potential model of migration or mobility (see section IV) of that molecule on the metal surface.

Another cluster complex exhibiting cyclooctatetraene coordination to three metal centers is $C_6H_5CCo_3(CO)_6(C_8H_8)$[180a] (Figure 22). The cyclooctatetraene molecule is in a tub conformation attached to the cobalt triangle in such a way that three of the polyene's double bonds are coordinated to the three cobalt atoms with the fourth double bond being bent away from the metal triangle. Bonding here is apparently conventional and may be considered as a set of three double bond–single metal interactions with a mean Co–C distance of 2.19 Å. Likewise, the olefin portion of the C_8H_{10} ring in the tetraruthenium complex $Ru_4(CO)_{11}(C_8H_{10})$ is bonded only to one ruthenium atom. Whether

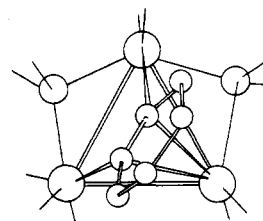**Figure 23.** Binding of a benzyne ligand shown in the skeletal structure of $Os_3(CO)_7[P(C_6H_5)_2]_2(C_6H_4)$ with $\bigcirc$ = Os, $\bigcirc$ = P, and O = C. To retain simplicity of perspective the CO ligands and the phenyl groups bound to phosphorus are represented by solid lines to the Os and P atoms, respectively.
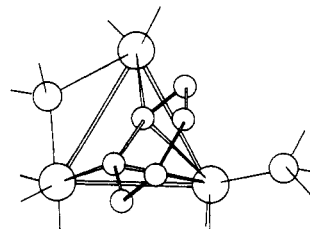

Figure 24. Benzyne binding in a cluster, analogous to that in Figure 23, shown in the skeletal structure for the $Os_3[C_6H_4]P_2$ core in HOs_3-$(CO)_7[P(C_6H_5)_2][P(C_6H_5)_3](C_6H_4)$ with $\bigcirc$ = Os, $\bigcirc$ = P, and O = C. The remaining CO ligands and phenyl groups are indicated by solid lines attached to Os and P atoms, respective. The hydride ligand is not shown.

this type of one-to-one coordination occurs between an olefin and a metal surface atom cannot be answered. Clearly, for metal cluster complexes to serve as *test* models of chemisorbed olefins on a metal surface, more monoolefin–cluster complexes must be structurally characterized.

Two other examples of cyclic hydrocarbons bonded to a triangular array of metal atoms are worth mentioning as possible models of analogous surface states. One is an example of a bicyclic ring system bound to a metal cluster, i.e., a 4,6,8-trimethylazulene complex of ruthenium, $(4,6,8-(CH_3)_3C_{10}H_5)$-$Ru_4(CO)_9$, in which the organic molecule is arched over a ruthenium triangle.[181] The other complex, $(C_5H_5)_4Rh_3H$, has one planar C_5H_5 ring above and parallel to the Rh_3 triangle; the other three are conventional η^5-C_5H_5 ligands bonded to single rhodium atoms.[182]

Coordination of olefinic or even acetylenic hydrocarbons to a clean transition metal surface is apt to be followed by scission of C–H or C–C bonds. However, if the surface is modified by partial coverage by another molecule like carbon monoxide, the bond scission reactions may be greatly inhibited. All the above derivatives of unsaturated hydrocarbons, in fact, have at least two types of ligands. No clusters with only hydrocarbon ligands have been reported or claimed.

d. Arene, Benzyne, and Phenyl Ligands

Arene–cluster complexes[183,184] involving mononuclear metal coordination of the arene to the cluster as in η_6-arene $Ru_6C(CO)_{14}$ complexes may not be good models of arene activation by metal surfaces. The coordination to several metal centers of large cyclic hydrocarbons possessing delocalized π systems as discussed above may more closely represent the initial interaction of arene molecules with some metal surfaces. Excellent models of a still higher degree of arene activation by a metal surface are found in two osmium–"benzyne" cluster complexes, $Os_3(CO)_7[P(C_6H_5)_2]_2(C_6H_4)$[185] and $HOs_3(CO)_7$-$[P(C_6H_5)_2][P(C_6H_5)_3](C_6H_4)$[186] (Figures 23 and 24). The spatial orientation of the C_6 ring to the Os_3 triangle is reminiscent of alkyne coordination to a metal triangle, the orientation being similar to the Δ mode. The dihedral angle between the Os_3 plane and the C_6H_4 ring is about 69°. Two osmium atoms and the benzyne ligand are almost coplanar, with mean $Os_{1,2}$–C distance of 2.16 Å. The mean Os_3–C distance is about 2.39 Å. All the C–C distances in the ring are equivalent, based on the

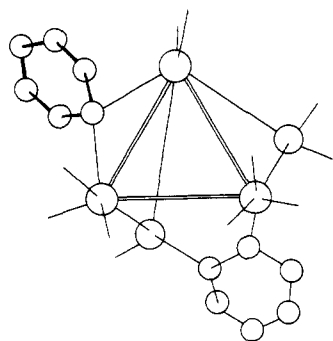**Figure 25.** An example of a bridging phenyl group, albeit an unsymmetrical one, shown in the upper left part of the skeletal structure of $Os_3(CO)_8[P(C_6H_5)_2](C_6H_5)[P(C_6H_5)(C_6H_4)]$ with $\bigcirc$ = Os, $\bigcirc$ = P, and O = C. Also depicted is the bridging $P(C_6H_5)(C_6H_4)$ group. The remaining CO ligands and phenyl groups are represented by solid lines emanating from Os and P atoms, respectively.
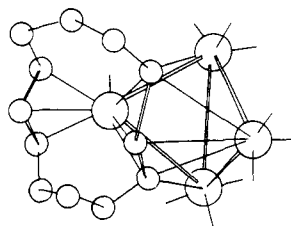

Figure 26. The stereochemical features of an allylic–multicenter metal atom interaction of an unsaturated cyclic hydrocarbon radical, $C_{12}H_{16}$, in $Ru_4(CO)_{10}(C_{12}H_{16})$ where $\bigcirc$ = Ru and O = C. The solid lines projecting from the ruthenium atoms show the stereochemical positions of the carbonyl ligands.

current stage of structure refinement. The shorter Os–C distances reported agree quite well with a value which might be predicted for a phenyl–metal surface interaction (2.12 Å) based on sums of the metallic radius and the single bond covalent radius of carbon. Interestingly, pyridine interactions with trinuclear clusters[292] generates ortho M–N and M–C σ bonds as in $HOs_3(NC_5H_4)(CO)_{10}$ analogous to the bonding proposed for pyridine chemisorbed on a metal surface.[293] A bridging phenyl group, which also may be considered representative of a stage of arene activation, has been observed in triosmium clusters, e.g., $Os_3(CO)_8[P(C_6H_5)_2](C_6H_5)[P(C_6H_5)(C_6H_4)]$[185] (Figure 25). The C_6H_5 ligand forms an unsymmetrical bridge between two osmium atoms with Os–C distances of 2.19 and 2.39 Å.

e. Hydrocarbon Radicals as Ligands

Many cluster complexes have hydrocarbon ligands in what can be considered varying degrees of C–H and C–C bond activation.[2] This type of complex is generated most commonly in stoichiometric reactions of ruthenium and osmium carbonyl clusters.[2] The coordination of a large unsaturated C_{12} ring to a metal cluster is shown in $Ru_4(CO)_{10}(C_{12}H_{16})$[187] and HRu_3-$(CO)_9(C_{12}H_{15})$.[188] In the former complex, the ring is bonded to a butterfly array of four ruthenium atoms via π-allylic coordination of one portion of the C_{12} ring to a "wing" ruthenium atom (Ru–C distance of 2.19 Å) as shown in Figure 26.[187] Another portion of the C_{12} ring is bonded to both "wing" ruthenium atoms by what resembles a bridging allyl group with a Ru(wing)—C_{allyl} distance of 2.28 Å. The hinge ruthenium atoms and the three carbons of this latter allylic linkage are nearly coplanar. The Ru (hinge)–C_{allyl} separations are about 2.14 Å. Such an arrangement could be a model representing the unique activation potential of step or kink sites on metal surfaces. The bonding of the C_{12} ring to the Ru_3 grouping in $HRu_3(CO)_9(C_{12}H_{15})$ is by a single π-allyl system. Two of the ruthenium atoms and the three carbons of the allylic portion of the C_{12} ring are nearly coplanar. The Ru–C_{allyl} bond distances are ~2.20 and ~2.01 Å, and the allylic C–C–C angle is 125°.[188]

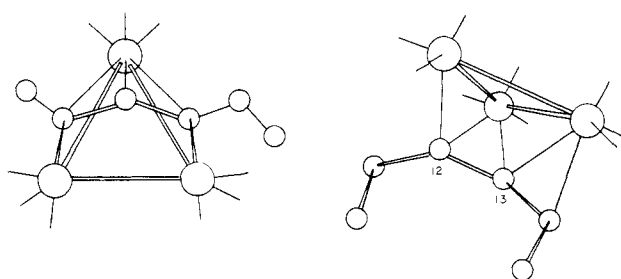Allylic bonding across a metal triangle is not uncommon

Figure 27. A multicenter allyl interaction of the C_6H_9 radical ligand with the three ruthenium atoms in $HRu_3(CO)_9(C_6H_9)$ isomers, "A" (right) and "B" (left) with $\bigcirc$ = Ru and O = C. The CO ligands are represented by solid lines projecting from Ru atoms. Hydrogen atoms are not shown in the figure.

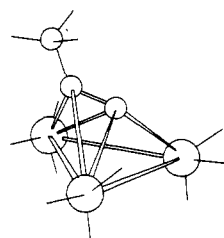**Figure 28.** Skeletal structure of $HRu_3(CO)_9[C\equiv CC(CH_3)_3]$, $\bigcirc$ = Ru and $\bigcirc$ = C, showing the multicenter (metal) interaction of $(CH_3)_3CC\equiv C$ through the acetylenic carbon atoms with the three ruthenium atoms. All ligands are depicted by solids lines projecting at the ruthenium atoms. Hydrogen atoms are not shown.

and represents a thermally activated stage of olefin or diene interaction with some metal clusters. Two distinct stages of this interaction are observed in the two isomers of $HRu_3(CO)_9(C_6H_9)$ (Figure 27). The "A" isomer has the organic radical bonded to the Ru triangle by a bent "allenic" system that can be considered to be based on two π bonds and one σ bond.[189] (Description of these complex structures in valence bond terms is really not an accurate description, but this terminology is employed here for simplicity in the description of the structures.[190]) The C–C distances in the "allenic" portion of the ligand are 1.367 Å, the "allenic" C–C–C angle is 142°, the Ru–C σ bond is 2.058 Å, and the other Ru–C allenic distances are in the range of 2.09–2.34 Å. An interesting feature of this complex is that two ruthenium atoms and two carbon atoms (C_{12} + C_{13}) of the organic ligand are nearly coplanar and form a dihedral angle of 57° with the Ru triangle.[189] This is quite different from the "B" isomer[192] and the $HRu_3(CO)_9(C_{12}H_{15})$ complex[188] in which two ruthenium atoms and five carbons atoms of the organic ligand (those composing and adjacent to the allylic system) are nearly coplanar, the plane of which forms an angle of 51° with the Ru triangle). In the "B" isomers,[191] the Ru–C σ bonds are 2.05 Å and the Ru–C π bonds 2.25 and 2.36 Å.

Superficially, the coordination of these organic groups is similar to that of alkynes to clusters. For both types of organic ligands, their orientation with respect to either an M_4 butterfly or M_3 triangle is similar; i.e., in the butterfly they are parallel to the hinge with σ-bonding to the hinge metal atoms, and in the M_3 array they are parallel to two metal atoms, σ-bonding to those two metal atoms and presumably π-bonding to the third. The M–C distances are very similar for both bond types regardless of the organic ligand as shown in Table XXIII.

An interesting cluster complex representing the coordination and activation of a terminal alkyne is $HRu_3(CO)_9[C\equiv CC(CH_3)_3]$ (Figure 28),[192] where the acetylenic carbon-carbon bond has been lengthened to 1.315 Å. The coordination is similar to that observed in $Ni_4[CNC(CH_3)_3]_4(C_6H_5C\equiv CC_6H_5)_3$[193] and is of the $\triangle$ mode. The Ru–C (unique carbon) bond is 1.947 Å and the other two Ru–C bonds are 2.21 and 2.27 Å. The hydride ligand is located below the Ru_3 plane.[192] This cluster is a very good model for alkynyl interaction with a metal surface with the

TABLE XXIII. Organometal Clusters Metal–Carbon Distances

complex	ligand	M–C distance, Å "σ bond"	M–C distance, Å "π bond"
$H_2Os_3(CH_2C)(CO)_9$[a]	(CH_2C)	2.04–2.05	2.17–2.35
$Os_3(CO)_{10}(S\text{-}cis\text{-}C_4H_6)$[b]	(C_4H_6)		2.20–2.30
$HOs_3(CO)_{10}[CHCH_2P(CH_3)_2(C_6H_5)]$[c]	$[CHCH_2P(CH_3)_2(C_6H_5)]$	2.16	
$Os_3(CO)_7[P(C_6H_5)_2]_2(C_6H_4)$[d]	(C_6H_4)	2.12–2.17	2.14–2.33
$HOs_3(CO)_7[P(C_6H_5)_2][P(C_6H_5)_3](C_6H_4)$[e]	(C_6H_4)	2.15	2.40
$HOs_3(CO)_{10}(CHCHC_2H_5)$[f]	$(CHCHC_2H_5)$	2.15	2.28–2.46
$Ru_6C(CO)_{14}[C_6H_3(CH_3)_3]$[g]	$[C_6H_3(CH_3)_3]$		2.24
$HRu_3(CO)_9[C≡C(t\text{-}C_4H_9)]$[h]	$[CC(t\text{-}C_4H_9)]$	1.95	2.21–2.27
$HRu_3(CO)_9(C_6H_9)\text{-}A$[i]	(C_6H_9)	2.06	2.09–2.34
$HRu_3(CO)_9(C_6H_9)\text{-}B$[j]	(C_6H_9)	2.05	2.22–2.36
$HRu_3(CO)_{10}[CN(CH_3)_2]$[k]	$[CN(CH_3)_2]$	2.03	
$HRu_3(CO)_9(C_{12}H_{15})$[l]	$(C_{12}H_{15})$	2.01	2.20
$Ru_4(CO)_{10}(C_{12}H_{16})$[m]	$(C_{12}H_{15})$	2.14	2.19–2.28
$H_3Ru_3(CO)_9(CCH_3)$[n]	(CCH_3)	2.08	
$Ni_3(CO)_3(CF_3CCCF_3)(C_8H_8)$[o]	(C_8H_8)	2.01–2.60	
$RC(Co)_3(CO)_9$[p]	(RC)	1.92	
$[Cu[CH_2Si(CH_3)_3]]_4$[q]	$[CH_2Si(CH_3)_3]$	2.02	

[a] A. J. Deeming and M. Underhill, *J. Chem. Soc., Dalton Trans.*, 1415 (1974). [b] M. Tachikawa, J. R. Shapley, R. C. Haltiwanger, and C. G. Pierpont, *J. Am. Chem. Soc.*, **98**, 4651 (1976). [c] M. R. Churchill and B. G. DeBoer, *Inorg. Chem.*, **16**, 114 (1977). [d] C. W. Bradford, R. S. Nyholm, G. J. Gainsford, J. M. Guss, P. R. Ireland, and R. Mason, *J. Chem. Soc., Chem. Commun.*, 87 (1972). [e] G. J. Gainsford, J. M. Guss, P. R. Ireland, R. Mason, C. W. Bradford, and R. S. Nyholm, *J. Organomet. Chem.*, **40**, C70 (1972). [f] J. J. Guy, B. E. Reichert, and G. M. Sheldrick, *Acta Crystallogr., Sect. B*, **32**, 3319 (1976). [g] R. Mason and W. R. Robinson, *Chem. Commun.*, 468 (1968). [h] M. Catti, G. Gervasio, and S. A. Mason, *J. Chem. Soc., Dalton Trans.*, 2260 (1977). [i] G. Gervasio, D. Osella, and M. Valle, *Inorg. Chem.*, **15**, 1221 (1976). [j] M. Evans, M. Hursthouse, E. W. Randall, and E. Rosenburg, *J. Chem. Soc., Chem. Commun.*, 545 (1972). [k] M. R. Churchill, B. G. DeBoer, and F. J. Rotella, *Inorg. Chem.*, **15**, 1843 (1976). [l] A. Cox and P. Woodward, *J. Chem. Soc. A*, 3599 (1971). [m] R. Belford, M. I. Bruce, M. A. Cairns, M. Green, H. P. Taylor, and P. Woodward, *Chem. Commun.*, 1159 (1970). [n] G. M. Sheldrick and J. P. Yesinowski, *J. Chem. Soc., Dalton Trans.*, 873 (1975). [o] J. L. Davidson, M. Green, F. G. A. Stone, and A. J. Welch, *J. Am. Chem. Soc.*, **97**, 7490 (1975). [p] B. R. Penfold and B. H. Robinson, *Acc. Chem. Res.*, **6**, 73 (1973). [q] J. A. J. Jarvis, R. Pearce, and M. F. Lappert, *J. Chem. Soc., Dalton Trans.*, 999 (1977).

possible exception of the hydride placement on the opposite side of the metal plane (although interstitial hydrides in the surface regime are certainly feasible).

A butenyl cluster, $HOs_3(CO)_{10}(CH=CHC_2H_5)$ formed from $H_2Os_3(CO)_{10}$ and 1-butyne, can be viewed as a model of terminal olefin C–H activation and coordination to an array of metal atoms (Figure 29).[194] The "olefinic" C–C distance is 1.40 Å and is oriented with respect to the osmium atoms such that it *may be considered* to be π-bonded to one osmium (Os–C distances of 2.46 and 2.28 Å) and σ-bonded by the terminal carbon to another osmium at a distance of 2.15 Å.[194] A related structure is established for $H_2Os_3(CO)_9(CCH_2)$ (Figure 30) which is derived from $H_2Os_3(CO)_{10}$ and ethylene.[195] The coordination of the organic radical is similar to that described above for the butenyl radical but with the *two* terminal ethylenic hydrogen atoms now substituted by osmium atoms. Thus, the nonhydrogen bearing carbon atom is coordinated to all three osmium atoms by two Os–C bonds at 2.05 Å and one at 2.17 Å. The remaining CH_2 carbon atom is within 2.35 Å of the third osmium atom. The "olefinic" C–C distance is 1.38 Å.[195]

Examples of alkyl radicals coordinated to a metal cluster are known and all are edge-bridging ligands. The complex $Cu_4[CH_2Si(CH_3)_3]_4$ illustrates edge-bridging alkyl groups.[196]
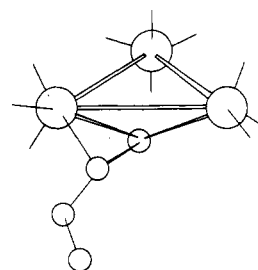

Figure 29. An example of a vinyl radical interaction with two metal atoms in $HOs_3(CO)_{10}(CH=CHC_2H_5)$. In the drawing ◯ = Os and ◯ = C; the CO ligands are shown by solid lines connected to the Os atoms. Hydrogen atoms are not shown.
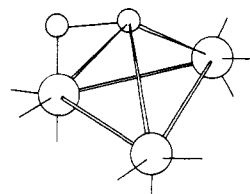

Figure 30. Multicenter interaction of the vinylidene radical, CCH_2, with the three osmium atoms in $H_2(Os_3(CO)_9(CCH_2)$. In this figure, ◯ = Os and ◯ = C; the CO ligands are shown as solid lines. Hydrogen atoms are not shown. The CH_2 carbon atom is at the upper left position in the drawing.

The structure is simply a square-planar array of four copper atoms about which are disposed simple bridging coplanar trimethylsilyl groups between copper atoms.[196] A similar structure for an alkoxy ligand has been reported in $Cu_4[OC(CH_3)_3]_4$.[197] Neither is a good model for alkyl or alkoxy bonding to a close-packed metal surface due to the coplanarity of all the metal atoms and ligand groups, a clearly impossible situation for a close-packed metal surface but not impossible for a rough corrugated surface of the appropriate symmetry and registry. An example of a bridging hydrocarbon anion in the form of a 1,3-dipolar $[CHCH_2P(CH_3)_2C_6H_5]$ ligand is found in $HOs_3(CO)_{10}[(CHCH_2P(CH_3)_2C_6H_5]$ where this ligand is found in a symmetrical bridging mode between two osmium atoms with an Os–C distance of 2.16 Å, in good agreement with a predicted value of 2.17 Å based on the osmium metallic radius and the single bond covalent radius of carbon.[198] The plane defined by the bridging carbon and the two Os atoms it bridges forms a dihedral angle of 109° with the osmium triangle and is thus a viable model for hydrocarbon fragment attachment to a metal surface. For the $(CH_3)_2N^+=C^-$ ligand, a similar bonding is established in the $HRu_3(CO)_{10}[CN(CH_3)_2]$[165] complex. The dihedral angle between the Ru_3 plane and that defined by the carbon and the two Ru atoms it bridges is 100°. The Ru–C distance is 2.03 Å, which is slightly shorter than the value of 2.11 Å obtained by summing the metallic radius and the covalent radius of carbon. Recently, the simplest example of an alkyl ligand, a methyl group, was reported in the complex $HOs_3(CO)_{10}(CH_3)$ which has a methyl group unsymmetrically bridging a cluster edge through an $Os–CH_2–H–Os$ interaction.[199] Interestingly, this methyl derivative is in equilibrium with a carbene structure, $H_2Os_3(CO)_{10}CH_2$, in which the carbene or methylene group bridges an edge.[199]

Carbyne hydrocarbon fragments coordinated to a metal array are found in the $RCCo_3(CO)_9$ class[200] of clusters and in analogous ruthenium and osmium complexes, $H_3Ru_3(CO)_9(CCH_3)$[201] and $H_3Os_3(CO)_9(CH)$.[199] In these clusters the carbon atom is an integral part of the cluster framework. The alkylidyne or carbyne groups are symmetrically face-bridging and normal to the M_3 triangle. The Ru–C distance is 2.08 Å and the Co–C distance is typically about 1.92 Å.

f. Hydrocarbon and Hydrocarbon Radicals on Metal Surfaces

There is not even one well-defined (structural or compositional) case of a hydrocarbon chemisorption state on a metal. Because the facility of either C–H or C–C bond breaking is high on a metal surface interaction with a hydrocarbon, saturated or unsaturated, the most fundamental issue of stoichiometry of the chemisorbed hydrocarbon species is totally unresolved.[2,4] Nevertheless, the data for the clusters and fundamental bonding considerations seem to allow certain projections: (i) chemisorption of a saturated hydrocarbon on most clean transition metal surfaces is not molecular or nondissociative in character—minimally a C–H or C–C bond must be cleaved to generate the bonding of a hydrocarbon radical (or biradical) to the surface; (ii) as in the hydrogen or hydride ligand, the bonding of an alkyl or aryl ligand to a metal surface will probably be multicenter in character; (iii) the binding of an alkyne or alkene molecule to a metal surface is unlikely to be of the simple σ–π metal–C_2 unsaturated form, namely, the Chatt–Duncanson–Dewar bonding mode, in that extensive metal atom–C_2 interaction may occur or C–H or C–C bond scission may be involved; (iv) aromatic hydrocarbon interaction may involve from two to six carbon atoms of a benzene nucleus or may involve C–H bond scission and then a complex interaction of the C_6 ring carbon atoms; and (v) the interaction of CR or CR_2 fragments will probably minimally involve two metal atoms in the surface. The simplistic model of hydrocarbon molecules, radical or polyradical interaction with a single metal atom based on the coordination chemistry of mononuclear metal complexes will, for the most part, be inadequate models of hydrocarbon chemisorbed states on metals *although the presence of other chemisorbed species on the metal surface may dramatically shift bonding and structural patterns closer to those representative of the mononuclear transition metal complex.*

Recent photoemission studies for chemisorption and reaction of acetylene and ethylene on $Pt(111)$[122] and $Fe(100)$[123a] surfaces indicate the presence of $CH_2{=}CH-$ and $CH_2{=}C-$hydrocarbon fragments. In contrast to the photoemission results, CH_3CH or CH_3C fragments appear to be formed upon chemisorption of acetylene on $Pt(111)$[89] as also indicated by vibrational analysis of electron loss measurements. More recent EELS studies by Demuth and Ibach[123b] suggest a CH species as on $Ni(111)$ in agreement with the earlier photoemission studies of Demuth.[123c]

8. Ligands Bound through Noncarbon Atoms

A substantial number of cluster complexes are known in which the ligands are bound to the cluster through noncarbon ligand atoms. Many of these are found in derivatives of the carbonyl cluster complexes obtained by simple substitution of a CO ligand by some donor molecule. Phosphines and phosphites are typical of this family of ligands. These strong donor molecules can replace one or more terminally bound carbonyl ligands and can promote changes in the mode of carbonyl bonding in the complex by increasing the electron density on the metal core. Thus, $Ir_4(CO)_{12}$ has no bridging CO ligands while $Ir_4(CO)_{10}$-$[P(C_6H_5)_3]_2$[202] has three. Bridging phosphines have never been observed, although phosphido bridges are established (vide infra). There is also a fledgling class[166] of phosphite metal clusters as exemplified by the trinuclear $\{HRh[P(OR)_3]_2\}_3$ complexes which have all phosphite ligands at terminal positions and the hydride ligands at edge-bridging positions.

Cluster complexes containing ligands coordinated to the metal framework by oxygen, sulfur, tellurium, nitrogen, phosphorus, and arsenic atoms are established. Most involve coordination of these atoms to an M_3 triangle, although bonding to an M_4 array is also known and often the coordinating atom is an integral element of the cluster framework (see the cubane clusters in section E.5). These ligands are typically three-, four-, or five-

TABLE XXIV. Metal–Ligand Parameters for Non-carbon Coordination

complex	ligand	M–L dist, Å
$Fe_4(CO)_{11}(NC_2H_5)(ONC_2H_5)$[a]	μ_4-NC_2H_5	2.03
$Co_4(CO)_{10}(PC_6H_5)_2$[b]	μ_4-PC_6H_5	2.244
$Co_4(CO)_{10}(S)_2$[b]	μ_4-S	2.26
$Co_4(CO)_{10}(Te)_2$[b]	μ_4-Te	2.54
$Fe_3(CO)_9(AsC_6H_5)_2$[c]	μ_3-AsC_6H_5	2.33
$Fe_3(CO)_9(NCH_3)$[d]	μ_3-NCH_3	1.93
$Fe_3(CO)_9[NNC(C_6H_5)_2]_2$[e]	μ_3-$NNC(C_6H_5)_2$	1.95
$HFe_3(CO)_9(S-i-C_3H_7)$[f]	μ_3-$S-i-C_3H_7$	2.14
$[H_3Re_3(CO)_9O]^{2-}$[g]	μ_3-O	2.12

[a] G. Gervasio, R. Rossetti, and P. L. Stanghellini, *J. Chem. Soc., Chem. Commun.*, 387 (1977). [b] R. C. Ryan and L. F. Dahl, *J. Am. Chem. Soc.*, **97**, 6904 (1975). [c] M. Jacob and E. Weiss, *J. Organomet. Chem.*, **131**, 263 (1977). [d] R. J. Doedens, *Inorg. Chem.*, **8**, 570 (1969). [e] P. E. Baikie and O. S. Mills, *J. Chem. Soc., Chem. Commun.*, 1228 (1967). [f] R. Bau, B. Don, R. Greatrex, R. J. Haines, R. A. Love, and R. D. Wilson, *Inorg. Chem.*, **14**, 3021 (1975). [g] G. Ciani, A. Sironi, and V. G. Albano, *J. Chem. Soc., Dalton Trans.*, 1667 (1977).

center bridge bonding in the clusters.

$HOs_3(CO)_{10}(SC_2H_5)$ is illustrative of an edge-bridging thiol derivative.[203] In this complex, the sulfur atom is symmetrically bridging with an Os–S distance of 2.40 Å and an Os–S–Os angle of 73°. The plane defined by the sulfur atom and the two osmium atoms it bridges form a dihedral angle of 76° with the Os_3 plane. Representative of edge-bridging phosphido groups are $HOs_3(CO)_7[P(C_6H_5)_2][P(C_6H_5)_3](C_6H_4)$ and $Os_3(CO)_7[P-(C_6H_5)_2](C_6H_4)$.[185,186] The osmium–phosphorus bridging distances range from 2.26 to 2.42 Å and the average is 2.33 Å.

Examples of triply bridging O-, S-, As-, and N-containing ligands are found in several trinuclear iron and rhenium complexes (Table XXIV).[204,205] Many of the iron complexes are based on an $Fe_3(CO)_9$ triangular unit containing one very long Fe–Fe distance (>3 Å). Above and below the Fe_3 triangle are located triply bridging AsC_6H_5, NCH_3, or $NNC(C_6H_5)_2$ groups completing a pseudo-trigonal bipyramidal framework. The complex $[H_3Re_3(CO)_9O]^{2-}$ is based on an equilateral $Re_3(CO)_9$ triangular unit above which is found a single, triply bridging oxygen atom and below which are located three edge-bridging hydrogen atoms.[206] Metal–ligand atom distances are given in Table XXIV. An example of a triply bridging thio ligand is $HFe_3(CO)_9(S-i-C_3H_7)$.[20] In this complex the sulfur atom, the hydrogen atom, and the two iron atoms that they bridge are coplanar, the plane forming a dihedral angle of 60° with the Fe_3 triangle. The S–Fe–Fe–H plane is tilted such that the sulfur atom is 1.50 Å above the Fe_3 triangle and equidistant from all three iron atoms.

The bonding of a ligand atom to four metal cluster atoms is established in $Fe_4(CO)_{11}(NC_2H_5)(ONC_2H_5)$[208] and $Co_4(CO)_{10}$-$(X)_2$,[209] where X may be PC_6H_5, S, or Te. In the first complex, the metal core is only slightly distorted from a square array, while the Co_4 complexes possess a distinctly rectangular metal atom configuration. In all cases, the μ_4-ligand is equidistant from the M_4 array; M–ligand atom distances are given in Table XXIV. The $Fe_4(CO)_{11}(NC_2H_5)(ONC_6H_5)$ complex, shown in Figure 31, also shows a very unusual coordination of the ONC_2H_5 group to the Fe_4 array with the ligand bisecting the Fe_4 square in such a manner that the oxygen atom symmetrically bridges two iron atoms and the nitrogen atom symmetrically bridges the other two.[208] The Fe–O and Fe–N distances are 1.94 and 1.93 Å, respectively.

These cluster complexes represent plausible models of ligands containing group 5 and 6 donor atoms adsorbed on a metal surface. The M_4 systems are intriguing, since they may be considered prototypical of adsorption on body-centered-cubic metal surfaces. The observed M–L distances vary up to 0.15 Å from values predicted from summation of metallic radii and single-bond covalent radii and generally are smaller than predicted. The observation of single atoms, e.g., O, S, and Te, bound
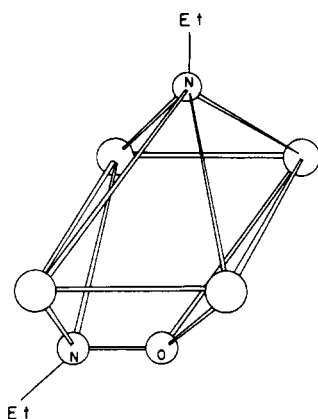
Figure 31. Multicenter interactions of the C_2H_5N radical (top) and C_2H_5NO (bottom) with the four iron atoms in $Fe_4(CO)_{11}(NC_2H_5)(ONC_2H_5)$ where $\bigcirc$ = Fe and O = O and N. The CO ligands and ethyl groups are represented by solid lines connected to the iron and nitrogen atoms, respectively.

TABLE XXV. Ligand Metal-atom Coordination Number

ligand	obsd metal-atom coordination no.	ligand	obsd metal-atom coordination no.
H	1, 2, 3	NR, PR	3, 4
CH_3	2	CO	1, 2, 3
C_6H_5	2	CNR	1, 2, 3
Cl, Br, I	1, 2, 3	$RC\equiv CR$	2, 3, 4
O, S, Te	2, 3, 4	$CH\equiv CH_2$	3
SR	2, 3	$C\equiv CR$	3

chemical exchange reactions in metal molecular clusters should be a revealing study. Since most clusters of interest in this context have at least two different ligand types, studies of chemisorbed states on surfaces derived from two or more molecules will be necessary. Interactions will be revealed in such studies by changes in binding energies of molecules elicited by the presence of a second chemisorbed molecule.

10. Summary

For the many modes of ligand coordination to a metal cluster core that are established, with only a few exceptions, these are *feasible* models for similar interactions between an adsorbate and a metal surface. The exceptions arise primarily from an unlikely spatial arrangement on a close-packed metal surface, e.g., the requirement of coplanarity of the ligand and the plane defined by the metal atoms. Other less likely models of chemisorbed surfaces would include the η^4-bonding of a diene to a single metal atom in a cluster.

In some cases, different types of ligands have similar orientations with respect to metal arrays. Thus, similar modes of coordination to a metal core are observed for alkynes, alkyne fragments, diene and allylic groups, and benzyne moieties. Alkyl and aryl radicals have only been structurally characterized in edge-bridging positions, alkylidenes only in edge-bridging modes, and alkylidyne only in face-bridging modes. As the substituents on a carbon atom are reduced, the mode of bonding to the cluster changes to one involving higher coordination to the metal atoms. Similar changes can easily be envisioned as occurring on metal surfaces during a catalytic sequence, especially surfaces which are highly stepped or are very rough on an atomic scale.[34]

The M_4 butterfly array found in some clusters, especially alkyne clusters, is also of potential significance in that it can be thought of as representing a step or kink site on a metal surface, positions believed to be highly reactive. In this regard, it is interesting to note that the highest degree of $C\equiv C$ bond reduction in alkynes by cluster complexes is observed in the M_4 butterfly clusters, i.e., the octahedral M_4C_2 type of cluster. The five-center interaction of chalcogens and also PC_6H_5 with square M_4 arrays is significant as a prototypical example of chemisorption on a metal surface that has square or rectangular metal packing in the top layer. The coordination of the NO atoms in the C_2H_5NO ligand across the Fe_4 square in $Fe_4(CO)_{11}(NC_2H_5)(ONC_2H_5)$ is also suggestive of a bonding mode for multiply bonded atoms in a ligand or molecule with metal surfaces that have square or rectangular M_4 subunits.

Perhaps the most important general conclusion that can be made regarding structure and stereochemistry in clusters is that many ligands exhibit multicenter metal atom interactions as shown in the partial list of Table XXV. Many of these ligand molecules or radicals are conventional unidentate ligands in mononuclear coordination complexes; their interactions are thought of in terms of two-center, two-electron bonds even though multicenter molecular orbitals must be considered if their chemistry in all its subtlety is to be explained. If the structure, stereochemistry, and bonding of such simplistic ligands are so substantially altered in going from mononuclear transition metal chemistry to the cluster regime, then we may reasonably expect

to a cluster complex is also significant since such species have been examined as adsorbates on certain metal surfaces and some adsorbate–substrate distances have been evaluated (Tables XIV and XV); cubane metal sulfur clusters were discussed above in an earlier section (E.5). It is unfortunate that the surfaces studied and those cluster complexes exhibiting single atom coordination do not involve the same metals.

The complex $(C_4H_4N_2)Ru_3(CO)_{10}$ illustrates another mode of ligand bonding to a metal triangle.[210] In this case the ligand is located along an M–M vector of an M_3 triangle and interacts with only those two metal atoms with a Ru–N distance of 2.135 Å.[210] The plane of the ligand and these two metal atoms is almost perpendicular to the plane of the three metal atoms. While this bonding has been observed for binuclear complexes, e.g., $(C_4H_4N_2)Fe_2(CO)_7$, the third metal is nonetheless present but not used for ligand coordination.[211a] In this regard, this complex is a possible model for such interaction between similar ligands and metal surfaces. Maximum coordination to metal atoms on the surface need not always occur.

9. Ligand–Ligand Interactions

Through-bond interactions of nonadjacent atoms have been extensively studied and documented in molecular chemistry, as in substituent effects of benzene derivatives, and in solid-state structures, as in ferrimagnetic materials. Such through-bond interactions for coordination compounds have been defined through nuclear magnetic and electron spin resonance studies and through chemical studies of cis and trans effects in octahedral[211b] and planar complexes.[211c] Similar phenomena should be observed in metal clusters. Specific ligands on one metal atom may exert pronounced effects upon the binding of ligands on other metal atoms in the cluster. Such transmission effects have been proposed to account for the labilization of carbonyl ligands by distant phosphine ligands in the reaction of $Ir_4(CO)_{12}$ with phosphines.[211d] Here there is a *formal* analogy to the indirect interaction between adsorbates on a metal surface such that ordered overlayers are expected. For two adatoms (ligands) on a metal surface interacting with the electric field each transmits its influence from one to the other. The interaction on the same crystal plane is not necessarily isotropic, and it is an oscillatory function of the adatom separation, either attractive or repulsive, with a periodicity which is determined in part by the electronic structure of the surface. The through-bond interaction between adsorbed ligands provides, among other effects,[37a] a long-range ordering force customarily observed in ordered overlayers by LEED. Critical comparison of geometry and electronic interactions on chemisorbed metal surfaces to the geometry effects on NMR spin–spin coupling constants and on

a complex and typically multicenter interaction on clean metal surfaces or at least on some metal surfaces—and that the crystallography of that surface will be a very important structure-determining factor. Since the definitive studies of atomic adsorption on metal surfaces establish *multicenter* metal (adsorbate atom interactions; the formal and topological features of a metal cluster), the metal surface analogy appears to be valid. However, the critical molecular detail of stereochemical correspondence between appropriate and comparable (metal and crystallography) molecular clusters and chemisorbed states for surfaces may or may not be valid. There presently are insufficient structural data for the chemisorbed state to even begin to test this stereochemical feature of the analogy.

III. Thermochemistry and Energetics of Bonding in Clusters and at Surfaces

A. Introduction

Comparisons of the heterogeneous surface thermochemistry of metal clusters and of chemisorption on extended surfaces can, in principle, provide important insight into the nature of chemical bonding on these materials. The major considerations in chemical bonding for both classes of materials are: the number of metal atoms involved per bonding site, orientation, and electronic character. In the case of adsorption on extended metal surfaces, additional factors to be considered are the availability and mobility of the valence band electrons, and the occurrence of extensive local and long-range interactions. Multiple adsorption states can exist in both cases although, once again, their nature and behavior will show interesting distinctions between the two classes. Reference is recommended to recent reviews for an extended discussion of the role of surface chemical bonding in chemisorption.[5,212]

Evidence is increasing with reference to chemisorption on metal surfaces that the adsorbed species is chemically bonded primarily to a small number of nearest metal atom neighbors. This has led to a major theoretical effort in the modeling of chemisorbed systems based on metal–adatom models composed of localized bonded complexes.[213] The localized bonding approach offers a better insight into the electronic nature of the chemisorptive bond than into the determination of the binding energies.[214] Calculations of the energetics based on cluster model concepts probably will improve by the application of more rigorous calculational methods.

Photoelectron spectroscopy is widely used as a probe of chemical bonding in chemisorbed metal systems and in almost every case, interpretation is based on comparisons of the spectra for the chemisorbed system to that of a molecule–metal atom configuration. For example, the importance of this approach was first pointed out by the early work of Conrad et al. on $Rh_6(CO)_{16}$.[215a] In a subsequent study of the photoelectron spectra of transition metal carbonyl complexes in comparison with the spectra of chemisorbed CO, strong similarities in the spectra are observed by Plummer, Salaneck and Miller.[215b] The evidence for the analogy between the two systems will be considered in more detail in the following sections dealing with the energetics of binding on pure single crystal surfaces, on complex surfaces, and with the vibrational properties of chemisorbed surfaces and metal clusters. Although an essential underlying relationship is indicated by all the results, the apparent commonness which exists in the interpretation of the nature of the chemical bonding in the two classes must be approached cautiously. Although a strong similarity exists between the photoemission spectra for the two chemical bonding systems, this does not necessarily indicate strong similarities in chemical bonding in the two cases.

It is instructive as a zero-order approximation to compare binding energies in diatomic metal molecules with those of the corresponding chemisorbed state. As pointed out by Ehrlich,[216]

TABLE XXVI. Bond Dissociation Energies of Diatomic Molecules and Strength of the Corresponding M–H Chemisorption Bond (kcal/mol)

	Ni–H	Cu–H	Ag–H	Au–H	Pt–H	Al–H
molecule	60[a]	66[a]	53[a]	74[a]	83[a]	67[b]
chemisorption	63[c]	56[a]	<52[c]	<52[d]	57[e]	44[f]

[a] A. G. Goyden, "Dissociation Energies and Spectra of Diatomic Molecules", Chapman and Hall, London, 1968. [b] B. deDarwent, NSRDA-NBS 31, 1970. [c] K. Christmann, G. Ertl, O. Schober, and M. Neumann, *J. Chem. Phys.*, **60**, 4528 (1974). [d] I. O. Hayward and B. M. W. Trapnell, "Chemisorption", London, 1964, p 234. [e] K. Christmann, G. Ertl, and T. Pignet, *Surf. Sci.*, **54**, 365 (1976). [f] O. Gunnarsson, H. Hjelmbert, and B. I. Lundquist, *Phys. Rev. Lett.*, **37**, 292 (1976). (Theoretical value, experiments indicate that H_2 chemisorption is endothermic, i.e., $E_{M-H} < 52$ kcal/mol.)

such a correlation can only be significant if the valence behavior of the atom in the metal crystal has some constant relationship to that of the same atom in the vapor. This relationship does not appear to be systematically maintained for either the metal vapor–metal solid or for the metal hydride–chemisorbed hydrogen analogies. Bond dissociation energies of diatomic molecules and strengths of the corresponding metal–hydrogen chemisorption bond are shown in Table XXVI. The values are sufficiently close considering the fact that a diatomic molecule is being compared with a surface state. Accurate bond energy data for the metal–hydrogen bond in coordination complexes are not available but estimates indicate a range ~50–80 kcal/mol. The localized nature of the surface chemical bond is implicit in this comparison.[214] Such an analogy has been effectively applied to the binding of carbon monoxide to metals in terms of binding energies, electronic spectra, and stretching frequencies. Recently, accurate values have been obtained using electron energy loss spectroscopy (EELS) for the C–O and M–CO stretching frequencies of chemisorbed carbon monoxide on single-crystal nickel and platinum (Figure 38).[217,218] It appears that the shape of the metal–molecule potential energy curve near the equilibrium internuclear separation is remarkably similar for CO on the extended surface and for that bound in a molecular cluster when carbon monoxide chemisorption energies are compared to those of the metal–CO bond dissociation energies in mononuclear and polynuclear carbonyl coordination compounds. For example, the bond energy in nickel carbonyl falls within the range of known values for CO chemisorption energies on nickel.[214] Hence, a description of the chemisorption energetics of both carbon monoxide as well as the entire related class of simple diatomic molecules can be usefully considered in relation to the corresponding molecules in molecular metal cluster chemistry. The existence of important distinctions must, of course, also be recognized. These are associated with contributions from the metallic electrons and the higher coordination (metal–metal interactions) characteristics of the extended metal surfaces.

All data for the bond energies of the metal–ligand bond in metal clusters are derived from measured heats or enthalpies of formation from the metal and the ligand. All bond energies are averaged bond energies—averaged over all ligand sites in the cluster. Substantial uncertainties in these average bond energies exist because the partitioning of the enthalpy contributions among the metal–metal and the metal–ligand interactions cannot be free of assumptions. Far more accurate average metal–ligand bond energies can be derived from the measured enthalpies of formation of mononuclear metal coordination complexes and these actually serve as a basic reference point. For the same reason, the values derived from calorimetric data for average metal–metal bond energies in metal clusters have an uncertainty in magnitude. Uncertain too are the metal–metal bond energies at the surface and only the values derived from bulk metal–metal bond energies can be used in the comparison of surface and cluster regimes.

TABLE XXVII. Metal–Metal "Bond Energies" [a] **($D_0[M_2(g)]$,** [b] **CBE (Calculated "Bonding" Energies),** [c] **and VSBE (Calculated Valence State Bonding Energies)** [d] **Values for the Transition Metals**

	Sc	Ti	V	Cr	Mn	Fe	Co	Ni	Cu	Zn
D_0	38 ± 5	38 ± 5	57 ± 4	36 ± 7	10 ± 7	29 ± 5	39 ± 6	53 ± 5	47 ± 3	(2)
CBE	30	28	25	16	10	16	20	24	27	16
VSBE	45	39	(33)	(26)	(17)	26	34	(44)	(56)[e,f]	62

	Y	Zr	Nb	Mo	Tc	Ru[f]	Rh	Pd	Ag	Cd
D_0	37 ± 5	(70)	(80)	(70)	(65)	(70)	66 ± 5	25 ± 5	39 ± 2	1.8 ± 0.2
CBE	34	36	35	26	23	29	27	23	23	13
VSBE	48	45	(40)[e]	(24)[e]	30	38[e]	(43)[e,f]	(49)[e,f]	(54)[e,f]	(56)

	La	Hf	Ta	W	Re	Os	Ir	Pt	Au	Hg
D_0	58 ± 5	(80)	(90)	(95)	(98)	(95)	(92)	90 ± 10	53 ± 2	3.2 ± 0.5
CBE	34	37	37	34	27	31	33	34	29	8
VSBE	43[e]	50	(44)	(40)	34	43	(47)	(53)	(57)[e,f]	(62)

[a] All data taken from compilations or calculations by L. Brewer.[219,220] [b] Values given in kcal/mol. [c] Heats of atomization of the element in kcal/mol per bonding electron per atom at 298.15 K or at the melting point, whichever temperature is lower. [d] Bonding energies in kcal/mol per bonding electron per atom of the $d^{n-2}sp$ valence state in the hexagonal close-packed structure. Values in parentheses are predicted for unstable structures. [e] Bonding energy is given for the $d^{n-1.7}sp^{0.7}$ state. [f] The number of bonding electrons are nonintegral for Ru, Rh, Pd, Cu, Ag, and Au (respectively, 5.4, 4.4, 4.3, 2.4, 2.4, and 2.4 electrons).
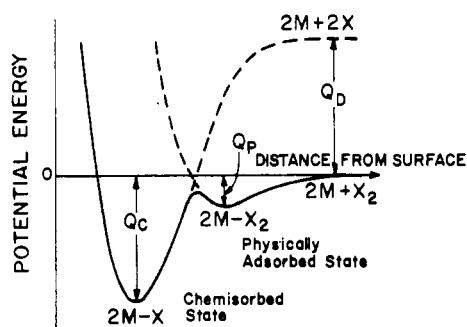

Figure 32. Schematic of the variation in potential energy with distance from the surface associated with dissociative adsorption of a diatomic molecule X_2. Intersection of the potential energy curves for the molecule and atom below the energy zero results in nonactivated adsorption. Q_P is the heat of physical adsorption of the molecule. Q_C is the heat of chemisorption, and Q_D is the heat of dissociation of the free molecule. The binding energy per atom is $(Q_C + Q_D)/2$.

Figure 33. Thermal desorption spectrum obtained after saturation adsorption of hydrogen on W(111) (after Tamm and Schmidt[221]).

B. Metal–Metal Bond Energies at Metal Surfaces

There exists no experimental technique for the direct measurement of metal–metal bond energies for surface metal atoms in a metal. However, a magnitude estimate for the surface bond energies can be obtained from the bond energies in the bulk. Brewer[219,220] has calculated the bonding energy (CBE) of metals from the heats of atomization of the metal and expressed these in kcal/mol per bonding electron per atom at 298.15 K (Table XXVII). Utilizing spectroscopic data, Brewer[219,220] adjusted the bonding energies so as to obtain the bonding energy of the d^{n-2} sp valence state of the hexagonal close-packed structure per bonding electron per atom. These calculated values are presented in Table XXVII as the valence state bonding energies (VSBE). Also listed in Table XXVII are the dissociation energies of the gaseous M_2 molecules (D_0).

C. Energetics of Chemisorption on Single-Crystal Metal Surfaces

Quantum mechanical descriptions of adsorption on metals postulate in a simplified picture that the potential energy of a molecule as a function of its distance from the surface in one dimension shows two minima, a shallow one due to purely physical forces and a deeper one closer to the surface resulting from chemical forces. These concepts are illustrated in Figure 32 where dissociative adsorption of a molecule is illustrated. One
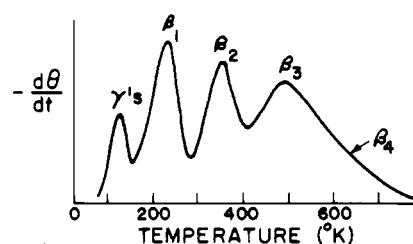
important corollary of this approach is that the chemisorbed state may be preceded on the surface by a weakly adsorbed precursor state. In the common case of nonactivated adsorption, the heat of adsorption is given to a good approximation by the activation energy for desorption. In most strongly chemisorbed systems, the activation energy for adsorption is relatively small or nonexistent. Figure 32 shows that the adsorbate binding energy is equal to the heat of adsorption for nondissociative adsorption and is equal to the heat of adsorption plus the heat of dissociation in the case of dissociative adsorption.

The thermal desorption technique is the most widely used method for estimation of activation energies for desorption and to approximate the heat of adsorption. It is also widely used for determining the nature of multiple bonding states on surfaces. It is based primarily on measuring the decrease in surface coverage systematically in terms of the gas desorption rate upon uniformly increasing the temperature of a chemisorbed surface until all the adsorbed gas has been desorbed. From suitable analysis of the pressure changes and knowledge of the desorption mechanism, important information on both the adsorption energies and the nature of multiple binding states can be obtained as a function of surface coverage.[221,222] A typical desorption spectrum, indicated in Figure 33, shows the multiplicity of binding states for a hydrogen–tungsten system corresponding to a different desorption energy in each case.

Heats of adsorption can be measured more accurately using equilibrium measurements of the isosteric heats of adsorption based on application of the Clausius–Clapeyron equation. The coverage dependence on single-crystal surfaces can be followed in terms of the changes in work function or of LEED intensities corresponding to a given surface structure at constant pressure of the gas. Adsorption isosteres can be constructed from the adsorption isobars and the heats of adsorption calculated. Abrupt changes in the heat of adsorption are observed. They are cor-
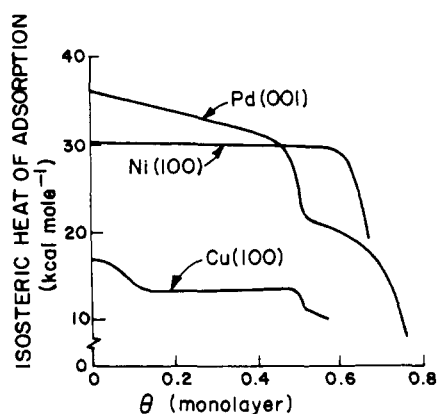
Figure 34. Variation of isosteric heat of adsorption for carbon monoxide on the (100) planes of Pd, Ni, and Cu. Abrupt decreases in heat of adsorption at high coverage have been attributed to strong repulsive interactions between the adsorbed molecules (after Tracy and Palmberg (1969) and Tracy (1972), ref 223).

related with changes in surface structure indicated by the LEED measurements and interpreted in terms of repulsive lateral interactions among the adsorbed molecules. This is indicated in Figure 34 for the chemisorption of CO at room temperature on the (100) planes of some fcc metals.[223] The concept of multiple binding states indicated by these results is generally characteristic of adsorption on uniform clean surfaces of single-crystal metals. It can be due either to differences in the nature of binding states on the surface possessing inherent or structural heterogenity (intrinsic) or to heterogenity characteristics of a uniform surface induced by the lateral interactions of the adsorbed molecules (extrinsic). The latter effect is a fundamental characteristic of chemisorption on metal surfaces. In this case the observed dependence of binding of ligands to metals in molecular clusters which vary in size presents an interesting basis for comparison of binding energies between the two classes.

The strengths of the substrate adsorbate bond corresponding to the initial state of adsorption on clean single-crystal metal surfaces for some common gaseous adsorbates may vary over a broad range as indicated in Table XXVIII. It is interesting to note, however, that the average bond energy in a given transition metal carbonyl often is within the same range for heats of chemisorption of CO on the same metal.[214] The average strength of the Ir–CO bond, in $Ir_4(CO)_{12}$, for example, is concluded to be about 45 kcal/mol[224] compared to the adsorption energy on iridium (111) of 34 kcal/mol. The scarcity of this kind of chemical bonding data indicates an area where systematic comparable measurements would be very informative. Since systematic measurements of the energetics of adsorption on clean, well-defined single-crystal metal surface is just beginning any extended comparison with the thermochemistry of cluster compounds is necessarily rather limited at present. Extensive measurements of solid metallic compounds, e.g., metal hydrides, exist but comparison of bonding strengths in these materials to metal cluster hydrides is obscured by the presence of a large crystal bonding component in the former case.

D. Energetics of Chemisorption on Complex Surfaces

It is not appropriate at this state of development to attempt to make any detailed consideration of chemical bonding on alloy, polycrystalline, or stepped surfaces although much might be achieved using these considerations to clarify the proposed connection between bonding on surfaces and in clusters. It is informative, however, to consider some general aspects of chemisorption in certain cases where a direct connection in the energetics of bonding and adsorption between the two systems is indicated.

TABLE XXVIII. Strength of the Substrate–Adsorbate Bond E_b (kcal/mol) on the Most Densely Packed Planes of Some Transition Metals

	N	O	H	NO	CO
Fe(110)	140[a]		64[a]		
Ni(111)	135[b]		63[p]	25[b]	27[c]
Cu(111)			56[p]		12[d]
Ru(001)					29[a]
Pd(111)	130[b]	87[b]	62[q]	31[b]	34[e]
Ag(111)		80[f]		25[h]	6.5[g]
W(110)	155[i]	8[j]			50–66
Ir(111)	127[k]	93[l]	63[m]	20[k]	34[g]
Pt(111)	127[n]		57[r]	27[n]	32[o]

[a] F. Bozso, G. Ertl and M. Weiss, to be published. [b] H. Conrad, G. Ertl, J. Kuppers, and E. E. Latta, *Surf. Sci.*, **50**, 296 (1975). [c] K. Christmann, O. Schober, and G. Ertl, *J. Chem. Phys.*, **60**, 4719 (1974). [d] J. Pritchard, *J. Vac. Sci. Technol.*, **9**, 895 (1972). [e] G. Ertl and J. Koch, *Z. Naturforsch.*, **25a** 1906 (1970). [f] H. A. Englehardt and D. Menzel, *Surf. Sci.*, **57**, 591 (1976). [g] G. McElhiney, H. Papp, and J. Pritchard, *ibid.*, **54**, 617 (1976). [h] R. A. Marbrow and R. M. Lambert, *ibid.*, **61**, 317 (1976). [i] P. W. Tamm and I. E. Schmidt, *ibid.*, **26**, 286 (1971). [j] P. W. Tamm and L. E. Schmidt, *J. Chem. Phys.*, **54**, 4775 (1971). [k] W. H. Weinberg, personal communication. [l] V. P. Ivanov, G. K. Brekov, V. I. Savchenko, W. F. Egelhoff, and W. H. Weinberg, *Surf. Sci.*, **61**, 207 (1976). [m] J. Kuppers and A. Plagge, to be published. [n] C. M. Comrie, W. H. Weinberg, and R. M. Lambert, *Surf. Sci.*, **57**, 619 (1976). [o] G. Ertl, M. Neumann, and K. M. Streit, *ibid.*, **64**, 393 (1977). [p] B. deDarwent, NSRDA-NBS 31, 1970. [q] G. A. Somorjai, 1977. [r] K. Christmann, G. Ertl, and T. Piagnet, *Surf. Sci.*, **54**, 365 (1976).

The electronic properties of chemical bonding can vary considerably between a metal atom on an extended surface and in a grouping characteristics of a small cluster. Thus the energetics of chemical bonding in alloy surfaces which may possess intermediate bonding properties should be especially instructive. This approach is particularly pertinent because of the recent availability of physical and chemical methods for selectively probing the bonding behavior of atoms in alloy metal surface which are well defined both in structure and in composition.[225]

1. Adsorption on Alloy Surfaces

There are two important effects in chemical bonding of atoms on alloy metal surfaces which can differ significantly from that on a single-component metal surface. The average valence electron properties of atoms A may be directly influenced by the near-neighbor presence of atoms B. This is the so-called "ligand" effect,[226] resulting from the influence of metal atoms in the proximity of a given adsorption site. This would have an analogy with metal cluster compounds containing more than one kind of metal atom. Such comparisons have not as yet been explored to our knowledge. It is also known for certain metal binary systems such as the group 8/1B elements that to a first approximation this effect is sufficiently small to be ignored in general. The chemisorptive properties of an alloy surface in this case will simply reflect a superposition of the behavior of the pure constituents weighted by their mole fractions assuming the ligand effect can be so neglected and that only a single metal atom is involved in the individual chemisorption bond. Another interesting effect, called the "ensemble" effect, occurs if more than one atom is involved in the bond formation.[227] In such a case, distribution and configuration of ensembles of A and B will be the structure-determining factor. The surface configurations for this situation would show important differences in bonding between terminal and bridging sites.

The spacing and configuration of the adsorption sites for a single adsorbed molecule would be defined for an alloy surface of a determined composition and crystallography to an extent similar to clusters where the spatial arrangements of bonding sites is determined by the number and position of metal atoms. Although application of the ensemble effect analogy between
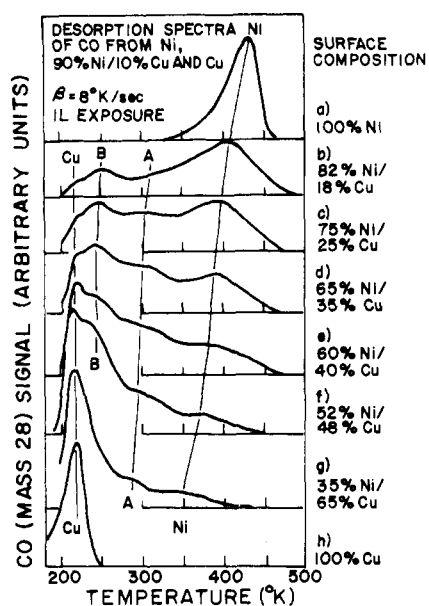
Figure 35. Thermal desorption spectra of CO on (110) planes of Cu/Ni alloys with varying surface composition (after Yu et al.[228]).
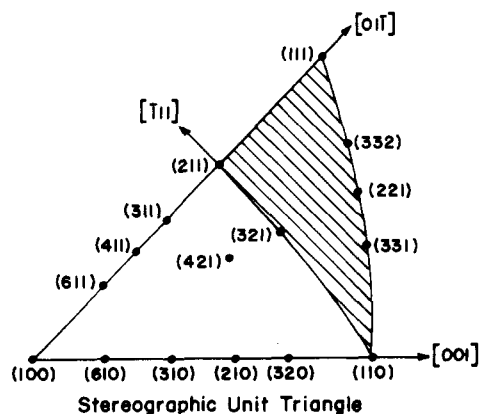

Figure 36. Stereographic triangle of the normals to various planes of tungsten. Planes located in the shaded area are predicted to be unreactive for dissociative N_2 chemisorption at 300 K (after Adams and Germer[235]).

TABLE XXIX. Heats of Adsorption (kcal/mol) of CO on (hkl) Planes of Transition Metals

plane	(111)	(100)	(110)	(210)	(211)	(311)
Ni	26.5[a]	30[c]	30[d]			
Cu	12[e]	13.5[f]			14.5[g]	14.5[g]
Pd	34[b]	36.5[h]	40[i]	35[i]		35.5[i]
Pd (theory)	34[j]	36	40	35		35

[a] K. Christmann, O. Schober, and G. Ertl, *J. Chem. Phys.*, **60**, 4719 (1974). [b] G. McElhiney, H. Papp, and J. Pritchard, *Surf. Sci.*, **54**, 617 (1976). [c] J. C. Tracy, *J. Chem. Phys.*, **56**, 2736 (1972). [d] T. N. Taylor and P. J. Estrum, *J. Vac. Sci. Technol.*, **10**, 26 (1973); N. H. Madden, J. Kuppers, and G. Ertl, *J. Chem. Phys.*, **58**, 3401 (1973). [e] H. Conrad, G. Ertl, J. Kuppers, and E. E. Latta, *Solid State Commun.*, **17**, 613 (1975). [f] J. C. Tracy, *J. Chem. Phys.*, **56**, 2748 (1972); M. A. Chesters, J. Pritchard, and M. L. Sims in "Adsorption-Desorption Phenomena", F. Ricca, Ed., Academic Press, New York, 1972, p 277. (Tracy observed below O = 0.1 an increase of E to about 16.5 kcal/mol which is not believed to be representative for the perfect Cu(100) plane.) [g] H. Papp and J. Pritchard, *Sur. Sci.*, **53**, 371 (1975). [h] J. C. Tracy and P. W. Palmberg, *J. Chem. Phys.*, **51**, 4852 (1969). [i] H. Conrad, G. Ertl, J. Koch, and E. E. Latta, *Surf. Sci.*, **43**, 462 (1974). [j] G. Doyen and G. Ertl, *ibid.*, **43**, 197 (1974). In this semiempirical calculation the value for Pd(110) was adjusted with the experimental data.

alloy surfaces and clusters has not as yet been explored, its use can give information on the number and geometry of binding sites on surfaces and clusters. A quantitative understanding of this phenomenon for metal alloy surfaces does not as yet exist but the observed results can be usefully rationalized in terms of the dependence of the heat of adsorption on surface coverage. The heat of adsorption should be constant with coverage if only a single atom A is involved until all the A atoms are occupied and then should drop suddenly to the value for pure B atoms, assuming the absence both of a ligand effect as well as lateral interactions among adsorbed atoms. If a group of either A or B atoms contribute to surface bonding, then different adsorption energies should be associated with ensembles of different configurations. A spectrum of adsorption sites will result with a corresponding sensitive and continuous dependence of the adsorption energy on coverage. Such is the observed effect for thermal desorption spectra for copper–nickel alloys[228] as shown in Figure 35.

This type of interpretation was applied to the analysis of data measured by Sinfelt[229] by Burton and Hyman[230] on the catalytic activity of Cu–Ni alloys for hydrogenolysis of ethane to methane.

They concluded that the C_2H_6 molecules requires two adjacent neighbor nickel atoms in the surface for the reaction to proceed. The occurrence of mixed adsorption sites due to the ensemble effect, with adsorption energies between those for the pure constituent, is evident from Figure 35. Desorption peaks for the different alloy surfaces appear to represent a spectrum of states with different adsorption energies and, by implication, catalytic effectiveness; an extended discussion is available in a recent review.[231] The metal atom configurations defined in a given cluster geometry could be employed to construct similar analyses.

2. Effects of Crystallography and Stepped Structures

The geometric arrangement of the metal atoms obviously should affect surface chemical bonding in both extended metal surfaces and in cluster compounds. Taylor's[232,233] concept that distinctive configurations of metal atoms are associated with "active centers" in solid surfaces has long been considered to be important in the understanding of chemisorption and catalysis. The heats of adsorption would be expected to be higher, for example, on less densely packed planes where the coordination number is lower and more unsaturation exists. There should also be pronounced effects for different crystallographic surfaces characteristic of large variations in the directions and strength of the orbitals of the surface atoms. Although the availability of systematic data on the influence of crystallography on initial heats of chemisorption is rather limited, the general indication is that the crystallography of the surface has a surprisingly small effect on the steady-state adsorption energies.

It is significant that the initial heats of adsorption of hydrogen on different crystal planes of tungsten varies only from 33 to 40 kcal/mol.[234] Table XXIX presents data for carbon monoxide adsorption on various low index crystal planes of nickel, copper, and palladium.[214] The total variation is less than 20%, although there is a general tendency for an increase of the adsorption energy with decreasing coordination number for the surface atoms among the three most densely packed planes, e.g., (111) < (100) < (110). On the other hand, the variation of the adsorption energy with coverage for different crystal planes of the same metal is at least as large as those among the same planes, for the initial heats of adsorption on different metals. Apparently, the differences due to interactions among adsorbed particles and among different adsorption sites are about the same magnitude as the variations of the single adsorbate bond energy with surface crystallography. It should be noted, however, that the effect of surface crystallography is often more important with respect to variations in the surface reaction kinetics. This is clearly illustrated by the work of Adams and Germer[235] shown in the stereographic plot (Figure 36) of sticking coefficient as
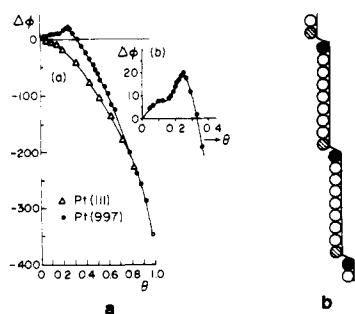
Figure 37. (a) Variation of the work function as a function of hydrogen coverage on a "flat" Pt(111) surface (triangles) and on a stepped Pt(S)-[9(111) × (111)] plane (circles) (after Christmann and Ertl[214]). (b) Model for the Pt(S)-[9(111) × (111)] at monolayer coverage with hydrogen illustrating the existence of three different types of adsorbed H atoms (after Christmann and Ertl[214]).

a function of crystallography for the dissociative adsorption of nitrogen on tungsten. The adsorption rate of nitrogen appears to be directly dependent on the proportion of sites present in the (1 × 1) geometric configuration on the surface. Controversial reports on the sensitive dependence of sticking coefficients on surface crystallography upon careful analysis of molecular adsorption kinetics have often been shown to depend more on the occurrence of a small but distinctive difference in activation energies for dissociation in defining a relatively low adsorption reactivity than for variations in the heats of adsorption with crystallography.

Taylor's concept of active centers[232,233] on catalytic surfaces also implies that surface imperfections such as, for example, those associated with step- and kink-sites are likely to be important in defining surface bonding and reactivity. Although some dramatic effects have been reported for specific cases such as the chemisorption of hydrogen on stepped Pt(111),[236] extensive studies indicate that the influence of steps on the energetics of adsorption is in general only about a few kcal/mol. This is about the same order of magnitude as the difference in heats of adsorption of CO among different crystal planes of the same metal (Table XXIX). Nevertheless, the data show that the adsorbate is more strongly adsorbed at steps; thus there is a small but distinctive higher binding energy on those sites. An interesting correlation was made between work function changes, binding geometries, and adsorption energy with coverage for hydrogen adsorbed on the Pd(111) and the Pd[(111)×9(111)] surfaces by Ertl et al.[237] where the heat of adsorption is constant at about 20 kcal/mol for the former but starts out at 24 and then steadily decreases to 21 with coverage for the latter. This is taken to indicate that the initial adsorption takes place somewhat more strongly on the steps; thereafter, when the stepped surface becomes saturated, adsorption proceeds in similar fashion for both surfaces.

The work functions show two discontinuities at low coverages on the palladium stepped surface. Two somewhat different bonding states at steps and bonding states on terraces could account for these discontinuities. The variation in the work function and the corresponding model for adsorption illustrating the three different binding sites on the stepped surface are shown in Figure 37.

The small but distinctive difference in adsorption associated with the presence of steps on crystal surfaces suggests a useful analogy with the role of geometrical irregularities on clusters in ligand bonding. It is important to note that whereas the steady-state energetics of adsorption are not very strongly influenced in general by surface imperfections, the kinetics of adsorption can be more strongly affected. Ligand mobility studies of molecular metal clusters indicate that the binding energies of ligands at different sites, e.g., terminal and briding sites, are not significantly different, an observation that is consistent with the data cited above for the chemisorbed state.

TABLE XXX. Calculated Average Metal–Metal Bond Energies in Metal Clusters

cluster	metal–metal bond energy, kcal/mol	cluster	metal–metal bond energy, kcal/mol
$Fe_3(CO)_{12}$	19.1	$Rh_4(CO)_{12}$	25.3
$Ru_3(CO)_{12}$	28	$Rh_6(CO)_{12}$	23.5
$Os_3(CO)_{12}$	30.9	$Ir_4(CO)_{12}$	30.8
$Co_4(CO)_{12}$	34		

TABLE XXXI. Average Metal–Carbon Monoxide Bond Energies[a] in Mononuclear Metal Carbonyls

Cr	25.7	Fe	28	Ni	35.1
Mo	36.3				
W	42.6				

[a] In kcal/mol.

E. Metal–Metal Bond Energies in Metal Clusters

There is only one direct measurement of a metal–metal bond energy in metal coordination complexes. Electron spin resonance studies of the dimer $[\eta^3\text{-}C_3H_5Fe(CO)_3]_2$, in which the iron coordination spheres are quite crowded and the iron–iron bond is unusually long (3.13 Å) establish an explicably low iron–iron bond energy of 13.5 kcal/mol.[238] Connor[239] has estimated, from calorimetric data, bond energies of the metal–metal bond in the dinuclear $M_2(CO)_{10}$ molecules to be 23.9, 42.9, and 44.7 kcal/mol for the manganese, technetium, and rhenium complexes, respectively. These estimates are subject to the problems and uncertainties discussed below for metal clusters.

Connor[239] has also estimated metal–metal bond energies in molecular metal carbonyls from the measured standard enthalpies of formation by assuming that metal–metal and metal–carbon monoxide bond energies do not vary substantially for a set of complexes based on a common metal. For example, the enthalpies of formation are experimentally defined for $Fe(CO)_5$, $Fe_2(CO)_9$, and $Fe_3(CO)_{12}$. Connor[239] assumed that the average bond energies for the metal–metal bond, $\bar{M}$, the terminal metal–carbonyl bond, $\bar{T}$, and the bridging metal–carbonyl metal bond, $\bar{B}$, were constant in this series. With these assumptions and the enthalpies of formation for the three iron compounds, a value of 19.0 kcal/mol was obtained for the iron–iron bond. Within the iron set and within an analogous set of cobalt compounds, $\bar{M}$ was about half the value of $\bar{T}$, and $\bar{B} \cong \bar{T}$. Then with the assumption that the near equivalency of $\bar{B}$ and $\bar{T}$ would prevail in other clusters and that $\bar{M} \cong 0.68\bar{T}$ in clusters, Connor[239] calculated the metal–metal average bond energies in a set of clusters to be as shown in Table XXX. With the rather gross assumptions made, these bond energies are best considered only as estimates. Because of the energy partitioning problem, only estimates of these bond energies can be obtained.

F. Metal–Ligand Bond Energies in Metal Clusters

Enthalpies of formation have been measured quite accurately for mononuclear metal carbonyl complexes. These data then directly yield accurate values for the average metal–carbonyl bond energies in kcal/mol listed in Table XXXI. With the assumptions cited in the previous section that in a metal cluster there will be near equivalence of terminal M–CO and bridging $M_x(CO)$ bond energies and that these values are larger than the average metal–metal bond energies,[239,240] specifically $\bar{M} = 0.68\bar{T}$, the metal–carbonyl bond energies in polynuclear metal carbonyl complexes were estimated in kcal/mol as in Table XXXII. The reference iron and cobalt complexes were utilized in the original calculations where it was assumed that $\bar{M}$, $\bar{B}$, and $\bar{T}$ would not vary substantially in a series of complexes with a common metal; these calculations showed the near equivalence

TABLE XXXII. Average Metal–Carbon Monoxide Bond Energies in Metal Carbonyl Clusters

	$\overline{T}$, kcal/mol[b]	$\overline{B}$, kcal/mol[c]
$Mn_2(CO)_{10}$	23.7	
$Re_2(CO)_{10}$	43.4	
$Fe_2(CO)_9$[a]	28	31.1
$Fe_3(CO)_{12}$[a]	28	31.1
$Ru_3(CO)_{12}$	41.1	
$Os_3(CO)_{12}$	45.4	
$Co_2(CO)_8$[a]	32.5	30.8
$Co_4(CO)_{12}$[a]	32.5	30.8
$Rh_4(CO)_{12}$	37.2	37.2
$Rh_6(CO)_{16}$	34.6	34.6
$Ir_4(CO)_{12}$	45.4	

[a] Reference compounds for the calculations. [b] Terminal M–CO. [c] Bridging $M_x(CO)$.

TABLE XXXIII. Comparison of Metal–Metal Bond Distances and Bond Energies for Bulk Metal and Metal Clusters

	metal (hcp)		metal cluster	
	VSBE[a]	MM dist[b]	BE (av)[a]	MM dist[b]
Mn	17	2.36–2.67	24	2.92
Tc	30	2.703	43	3.04
Re	34	2.741	45	3.02
Fe	26	2.482	19	~2.7
Ru	38	2.65	28	~2.9
Os	43	2.675	31	~2.9
Co	34	2.506	33	~2.5
Rh	43	2.609	35–37	~2.9
Ir	47	2.714	31	2.7–3.0

[a] In kcal/mol. [b] In Å.

of $\overline{T}$ and $\overline{B}$. The assumption of near constancy of $\overline{T}$ and $\overline{B}$ in a series seems reasonable since further calculation for the rhodium set shows a variance of less than 10% for the metal–carbonyl bond energies.[239,240]

G. Comparisons and Conclusions

The comparison of metal–metal bond energies of surface metal atoms with cluster metal atoms suffers from the necessary substitution of bulk metal–metal bond energies for surface values and from the extensive assumptions made in deriving metal–metal bond energies from the measured enthalpies of formation of metal clusters and also dinuclear complexes. There is only one directly measured metal–metal bond energy, as previously indicated for $[\eta^3\text{-}C_3H_5Fe(CO)_3]_2$. This value of 13.5 kcal/mol is much smaller than Brewer's (VSBE) value[219,220] for bulk iron of 30 kcal/mol but this discrepancy is expected because the iron–iron bond in the sterically congested iron complex is relatively weak. Comparison of the VSBE values of Brewer with the Connor estimates of average metal–metal bond energies in clusters is shown in Table XXXIII (kcal/mol), and the metal–metal distances (Å) are also compared. The comparative values are in fair agreement. With the exception of the manganese group, bulk metal–metal bond energies are on average about 30% higher than for the estimated bond energies in the clusters. However, the precise comparison that should be made is that between the bond energies in the clusters and those for the *surface metal atoms with a monolayer of chemisorbed carbon monoxide,* a comparison that simply is not feasible. Expected trends in metal–metal bond energies are shown in the limited data for the clusters. The metal–metal bond energy increases in going down a group with the exception of iridium which seems to have an anomalously low value (the thermal stability and chemistry of $Ir_4(CO)_{12}$ would suggest an average iridium–iridium bond energy substantially higher than for the cobalt and the rhodium values in the related tetrametal clusters). In going from the manganese to the cobalt groups, bond energies are expected
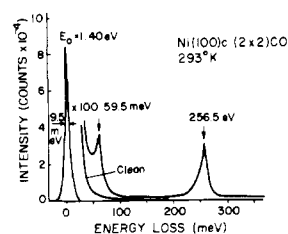
Figure 38. High-resolution electron energy loss spectra for CO adsorbed on Ni(111), $\theta - 0.5$ (after Andersson[217]).

TABLE XXXIV. Comparison of Average Metal–Carbonyl Bond Energies (kcal/mol) for Surfaces and Clusters

CO on metal	metal carbonyl	
Ru(001) 29	$Ru_3(CO)_{12}$	28
Ir(111) 34	$Ir_4(CO)_{12}$	45
Ni(111) 27	$Ni(CO)_4$	35
Ni(100) 30		
Ni(110) 30		
W(110) 50–66	$W(CO)_6$	43

to increase in a given row. In this context, the technetium and rhenium bond energies (cluster case) seem anomalously high and again those for iridium, and possibly also for osmium, seem too low.

Included in Table XXXIII are bond distance data for bulk metals and the clusters. Consistently, the metal–metal distances in the dinuclear manganese group carbonyls are longer than the values for the bulk metals. On this basis, the estimated Tc–Tc and Re–Re bond energies appear to be too large. For the clusters, the metal–metal distances are remarkably similar to the distances in the corresponding bulk metal.

A comparison of metal–carbon monoxide bond energies for metal surfaces and metal clusters is presently limited rather severely because of the lack of chemisorption energies on clean metal surfaces of well-defined crystallography and coverage. These data will be forthcoming. Ultimately, the limitations in such a comparison will reside in the uncertainties in metal cluster bond energy data. Presently available data, limited to carbon monoxide, are listed in Table XXXIV. With such a limited data set about the only valid comment is that bond energies in the two regimes are similar except for iridium and tungsten. (Although the β_1 and β_2 states of CO on W(110) are dissociated, molecular CO is produced upon desorption.)

It appears to a first-order approximation that for both the surface and cluster regimes, the strength of the carbon monoxide bond to the metal atom or atoms is relatively insensitive to the crystallography or geometric features of the interaction. Surface coverage does affect the energetics of the molecule–molecule interactions on the surface. A similar effect should be operative in clusters, but no experimental data are available to test this projection.

IV. Mobility of Ligands on Metal Clusters and of Chemisorbed Species on Metal Surfaces

A. Introduction

Spectroscopic, calorimetric, and kinetic studies of metal clusters and of the chemisorbed molecules on metal surfaces have clearly demonstrated in some instances that the ligands of chemisorbed species are not stationary. Nonstationary states may arise from two basic processes. One is a dissociation process in which all bonds between the metal and the ligand or the metal surface and the chemisorbed species are broken. If the ligand or chemisorbed species is a molecule, the dissociated molecule appears as a discrete species in the solution for the cluster case, or in the gas or solution phase for the metal surface

case. The second possible process is nondissociative, and the molecule or radical moves or migrates about the periphery of the cluster, metal particle, or surface. Throughout the itinerary of the migration, an electronic correlation between metal orbitals and ligand orbitals is not lost; as a ligand bond(s) begins to bend and stretch, a new ligand bond(s) is formed. The migration process can have a very low activation energy, lower than the alternative dissociative process. Migration is a process of considerable importance in both the cluster and the metal surface regimes with respect to catalysis. It is of importance in many aspects of surface science such as adhesion, corrosion, metal embrittlement, and soil chemistry.

An unambiguous delineation of the mechanism of molecular mobility as either a dissociative or as a nondissociative migratory process cannot always be achieved through a single experimental probe, but generally a distinction between the two processes can be achieved. For metal clusters (solution state), nuclear magnetic resonance is *the* technique for ligand mobility studies.

For metal surfaces, a primary experimental technique for direct atomistic observation is field ion microscopy although an indirect indication of mobility may be realized from differential heats of diffusion and from kinetic studies. The mobility of adsorbed particles in different directions on a metal surface is determined by the two-dimensional energy profile across the unit cell of the substrate as indicated in Figure 39. The energy maxima determine the activation barriers; the positions of minimum energy will be the preferred initial adsorption energy, E_{AD} (neglecting lateral interactions between adsorbate particles); and the energy difference between various sites will determine the relative populations at nonzero temperatures. If the variation of the adsorption energy across the surface is considerably less than kT, i.e., $\Delta E_{AD} < kT$, the adsorbed particles will behave like a two-dimensional lattice gas. Such a situation may occur in cases of physisorption where the surface diffusivity is governed by the root-mean-square velocity and mean free path. If on the other hand $\Delta E_{AD} > kT$, the adsorbed particles will spend most of their time in localized vibrational states in the equilibrium sites and their diffusive motion will consist of transitions between equivalent sites. Typical of this highly localized behavior are ordered chemisorbed overlayers. It should be noted, however, that once a chemisorbed particle receives sufficient energy to surmount the activation barrier for surface diffusion, it may travel a significant number of lattice spacings before returning to a localized vibrational state, since little cooperative motion of the substrate atoms is involved. This is in sharp contrast to the motion of atoms within the crystal via vacancy or interstitial diffusion mechanisms where jump distances of more than one lattice spacing are extremely unlikely.

A rough insight into the energetic variations across a metal surface may be obtained by looking at experimental data on the activation energy for surface diffusion. The importance of diffusion measurements is twofold. First, it is useful for understanding the kinetic mechanisms of surface processes, such as catalytic reactions, desorption, and so on, to know ΔE_{AD} and hence the temperatures at which adsorbates become mobile. Second, the variation of $\Delta E_{AD}/E_{AD}$ with crystallographic orientation provides a valuable tool for assessing the relation of substrate structure to bonding.

B. Analysis of Ligand Migration by Nuclear Magnetic Resonance Studies

The nuclear magnetic resonance (NMR) experiment is an extremely effective technique whereby dynamic processes can be evaluated in terms of the activation parameters and of mechanism. In the application of NMR to cluster dynamics, there is the requirement that the ligand, whose mobility is in question, contain isotopes of reasonable concentration that have a mag-
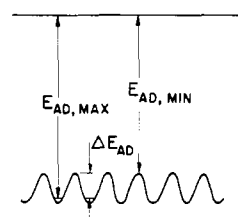

Figure 39. Periodic variation of the potential of an adsorbed particle along a surface direction.
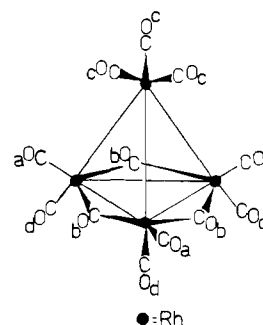

●=Rh

Figure 40. The solid state structure of $Rh_4(CO)_{12}$. The cluster has a basic C_{3v} symmetry with four ^{13}C NMR distinguishable carbonyl environments labeled a through d.

netic spin, I (ideally a spin of $^1/_2$), so that the high-resolution NMR experiment is a practical possibility. Most ligands of interest in chemisorption contain either carbon or hydrogen. Since the high-resolution proton and ^{13}C NMR experiments are routine today, there is no significant magnetic limitation in the NMR study of ligand mobility in clusters.[241]

Time scale does present a substantial problem. The time-scale window in the NMR measurement of dynamic phenomenon is relatively wide. Within the typically accessible temperature range of ~ -150 to 200 °C, dynamic processes that have rates in the range of about 10 to 10^6 per second may be quantitatively and mechanistically studied by the NMR method—or placed in terms of activation energies, the range is ~ 5 to 24 kcal/mol. However, the upper limit presents the serious limitation in this technique. The NMR technique can only sense the low- or lower-energy dynamic processes. Thus, if the *most facile* migration process in a cluster is associated with cluster features that cannot be duplicated for a metal surface, the cluster migration data will be uninformative in the analogy. There could be other more activated processes for the cluster, not detectable by NMR, that would be mechanistically analogous to the surface migration processes. Thus, we must carefully access mechanistic information for the clusters in terms of realistic applicability to a metal surface taking into account the detailed nature of the metal surface.[242] A real advantage of the NMR technique is the relative ease with which mechanistic features for migration can be outlined at the molecular level. This information is derived from an analysis of the permutational character[243] of the exchange process and the precise structural and stereochemical features of the cluster as determined by a crystallographic study.

One specific and ideal application should neatly illustrate the power of the NMR method. The metal carbonyl cluster, $Rh_4(CO)_{12}$, whose structure is shown in Figure 40, yields bonding information in the ^{13}C NMR experiment because the carbonyl (carbon monoxide) carbon atoms directly bonded to rhodium exhibit a fine structure due to spin–spin coupling of ^{13}C and ^{103}Rh nuclei, each of which has a nuclear spin quantum number, I, of $^1/_2$. Thus, there are four sets of multiplets that represent the four types of carbonyl environments: three are doublets due to $^{13}C-^{103}Rh$ spin–spin coupling, and these represent the three types of terminal carbonyl groups; the fourth is a triplet due to

TABLE XXXV. Summary of Surface Diffusion Results Using Field Emission Microscopy [d]

type of diffusion	$a^2 v \exp$ $(\Delta S^*/R)$, cm^2/s [a]	E_d, kcal	ΔS^*, cal/(mol deg) [b]	E_{des}, kcal	E_d/E_{des}
CO on W boundary free (110)		60 ± 5		$[90]$ [c]	$[0.66]$
CO on W boundary (110)		36		70	0.51
O on W boundary free	82	30 ± 1.5	13 ± 5	130	0.24
O on W 110 boundary	3×10^{-2}	24.8 ± 1	7 ± 5	125	0.2
O on W 100 boundary	1	22.7 ± 1	13 ± 5	125	0.18
H on W boundary free	3.2×10^{-4}	$9.6 - 16 \pm 3$	$[-2 \pm 5]$	65–82	0.20
H on W 110 boundary	1.8×10^{-5}	5.9 ± 1	$[-8 \pm 5]$	60	0.1
H on Ni boundary free	3.2×10^{-5}	7 ± 1	-7 ± 5	68–72	0.1
CO_2 on CO_2/W	$[10^{-3}]$	2.4		5.5	0.43
CO on CO/W		$[0.9]$		$[2.3]$	0.39
O_2 on O/W	$[10^{-3}]$	0.9		2.3	0.39
Xe on W	$[10^{-3}]$	$[3]$		9–10	0.3
Kr on W	$[10^{-3}]$	$[0.9]$		5.9	$[0.18]$
A on W	$[10^{-3}]$	0.6		1.9	0.3
K on W ($\theta = 0$)		6.9			0.11
K on W ($\theta = 0.6$)		18			
K on W ($\theta > 0.8$)		low			

[a] Column 2 gives the preexponential part of the diffusion coefficient. [b] Column 4 lists activation entropies. The symbols X/W refer to an X-covered W surface. [c] Values in brackets are preliminary or represent only rough estimates. [d] See R. Gomer, ref 261.

coupling of ^{13}C with two ^{103}Rh nuclei, and this represents the three bridging carbonyl groups, each of which is bonded to two rhodium atoms. The ^{13}C spectrum is temperature dependent; as the temperature is raised from −65 °C, the multiplets broaden and merge, a feature characteristic of dynamic exchange, and at +60 °C, the spectrum is a binominal quintet.[244,245] Interpretation of the spectral data is unambiguous; there is a rapid intramolecular exchange of carbonyl groups such that, on this NMR time scale of approximately 10^{-2} s, all carbonyl groups sense an equivalent environment. The limiting high-temperature (+60 °C) spectrum of a quintet shows that on a time-averaged basis all carbonyl atoms are spin coupled with all four rhodium atoms: $2nI + 1 = 2(4 \times \frac{1}{2}) + 1 = 5$. Retention of $^{13}C-^{103}Rh$ spin–spin coupling in the limiting spectrum unequivocally establishes that the averaging of carbonyl environments does not occur through a dissociative or bond-breaking process.

In addition to the opportunity to establish the activation parameters for cluster migration processes, there is the possibility of a reasonable mechanistic delineation of a ligand migration process in a cluster through NMR studies in which the permutational character of the process may be elucidated through line-shape studies[243] or by appropriate substitution (for example, site blocking or with diastereotopic ligand probes or both).

The major part of the mobility discussion will center on metal clusters simply because the available data for surfaces are limited and are often only inferential on a molecular scale. Since there are mechanistic implications in the cluster data, the mechanisms and their possible relation to a surface are fully explored in the latter part of this section. In the following section is a description of the potential in crystallographic analysis for sensing the physical nature of ligand migration in metal clusters. Discussion of surface mobility is largely limited to a description of those techniques that have substantial promise for probing the energetics and mechanisms of mobility of chemisorbed species.

C. Mechanistic Data for Ligand Migration in Metal Clusters from Crystallographic Data

Cluster structures are generally described in terms of idealized structures although crystallographic studies often show significant deviations from an idealized, high-symmetry model. These deformations that ostensibly result from crystal packing forces may relate in a physical sense to the lowest energy (or lower

energy) rearrangement(s). Specifically, the lowest energy deformation mode in crystal packing for a given cluster may directly correspond to the early or initial reaction path for ligand migration in that cluster. Crystallographic data have been effectively utilized in the definition of the physical processes for molecular rearrangements in simple coordination compounds.[246-251] Unfortunately, the quality of the crystallographic data of a significant fraction of the metal cluster structural studies to date is insufficient to permit such an analysis. For this specific application and for a general improvement in the accuracy of bond distances and angle data, many of the key clusters like the $M_4(CO)_{12}$ set should be carefully reinvestigated by X-ray diffraction (in many instances the limiting factor will be the quality and the size of the crystal).

Another aspect of the crystallographic data that might provide useful information about physical rearrangement mechanisms is the thermal motion characteristics of the atoms in the solid state. Here again, excellent data sets are necessary; also the cluster molecules should reside in sites of noncrystallographically required symmetry. The thermal motion data could be analyzed with the aid of existing programs for correlated motion of certain atoms within a cluster molecule which motion might then relate to the initial part of a ligand migration process. In this ligand migration section, we cite only the potential of this method of analysis; to date, no applications have been reported for clusters.

D. Metal Surfaces—Field Emission Microscopy Studies of Migration

Most information has been obtained by observing the spreading of nonuniform adsorbate layers on small tips by means of field emission microscopy.[252,253] The high magnification ($\sim 10^6$) and spatial resolution (~ 20 Å) of the field emission image make it possible to follow migration processes having velocities of angstroms per second, and thus provide the best and in many cases the only method for direct study of surface diffusion under controlled conditions. One difficulty is that such diffusion experiments often measure averages over the emitter surface even when diffusion in a single region of the emitter is observed because the rate of supply of diffusing adsorbate may be limited by diffusion over other portions of the surface. This imposes fundamental limits on the accuracy and detail obtainable using this technique.
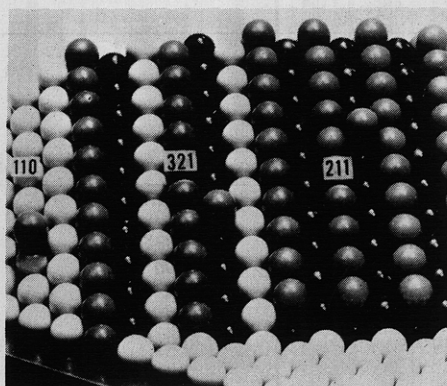
Figure 41. Hard-sphere model of the body-centered cubic lattice showing planes for which the surface diffusion directions are less directional (110) and planes where the surface mobility is highly directional (321) and (221). Number of nearest neighbors atoms: dark gray, 5, light gray, 6, and black, 7 (after Ayrault and Ehrlich[258]).
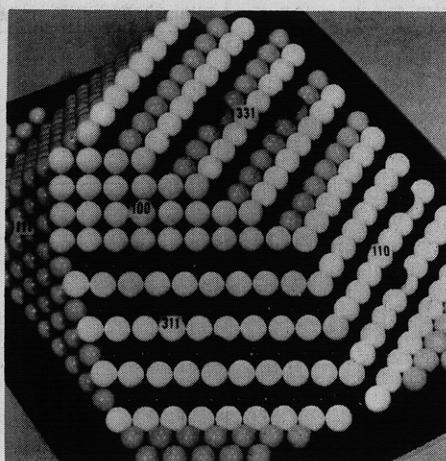
A summary of surface diffusion results for chemically and physically adsorbed gases using the field emission method is shown in Table XXXV. The nature of the activation for surface diffusion along a given direction was illustrated in Figure 39. Values for the diffusion coefficient of the migration, its activation energy, and the heat of desorption have been estimated[253] from the relations:

$$x = 2(Dt)^{1/2} \tag{1}$$

$$D \cong a^2 \nu \exp[-(E_d/kT)] \tag{2}$$

$$E_{des} \cong E_d + 3kT \ln(\bar{x}/2a) \tag{3}$$

where x represents the linear distance advanced by the boundary, $\bar{x}$ the average distance traversed before evaporation, D the diffusion coefficient, a the jump length ($\sim$3 Å), and ν a jump frequency ($\sim 10^{12}$ s^{-1}); E_{des} and E_d are the activation energies for desorption and diffusion, respectively. In this way diffusion energies for atomic hydrogen on tungsten between about 6 and 16 kcal/mol have been obtained (Table XXXV), depending on coverage and surface orientation. For H on Pt a value of about 5 kcal/mol was derived. These data imply a value for $\Delta E_{AD}/E_{AD}$ in the range 0.1–0.2 for H/W and O/W (column 6, Table XXXV), which is probably of the right order of magnitude for gas/transition metal chemisorption systems in general.

As pointed out by Gomer,[253] relations 2 and 3 are only approximately valid owing to the nature of the measurement, and it is necessary to examine each experiment with great care. An ingenious method of circumventing this difficulty has been proposed.[254,255] By the use of probe hole techniques in the field emission experiments, it should be possible to observe concentration fluctuations for thermodynamically equilibrated layers over small regions of the tip under conditions where the adsorbate is mobile, and in this way eliminate uncertainties due to correlated transport over adjacent regions. The diffusion coefficient could then in principle be determined from the relaxation time and time correlation function of the emission fluctuations. While preliminary measurements have indicated this method is feasible,[253] no experimental results have yet been reported.

E. Metal Surfaces—Field Ion Microscopy Studies of Metal Atoms on Metal Surface

Although of rather limited usefulness in chemisorption of nonmetallic atoms, field ion microscopy (FIM), which is closely related to field emission microscopy, is of considerable intrinsic interest because it allows direct observation of individual adsorbate metal atoms and much more straightforward determination of diffusion parameters. The principal application of FIM to chemisorption is to the study of surface diffusion of individual metal atoms on single-crystal planes. Hard-sphere models of

Figure 42. Face-centered cubic lattice modeled in hard spheres showing the variety of bonding sites and directions of preferred surface mobility as a function of crystallography. Nearest neighbor color code, white, 7, light gray, 8, dark gray, 9, black (front) 10, and black (right) 11. The surface diffusion features of the hard-sphere models display useful correlations with the observed mechanisms of atomic motion (after Ayrault and Ehrlich[258]).

TABLE XXXVI. Summary of Surface Diffusion Results Using Field Ion Microscopy [a]

	surface diffusion activation energy, (kcal/mol)	D_6 for surface diffusion, cm^2 s	ΔS, eu
W on W(110)	21.2	2.6×10^{-3}	2
	19.9	2.1×10^{-3}	
on W(211)	12.3	3.0×10^{-8}	−22
	13.0	3.8×10^{-7}	
on W(321)	20.1	3.7×10^{-4}	−4
	19.4	1.2×10^{-3}	
Ta on W(110)	17.9	4.4×10^{-2}	
on W(211)	11.2	0.9×10^{-7}	
on W(321)	15.4	1.9×10^{-5}	
Mo on W(211)	12.8	2.4×10^{-6}	
Re on W(110)	23.9	1.5×10^{-2}	
on W(211)	20.3	1.1×10^{-2}	
on W(321)	20.4	4.8×10^{-4}	
Ir on W(110)	18.0	8.9×10^{-5}	
on W(211)	13.4	2.7×10^{-5}	
Pt on W(110)	$\sim$14	$\sim 10^{-4}$	
Rh on Rh(111)	3.6	2×10^{-4}	0
on Rh(311)	12.4	2×10^{-4}	0
on Rh(110)	13.9	3×10^{-1}	11
on Rh(331)	14.8	1×10^{-2}	4
on Rh(100)	20.2	1×10^{-3}	−1

[a] See R. Gomer, ref 261.

close-packed crystal surfaces showing preferred directions of surface diffusion on stepped or corrugated crystallographic planes are schematically illustrated in Figures 41 and 42. It is possible to follow the random walk of a given atom as a function of temperature and thus to obtain activation energies of surface diffusion. In this manner the diffusivity of a variety of 5d transition metal adatoms on tungsten surfaces[256] and of self-adsorbed atoms on different tungsten[257] and rhodium[253] planes has been studied (Table XXXVI). Although the activation energies thus obtained vary strongly with crystallography, in general they are still considerably smaller than the binding energies. Diffusion is found to occur most easily over the smoother planes, with a notable exception being the W(110) surface, where the barrier revealed by experiment is anomalously high.[257]

The directional effects observed in these experiments are

TABLE XXXVII. Summary of Surface Diffusion Results from Mass Transport Studies[c]

	surface diffusion activation energy, eV[a]	D_0 for surface diffusion, cm²/s	atm, Torr	temp range (T/T_m), °C	method[b]
		(i) Fcc Metals			
Au(100)	2.35 (1.82)	4×10^5	H_2	0.7–0.995	a
Cu(100)	2.0 (2.16)	4.2×10^3	H_2	0.81–0.95	b
Cu	0.57 (2.16)		$<10^{-10}$	~0.3	c
Ir(111)	2.3			0.65–0.8	c
Ni(100)	1.5 (2.96)	2.6	$<10^{-8}$	0.7–0.9	a
(100)[001]	1.7 (2.96)	12.8			
		1.2×10^{-7}			
(110)[110]	1.8 (2.96)	23.9			
		3.0×10^{-6}			
Ni	0.91 (2.96)		$<10^{-10}$	0.3–0.44	c
Pd	0.91 (2.77)		$<10^{-10}$	~0.3	c
Pt	1.3 (2.97)		$<10^{-10}$	0.27–0.4	c
Rh(111)	1.78		$<10^{-10}$	0.5–0.66	c
		(ii) Bcc Metals			
Fe	2.61 (2.49)	5×10^5	H_2	0.58–0.65	a
Mo	2.3 (4.01)		10^{-10}	0.6	c
Mo(110)*	3.0 (4.01)	4×10^2		0.76–0.83	a
Mo(100)*	4.17 (4.01)	2.9×10^4		0.66–0.83	a
Ta	2.61 (4.29)		10^{-10}		c
W	2.96 (6.65)	0.5	10^{-10}	0.51–0.6	c
W(100)*	5.57 (6.65)	7.6×10^4		0.67–0.86	a

[a] Data from J. M. Blakely,[35] and references therein. [b] The numbers in parentheses are the activation energies for volume self diffusion; the values quoted are from N. L. Peterson, Solid State Phys. **22**, 409 (1968). [c] (a) Flattening of surface corrugations; (b) development of grain boundary grooves; (c) field emission studies.

exactly those suggested by the atomic arrangement of the planes. Interestingly, on the (211) and (321) planes of bcc tungsten (Figure 41), and on the (110), (331), and (311) planes of fcc rhodium (Figure 42), motion is strictly one dimensional along channels formed by close-packed atom rows. Indeed, in the rhodium experiments it was reported[258] that not a single jump from one channel to another was ever observed.

The behavior of the boundaries delineating the planes was also explored. On tungsten, the edges of the planes for which quantitative data are available were all found to act as reflecting barriers. The same was true for the rhodium planes studied except for the (331) and (100) planes, where an entirely different behavior pattern was found.[258] On these planes adatoms regularly escaped during observation with no indication that the edges acted as reflecting barriers.[257]

On the basis of the presently available results, it is thus clear that, while surface structure can often serve as a useful guide in predicting and correlating atomic properties, the atomic arrangement of a plane is not always decisive in controlling the detailed motions of adatoms. In particular, the effect of neighboring adatoms on the diffusion parameters can be significant. Correlation effects arising from interactions with nearby adatoms have been found to be significant even at interatomic distances greater than 7.5 Å.[258] (In fact correlation effects, rather than any peculiarity of the substrate lattice, have been suggested[258] to account for the anomalous diffusion behavior observed on tungsten planes.)

Unfortunately, adsorbates like O, H, or CO are not imaged even for gases for which the imaging field is not so high as to cause field desorption.[259,260] The reason seems to be that such adsorbates do not have sufficient local density of states just above the Fermi level (under high field conditions) to appreciably enhance the ionization probability of image gas atoms.[253]

F. Metal Surfaces—Mass Transport Studies

A number of surface self-diffusion measurements have also been based on mass transport phenomena, including flattening
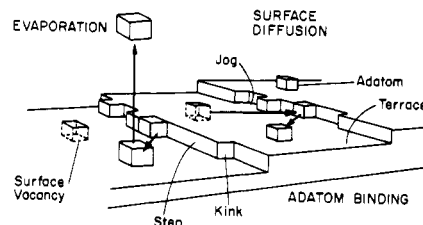
Figure 43. Schematic model of single crystal surface showing characteristic parent and line imperfections important in surface mobility and evaporation.

of surface corrugations, growth and development of grain boundary grooves, smoothing of individual surface scratches, sintering of spherical crystals, and blunting of needle-type specimens used in field emission microscopy. A schematic model of a single-crystal surface showing characteristic point and line imperfections is illustrated in Figure 43. The principles involved in describing these phenomena on surface diffusion are closely related and have been surveyed by Blakely.[35] Table XXXVII lists some surface diffusion results obtained from experiments of this type. Although there are still some significant disagreements among the available data, the surface diffusion activation energy is in most instances an appreciable fraction of that for volume diffusion. The directional anisotropies observed on Ni(110) are consistent with the qualitative trends demonstrated in the field ion microscopy measurements.

Numerous studies involving mass transport have also been made of the effects of differentially adsorbed impurities (such as chalcogens and halogens) on surface self-diffusion. Contrary to what might be expected, adsorption usually provides large increases in the self-diffusivity of the metal. For example, chemisorption of chlorine, bromine, or iodine produces spectacular increases (up to 10^4) in the surface self-diffusion coefficient for copper.[262] The diffusivities thus obtained ($>10^{-3}$ cm² s⁻¹) are difficult to interpret in terms of solid-state mass transport mechanism and tend to support the notion of the existence of a two-dimensional liquid phase.[262] In fact, the halogens, which
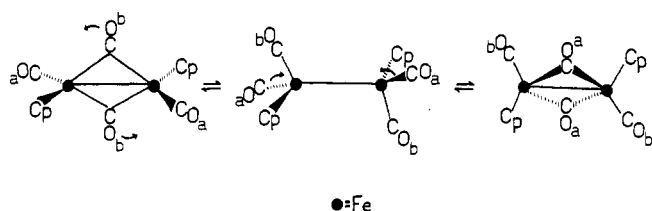
●=Fe

Figure 44. Proposed pairwise ligand exchange mechanism in *trans*-$(\eta^5\text{-}C_5H_5)_2Fe_2(CO)_4$. The trans fashion in which bridge opening and reclosure occurs is stereochemically unattainable for ligands bound to a flat metal surface.

●=Fe

Figure 45. Pairwise exchange scheme for *cis*-$(\eta^5\text{-}C_5H_5)_2Fe_2(CO)_4$. An internal rotation about the Fe–Fe bond is required for the terminally bound carbonyls "a" to attain the trans relationship required for ligand migration in this mechanism.

are known to form low-melting-point compounds with metals, were specifically chosen to test the hypothesis of a lower surface-adsorbate melting point and, hence, higher surface diffusion activity.

A lower surface melting point implies a weakening of metal–metal bonds in the outermost substrate layers, an effect which might be expected for other more catalytically interesting adsorbates as well. Frequently, the chemisorption process is accompanied by various forms of reconstruction of the substrate surface mesh. Undoubtedly the relative substrate–adsorbate electronegativities, along with the relative ionic radii, are critical parameters influencing this chemisorption-induced surface mobility.

G. Ligand Migration in Clusters

Nuclear magnetic resonance studies of metal clusters show in the temperature range of $\sim$−150 to +100 °C *facile ligand migration only for ligands of demonstrated capability for bridge bonding*, three-center and four-center bonding, **6** and **7**, with two and three metals, respectively, as well as conventional terminal two-center bonding, **5**, with a single metal atom.[294] Such bonding

●=metal

5   **6**   **7**
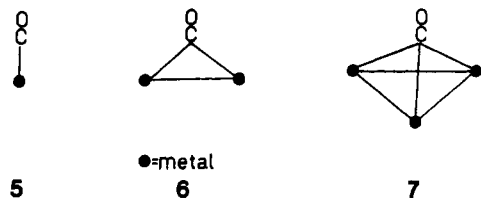
capability is an eminently reasonable requirement because, in the *conceptually* simplest case of ligand migration from one metal atom to an adjacent one, there must be a state in which the ligand atom will be centered between the two metal atoms. This state need not be a minimum (intermediate) in the energy surface representing the migration process; it may be the maximum or a local maximum. Nevertheless, if this state is a local minimum, then it would seem reasonable to expect facile migration provided other conditions are met. The paradigmatic ligand is carbon monoxide which shows all three bonding modes, **5, 6,** and **7,** in metal clusters and which is a mobile ligand in dinuclear and polynuclear metal carbonyl complexes. The hydrogen or hydride ligand is similar to carbon monoxide in bonding modes and in mobility although the NMR data that define hydrogen mobility are less extensive than those for carbon monoxide. Terminal and bridging bonding modes are established for alkyl, aryl, halide, nitrosyl, and organic isocyanide ligands in metal complexes, but NMR data that define ligand mobility are available only for organic isocyanides. Terminal and bridge bonding modes are well established for acetylenes, but a high barrier to acetylene migration may stem from a relatively large disparity in energy between a terminal and a bridging interaction. In those cases where acetylene bridges between two, three, or four metal atoms, shown systematically in **8-10**, there is an extensive rehybridization of the acetylenic carbon atom orbitals so as to form relatively strong metal–carbon σ bonds as contrasted to the conventional terminal σ–π interaction with a single
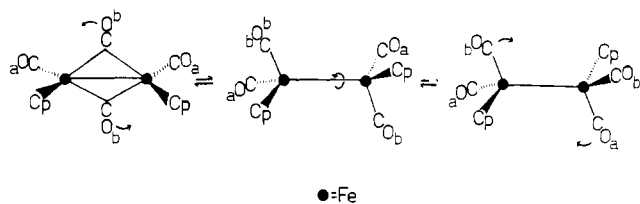
8   **9**   **10**
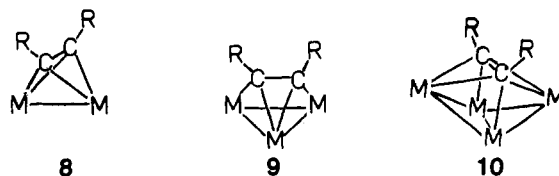
metal atom, **11**, where the extent of rehybridization is not marked. Obviously, facile migration is not expected if terminal and bridging states differ substantially in energy. If the ligand is

11

a two-electron donor in a terminal position and a greater than two electron donor in a bridging position, facile migration of this ligand will not be likely (unless pairs of terminal and bridging ligands move systematically and simultaneously) because of the electronic perturbation at the various metal centers produced in the transition or intermediate states.

The NMR data that provide mechanistic information about ligand transfer between two metal atoms in a dinuclear metal cluster generally do not relate in a meaningful fashion to possible migration mechanisms on a metal surface. In dinuclear clusters such as *trans*-$(C_5H_5)_2Fe_2(CO)_4$ (Figure 44), in which the ground state is doubly bridged,[263] there is carbonyl exchange that is proposed to occur through pairwise bridge opening and reclosing in a trans-pseudoplanar fashion.[264] This trans-pseudoplanar relationship cannot be attained on a perfectly flat metal surface where there are essentially only two degrees of spatial freedom. Furthermore, for dinuclear species such as *cis*-$(C_5H_5)_2Fe_2(CO)_4$ (Figure 45), the exchange of bridging and terminal carbonyls has the additional requirement (at least for the low-energy process) of rotation about the Fe–Fe axis for carbonyls $(CO)_a$ to attain a trans-pseudoplanar relationship.[264] Rotation of this type simply does not relate to metal atoms of a flat close-packed metal surface.

A second, mechanistically distinct process reported for the monocarbonyl bridged $(C_5H_5)_2Rh_2(CO)_3$ (Figure 46) is postulated to involve a one-for-one bridge-terminal exchange in a nonplanar fashion.[265] Unlike the mechanism which operates for $(C_5H_5)_2Rh_2(CO)_4$, this process might be envisaged for a flat metal surface, but the key factor here is the dihedral angle defined by the two (M_2CO) planes in transitional states; if the angle is very large (180°), the analogy is invalid (Figure 46).

One piece of structural and mechanistic information is evident from the data available for dinuclear metal carbonyl complexes. If the metal–metal separation is large ($\sim$3.0 Å or greater), the ground-state structure is less likely to have carbonyl groups bridging the metal bond, and if this separation is very large, the activation energy for carbon monoxide migration from one metal atom to another probably may increase. Relevant exchange data on this point are available from studies of trinuclear clusters. For example, $Fe_3(CO)_{12}$, which has a ground-state structure in which one of the triangular edges is bridged by two carbonyls,[266] displays a very low barrier of $\sim$5 kcal/mol for carbonyl ligand migration,[267] whereas $Os_3(CO)_{12}$ which has D_{3h} symmetry[268] and
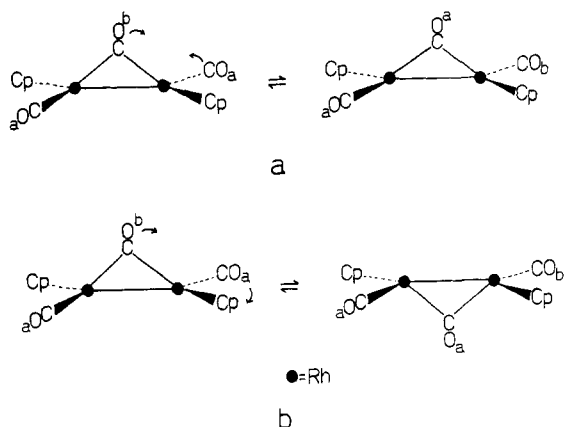
Figure 46. Two possible pathways for the postulated one-for-one exchange mechanism cis-$(\eta^5$-$C_5H_5)_2Rh_2(CO)_3$. In (a) the dihedral angle defined by the two (Rh$_2$CO) planes is small, whereas in (b) the dihedral angle is large. The former stereochemical relationship may have bearing on ligand migration at a flat metal surface, whereas the latter would not.
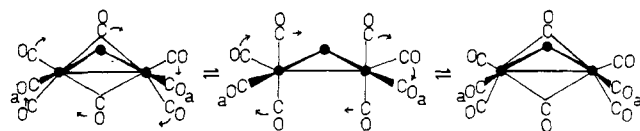

Figure 47. Synchronous exchange of six ligands between two metal centers in an M$_3$ cluster. The six ligands define a near plane perpendicular to the M$_3$ skeleton. Carbonyl ligands "a" lie parallel with the M$_3$ plane and, hence, do not participate in the ligand migration.

Figure 48. Concerted "merry-go-round" exchange of six ligands about three metal centers. The migrating carbonyl ligands are parallel to the M$_3$ plane.
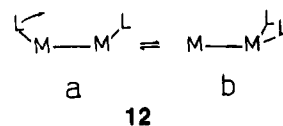

Figure 49. Exchange mechanism proposed for C_{3v} $(\eta^5$-$C_5H_5)_3Rh_3(CO)_3$. The carbonyl ligands form an all cis array, and their motion approximately defines a common conical surface. This mechanism may relate directly to ligand mobility on a flat metal surface.

12

no bridging carbonyl groups undergoes no, or a low rate of, ligand migration at elevated temperature.[269] Similarly Rh$_4$(CO)$_{12}$ has three edge-bridging carbonyls[139] and exhibits facile ligand exchange at low temperatures,[244,245,270] whereas Ir$_4$(CO)$_{12}$ has a ground-state structure with *no* bridging carbonyl ligands.[139] In bulk transition metals, the closest distance of approach for two metal atoms is less than 3.0 Å except for zirconium and hafnium; actually, the closest approach distance for the vast majority of these transition metals falls in the narrow range of ~2.46 to 2.64 Å. Since at most there may be a slight contraction of metal–metal separation in going from the bulk to the surface, the distance criterion that *may*, in extreme cases, be of importance in exchange in dinuclear as well as polynuclear metal complexes, should not be limiting in the metal surface case because here the separations are generally below the critical values for bridging ligands. Nevertheless, one might expect that ligand migration rates for metal surfaces would fall as the atomic number of the metal within a periodic group is increased. This decrease may partially reflect a metal–metal separation factor, but it undoubtedly has its major origins in electronic factors since decreases in rearrangement rates for *mononuclear* metal complexes are also observed to correlate with an increase in the metal atomic number. The impact of electronic factors is unequivocally characterized in the structural observations that Ir$_4$(CO)$_{12}$ has no bridging carbonyl ligands[139] as do isocyanide (electronically similar to carbon monoxide) derivatives,[271] whereas the electronically dissimilar phosphine ligand derivatives all have bridging carbonyl ligands in the solid and solution state structures.[202,272] *Increased electron density on a carbonyl cluster by substitution with strong donors or by formal negative charge favor the formation of carbonyl bridges because the bridging carbonyl is a better acceptor than a terminal carbonyl.*

In polynuclear or cluster molecules, there is generally coordination saturation: all the bonding molecular orbitals are filled. For this reason, a localized ligand migration between two metal atoms in the cluster, as schematically outlined in **12a** and **12b**, is relatively unfavorable simply because local sites of coordi-

nation unsaturation and, so to speak, over saturation would be generated in **12b** if there is coordination saturation in the cluster ground state (**12a**). Thus, there must generally be a concerted motion of two or more ligands if the process is to be facile. For a metal surface at less than monolayer coverages, localized and nonconcerted ligand migrations may occur to a limited extent. At full monolayer coverage—at least a full monolayer coverage on a perfect metal face where there are no defects—ligand migration rates may decrease markedly since some concerted motion of ligands would be required. This idealized limit for metal surfaces would then be more closely analogous to the typical coordinately saturated metal cluster.

What is the nature of the multicenter mechanisms of ligand migrations in metal clusters?[242] Two apparently common low-energy processes in trinuclear metal carbonyl clusters or in larger clusters that have triangular polyhedral faces, e.g., tetrahedra and octahetra, are (i) the more or less synchronous motion of six carbon monoxide ligands between two metal atoms as shown in Figure 47 and (ii) the synchronous motion of six carbon monoxide ligands between three metal atoms as shown in Figure 48. Neither of these two merry-go-round like processes can occur at a metal surface, at least, at a flat close-packed section because such a number (two or three per metal atom) of carbon monoxide ligands could not be bound to a single metal atom, and most critically because both mechanisms (Figures 47 and 48) require a near-coplanar array of metal atoms, bridging carbonyls and terminal carbonyls, a geometric feature not feasible for a close-packed metal surface although possible for spherulites where triangular metal faces obtrude and for certain corrugated crystallographic faces of single crystals. A third distinct mechanism for ligand migration in trinuclear and larger clusters is the concerted motion of carbonyl ligands about the edges of a triangular metal face where the carbonyls and the metal centers define a common conical surface (Figure 49). In contrast to the previously described mechanisms, this process may be directly related to mobility of chemisorbed species on a flat metal surface because the ligand migration occurs entirely above the cluster face, as in the C_{3v} isomer[273] of $(\eta^5$-$C_5H_5)_3$-Rh$_3$(CO)$_3$.[274]

Mobility of chemisorbed species on metal spherulites is

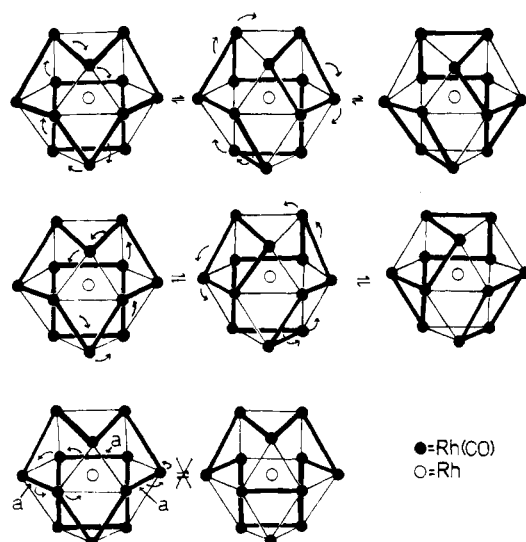**Figure 50.** Postulated six-center ligand migration processes for $Rh_{13}(CO)_{24}H_2^{3-}$ in which 21 carbonyl environments are equilibrated. The broader lines between rhodium centers represent edge-bridging carbonyls, and each rhodium center of the framework has a single terminal carbonyl attached which is not depicted, but which participates in the fluxional processes. The proposed mechanism entails the synchronous motion of three bridging carbonyls to terminal positions and three terminal carbonyls to edge-bridging positions about a hexagonal belt of the cluster. This occurs in three distinct fashions so as to generate an equivalent configuration in each instance. The third of these exchange processes is accessible only after operation of either of the first two routes. The operation of route one followed by route three is depicted on the first line of the figure, and the operation of route two followed by route three is shown on the second line of the figure. The third line of Figure 50 depicts ligand migration involving bridging carbonyls "a" which would generate a nonequivalent configuration; this process is not observed in the NMR spectra.

possibly modeled in the ligand migration process observed for $Rh_{13}(CO)_{24}H_3^{2-}$. This cluster has a polyhedral cage of rhodium atoms that precisely describe a 13-atom piece of a hexagonal close-packed metal (Figure 1).[275] NMR studies show that the carbonyl groups do migrate but only 9 of the 12 edge-bonding ligands participate in the low-energy exchange process.[169] This low-energy process seems to require a synchronous edge-terminal carbonyl exchange involving six metal centers and nine carbonyl ligands as illustrated in Figure 50 (carbonyl ligands labeled "a" in Figure 50 cannot participate in this process without generating inequivalent configurations). Hydrogen atoms migrate in this cluster simultaneously with the carbonyl ligands.[169] These dynamic processes are not relevant to a flat close-packed metal surface, only to small metal spherulites.

Ligand migration is generally fast in tetrametal dodecacarbonyls, $M_4(CO)_{12}$, and their derivatives in which one or several of the carbonyl ligands have been replaced with phosphine or organic isocyanide ligands. Depending upon the metal and the nature of the substituent, the ground-state (crystalline and solution-state) structure typically has the idealized T_d form with all ligands terminal or the C_{3v} form with one face of the tetrahedron bridged on all three edges by carbonyl ligands. The collective structural and dynamic nuclear magnetic resonance (DNMR) data clearly indicated that the idealized "T_d" and "C_{3v}" forms are very close in energy. Most of the NMR data for the carbonyl migration process in these clusters can be neatly explained by postulating facile "T_d" ⇌ "C_{3v}" intrconversions with either the "T_d" or "C_{3v}" form, an intermediate in the migration process(es) (Figure 51). Here the physical process is similar to that depicted by Figure 48.

In addition to the large $Rh_{13}(CO)_{24}H_3^{2-}$ cluster mentioned above, many of the intermediate-sized clusters undergo facile ligand migration processes. The large clusters would seem, on general principles, the better potential models of a metal surface
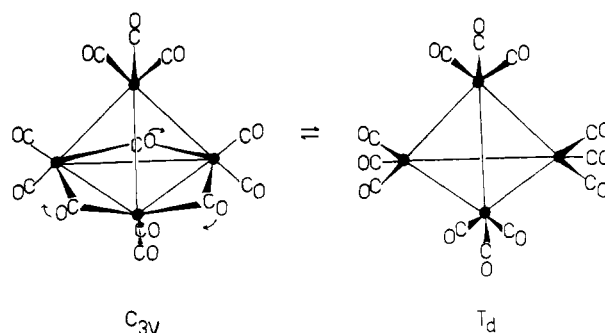

Figure 51. T_d ⇌ C_{3v} interconversions in the $M_4(CO)_{12}$ class. From the T_d form, the formation of the three edge-bridging carbonyls, so as to generate the C_{3v} form, may occur with equal probability about any of the four cluster faces.

with chemisorbed molecules. Notably, the individual metal atom coordination number for ligand atoms is substantially lower in the large clusters than in tri- and tetranuclear metal clusters. This coordination number remains relatively small for the six-atom clusters, a large class for which NMR ligand migration studies are fairly detailed. A casual interpretation of the NMR migration data for octahedral clusters would suggest that a high symmetry in the ligand array tends to raise the activation energy for the migration process. For example, $Rh_6(CO)_{16}$, which has a regular tetrahedral array[147] of carbonyl ligands with four face-bridging ligands, **13**, shows no evidence at 80 °C of ligand exchange that is fast on the ^{13}C NMR scale (note that exchange could be occurring in this cluster at rates of ~1/s at 80 °C and escape detection in the NMR experiment).[277] A related carbonyl cluster

●=Rh

13
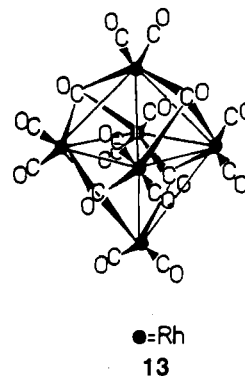
$Co_6(CO)_{14}^{4-}$ has O_h symmetry with a terminal carbonyl at each cobalt site and with a face-bridging carbonyl on each of the octahedral faces.[144] Probably this cluster will also exhibit no evidence of fast ligand migration. Both these clusters bear formal resemblances to a full monolayer coverage on a metal surface, for example, a close-packed metal array with a carbon monoxide molecule triply bridging each set of three metal atoms. One could argue that in these clusters ligand migration would have a high activation energy because the coordination saturation, the high symmetry, and the absence of defect (surface layer "holes") sites would require a highly concerted ligand migration process.

$Rh_6(CO)_{15}^{2-}$ which has only C_{3v} symmetry[143,278] with grossly inequivalent octahedral faces displays a fast CO ligand exchange[277] process that easily can be visualized (Figure 52) by a process in which an equivalent structure is formed by a concerted shift of the three face-bridging carbonyls to edge-bridging position as three terminal CO ligands shift to face-bridging positions and three edge-bridging carbonyls go to terminal positions.[277] In a sense, the $Rh_6(CO)_{15}^{2-}$ structure is like a defect structure from which intermediates that lead to ligand migration readily can be generated without unfavorable coordination numbers or geometries at any metal atom sites. All carbonyl environments in this cluster are equivalent on the NMR time
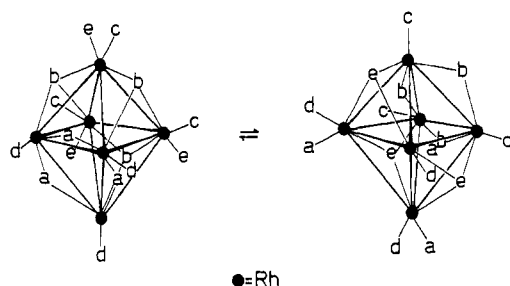
Figure 52. A postulated mechanism for ligand migration in $Rh_6(CO)_{15}^{2-}$. Edge-bridging carbonyls "a" move to terminal positions as face-bridging carbonyls "b" move to edge-bridging positions and terminal carbonyls "e" move to face-bridging positions. This generates an equivalent molecular configuration.
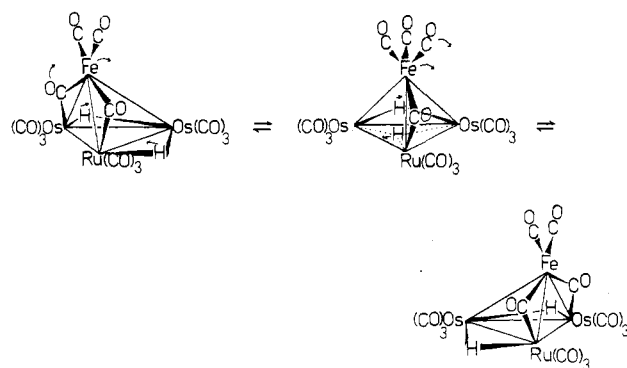

Figure 53. Synchronous carbonyl and hydride migration in concert with a deformation of the metal framework postulated for $H_2FeRuOs_2(CO)_{13}$. The net effect of the motion is to generate the molecular enantiomer of the original configuration.

scale at $-70\ °C$ (^{13}C spectrum is a binomial septet). Also of note is the highly symmetrical, trigonal prismatic $Rh_6C(CO)_{15}^{2-}$, 14,[279] which also shows no rapid (NMR time scale) ligand migration at 20 °C.[280] The sets of three bridging and three carbonyl

14   **15**

groups associated with the triangular faces of $Rh_6C(CO)_{15}^{2-}$ do not form a common plane or conical surface. On the other hand, $Rh_7(CO)_{16}^{3-}$, 15, a geometric relative of $Rh_6(CO)_{15}^{2-}$ which has a capped octahedral form of idealized C_{3v} symmetry,[4] displays an exchange of one set of three terminal carbonyls with a set of three edge-bridging carbonyls associated with the unique edge, all of which ligands share a common conical surface.[277] Clearly, ligand migration is quite facile in clusters where there are edge-bridging and terminal carbonyl ligands, which are either nearly coplanar with the metal face (Figure 48) or have a common conical surface (Figure 49).

Another facet of cluster mobility involves the deformation of metal–metal bonds as an integral part of the delocalization process. This behavior is exemplified by the exchange process
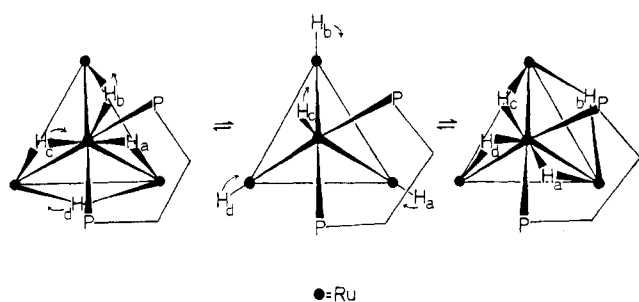

Figure 54. Proposed hydride and carbonyl exchange mechanism for $Fe_3(CO)_{11}H^-$. Migration of the hydride and carbonyl ligands forms a nonbridged intermediate which returns to the ground state by re-forming hydride and carbonyl bridges at the adjacent Fe–Fe edge. This rearrangement requires a change in the Fe–Fe bond distances.

postulated for $H_2FeRuOs_2(CO)_{13}$, and depicted in Figure 53 where stretching and bending of the metal framework occurs in concert with both CO and hydride movement.[281] This dynamic behavior of the metal framework is also expected to operate in more subtle instances, such as $Fe_3(CO)_{11}H^-$; the proposed mechanism[282] (Figure 54) requires a reorganization of the Fe–Fe bond lengths which differ in the ground state by $\sim0.11\ Å$.[283] Processes of this type, facile for metal clusters, may be more activated for metal surfaces where the number of M–M bonds is much larger, and so this serves as another point of potential distinction between cluster and surface mobility. A metal framework reorganization has also been postulated to account for the facile ligand rearrangement in $Ni_4[CNC(CH_3)_3]_7$ in which the bridging isocyanides migrate about the nickel polyhedron which is a flattened C_{3v} tetrahedron in the ground state and, presumably, a nearly regular tetrahedron in the excited state.[152]

Hydride ligands in metal clusters typically show a high rate of migration. Often these hydride migration processes are coupled with the migration of other ligands such as carbon monoxide, so that it is rather difficult to definitively delineate the permutational or physical character of the hydride ligand motions. This is not the case for the trinuclear cluster $\{HRh[P(OCH_3)_3]_2\}_3$ in which the hydrogen atoms are at edge-bridging positions.[166] These hydrogen atoms rapidly migrate about the Rh_3 triangle even at $-100\ °C$. Here the activation energy to exchange is less than ~8 kcal/mol.[166] In $H_4Ru_4[P(OCH_3)_3](CO)_{11}$, there are four edge-bridging hydrogen atoms.[284] These hydride ligands migrate rapidly at $-100\ °C$; inequivalence of the hydrogen atoms is evident in the proton NMR spectra only at $-124\ °C$.[284] This rearrangement could proceed either by hydride migration along tetrahedral edges or faces; the crystalline state of $H_4Re_4(CO)_{12}$ serves as a precedent for the latter path in that the hydride ligands in this cluster reside in face-bridging positions.[160] For an analogous $H_4Ru_4[(CH_3)_2PCH_2CH_2P(C_6H_5)_2](CO)_{10}$ cluster, a *synchronous* motion of all four hydride ligands has been established by an NMR study[168] (see Figure 55).

One of the most fascinating recent developments in cluster chemistry is the synthesis of quite large clusters by Chini and his co-workers.[288] In some of the large clusters that have hydride ligands, the hydrogen atoms are actually inside the cluster, e.g., $HNi_{12}(CO)_{21}^{3-}$ and $H_2Ni_{12}(CO)_{21}^{2-}$. The aforementioned $Rh_{13}(CO)_{24}H_3^{2-}$ cluster has the hydride hydrogen atoms positioned within the cluster and centered on the square faces of the polyhedron.[285] These hydride ligands migrate, as shown by NMR studies. Although this migration process is not mechanistically defined for this large cluster, the observations coupled with the established migration processes in smaller clusters present the possibility that hydrogen atom migrations in metal clusters and

●=Ru

Figure 55. Hydride exchange scheme for $H_4Ru_4(CO)_{10}[(C_6H_5)_2$-$PCH_2CH_2P(C_6H_5)_2]$. The synchronous motion of all four hydrides renders H_b and H_d magnetically equivalent.

metal surfaces may proceed rapidly at and within the periphery of the surface.

Conventional organic ligands in metal clusters do not exhibit the same type of mobility as carbon monoxide. Where olefinic π systems are present, ligand motion may occur in two different fashions. In clusters with delocalized ligand π systems such as in $Fe_2(CO)_5(C_8H_8)$, there may be rapid ring rotation about the metal framework as shown in **16**.[286] A second type of mobility

●=Fe

16
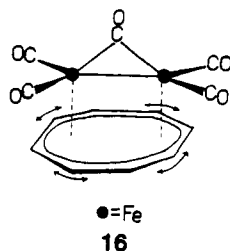
involves formal σ–π interconversions of the cluster–olefin bonding. $HOs_3(CO)_{10}CHCH_2$, depicted in Figure 56, apparently exhibits this behavior.[287] Ring rotation and σ–π interconversions do not require a coplanar ligand arrangement in the sense of that often required for CO mobility. Hence, the mobility of organic ligands in clusters *may* relate realistically to organic ligands chemisorbed on surfaces.

In the interaction of hydrocarbons with transition metals, especially clean transition metal surfaces, there is a high lability of the hydrogen atoms in the hydrocarbons, as sensed by a rapid H–D exchange in C_xH_y–C_xD_y mixtures, due to the facile scission of C–H bonds through an oxidative addition of C–H across metal–metal bonds at the metal surface. Because of the intrinsically lower reactivity of the molecular metal clusters, such C–H addition reactions are rare in cluster chemistry although $Ru_3(CO)_{12}$ and $Os_3(CO)_{12}$ exhibit a capability for stoichiometric C–H bond scission in organic molecules like ethylene and benzene at elevated temperatures.[2,3] In this context, some recent osmium cluster studies are noteworthy. Reaction of CH_2N_2 with the cluster hydride $H_2Os_3(CO)_{10}$ yields two new cluster species, a methyl and methylene complex that rapidly interconvert in solution.[199] An unusual feature of the methyl derivative is the unsymmetric character of the bridging interaction:
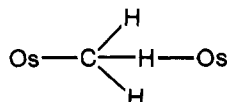
The equilibrium constant for methyl $\rightleftharpoons$ methylene is 3.5 at 32 °C. NMR data suggest structures a and b in Figure 57 for the methyl and methylene structures, respectively.[199] The equilibrium between a and b could serve as a rather neat model for H–D exchange in hydrocarbon reactions at metal surfaces, a model for the nearly pervasive hydrogen atom lability in hydrocarbons that interact at a metal surface. An equilibrium like that can also provide an indirect mechanism for methylene group migrations
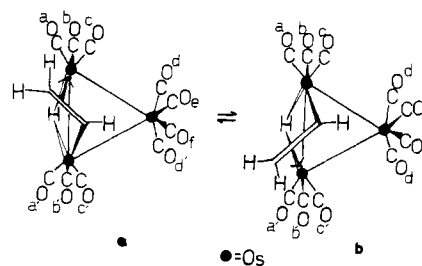

Figure 56. Formal σ–π interconversion in $HOs_3(CO)_{10}CHCH_2$. The organic ligand as a whole retains its position in the cluster.

●=Os

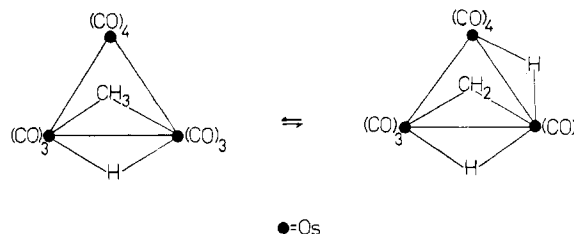**Figure 57.** Equilibrium between $HOs_3(CO)_{10}CH_3$ and $H_2Os_3(CO)_{10}CH_2$. Interconversion between the two species requires a methyl $\rightleftharpoons$ methylene transformation. The methyl group unsymmetrically bridges the Os–Os bond apparently with an $Os–CH_2–H–Os$ type of interaction.

on a surface if the reasonable assumption of relatively facile methyl group migration is made.

H. Conclusions

A precise and detailed comparison of surfaces and clusters for ligand migration processes in the contexts of the rates, of the energetics of the processes, and of mechanism is simply not possible, primarily because the requisite data are not available. In addition, the literature, extant for cluster rearrangement, is too often scant in experimental details; rates and activation energies are rarely reported for dynamic cluster processes. However, reasonably accurate estimates for activation energies can be made if the NMR spectra are reported. It is for the metal surface case that there is a substantial dearth of relevant data. However, techniques are available to redress this situation, and hopefully surface scientists will extensively examine the energetics of migration of chemisorbed species in the foreseeable future.

Hydrogen (hydride ligand) mobility on metal surfaces is high. For hydrogen on tungsten and nickel, the activation energy for surface diffusion (Table XXXV) is in the range of 6 to 10 kcal/mol, values that are only 10 to 16% that of the energy required for hydrogen (H_2) desorption from the metal surface. Hydrogen mobility in metal cluster hydrides is also quite high. Estimated activation energies for hydride migration in clusters are in the range of 3 to 9 kcal/mol. Activation energies for surface diffusion of carbon monoxide on the less reactive transition metals are now known. For tungsten, the activation energy for carbon monoxide diffusion is 36 to 60 ± 5 kcal/mol on the boundary and boundary-free (110) faces, respectively (however, there is the complication of dissociative chemisorption of carbon monoxide on such an extremely reactive metal as tungsten). These energies are very high compared to those established in transition metal carbonyl clusters where the range is ~3 to 20 kcal/mol as determined by NMR studies; nevertheless, the activation energies certainly exceed 20 kcal/mol in certain clusters. In fact, a severe limitation in the NMR method of analysis for ligand migration in metal clusters is that the time scale is such that processes that have activation energies in excess of about 20–25 kcal/mol are not detectable.

One unquestioned power of the NMR technique for the study of ligand mobility in clusters is its potential for providing mechanistic information. Available data from NMR studies of clusters

bear out this promise; some low-energy ligand processes are reasonably well delineated. Unfortunately, few of these identified processes are physically feasible on flat close-packed metal surfaces, although all are conceptually possible for tiny metal spherulites or highly irregular metal surfaces. As yet there is no mechanism, definitively established from NMR studies, in clusters where there is fast exchange of ligands that project at more or less the normal to a cluster polyhedral face; rather the typical low-energy process involves a ligand set that is more or less coplanar, or nearly coplanar, with a cluster face or share with metal atoms in a cluster face a common, shallow angled conical surface. Possibly future, detailed NMR studies of the very large metal cluster molecules or ions (like $Rh_{13}(CO)_{24}H_3^{2-}$, $Rh_{15}(CO)_{27}^{3-}$, $Rh_{14}(CO)_{25}^{4-}$, and $Pt_{19}(CO)_{12}^{4-}$ discovered by Chini and co-workers[288]) may discern ligand mobility processes that could be easily emulated on metal surfaces, perhaps even flat close-packed metal surfaces.

Ligand mobility on metal surfaces that have less than mono-layer coverage cannot be simulated in metal clusters, at least the type of molecular metal cluster that we know today. Es-sentially all known metal clusters are coordinately saturated and none, except $Pt_{19}(CO)_{12}^{4-}$, has less than one ligand per cluster surface metal atom.[288]

The discovery of large metal clusters which have hydride li-gands that lie below the cluster surface metal atoms does point to possible hydrogen migration mechanisms in metal surface chemistry that could have substantial significance with respect to mechanistic features of catalytic reactions. For example, in the hydrogenation of an ethylene molecule at a metal surface, the hydrogen atoms that are transferred to the surface bound ethylene molecule need not necessarily be transferred laterally from adjacent surface atoms but could actually emerge and be transferred from just below the surface of the metal struc-ture.

There is evidence of metal framework structural reorgani-zation in a limited number of metal cluster rearrangement pro-cesses. Normally one does not consider metal atoms to have substantial mobility at an external metal surface, but the acti-vation energies for metal atom motion and even migration is relatively low, especially if there are structural defects at the surface. In fact, there is documentation of facile surface re-constitution especially at the less thermodynamically favored, less closely packed faces (like the 110 face in cubic close packing) in the process of chemisorption.

Clearly, we see here the delineation of boundary conditions for the validity of the analogy between molecular metal clusters and metal surfaces which have chemisorbed molecules. The delineation is relatively sharp for flat close-packed metal sur-faces; there is unlikely to be much similarity between these surfaces and molecular metal clusters with respect to mecha-nistic features of ligand mobility or migration, at least for the low-energy migration processes in the clusters. The analogy, as related to stepped, kinked, or corrugated metal surfaces where spatial freedom above the surface is less limited, perhaps has more validity. Importantly, the limitations cited for mecha-nistic correlations between the flat surface and metal clusters are far less constraining for the type of metal surface of im-portance in catalysis where the surface is uneven, literally heterogeneous, and where in supported form, the metal particles are small and near spherical in form.

Additional physical studies in this area are critical to a further test of the analogy, especially where there is not a large dis-crepancy in the metal atom crystallography between the cluster and surface regimes. Much more kinetic and activation energy data are needed for ligand mobility on metal surfaces. Mecha-nistic analysis of rearrangements in certain classes of clusters is also required. In particular, the critical, previously cited, studies of large metal clusters may provide a much more incisive characterization of boundary conditions for the validity of the analogy in this area of ligand mobility.

V. Prospects for Further Study

The crucial issue in the analogy between metal clusters and chemisorbed states on metal surfaces is not, at this stage, one of validity but rather one of boundary conditions. Breakdown in the analogy does occur particularly where the crystallography of the metal atoms does not have a close correspondence in the two regimes. Since flat close-packed surfaces have no structural analogs in discrete metal clusters, the analogy between metal clusters and chemisorbed molecules on such flat surfaces is at best strained. For example, most of the common, low activation energy, ligand migration mechanisms in clusters simply are in-operative on close-packed, flat metal surfaces for purely geo-metric reasons. On the other hand, structural features of chemisorbed states of molecules on flat close-packed surfaces may be similar to those for the same molecules bound in a metal cluster. Needed now are more systematic and comparative experimental studies, studies in which the correspondences in metal, ligand, metal crystallography, and coverage are as close as possible. Delineation of boundary conditions in the analogy is not feasible without such systematic experimental informa-tion.

One of the distinctive features of coordination and of cluster chemistry is the effect of one type of ligand upon a ligand of another type. In clusters, the substitution of one ligand by one that is electronically dissimilar may lead to a different mode of binding of some ligands; for example, the substitution of carbonyl ligands in $Ir_4(CO)_{12}$ by strong donor ligands like phosphines ef-fects a shift of three terminal carbonyl ligands to edge-bridging sites in a common face. It seems reasonable to expect similar phenomena for metal surfaces. Study of mixed chemisorption states by surface scientists, although difficult, should be ex-tremely enlightening in the general context of surface science and in the specifics of the surface–cluster analogy.

The multicenter binding of organic molecules, fragments, and radicals in discrete molecular clusters is well documented particularly in the chemistry of ruthenium and osmium clusters. This multicenter binding of acetylenes, methyl radical, meth-ylene, vinylidene, benzene, carbynes, and the like is relatively well defined in a structural and stereochemical fashion. These cluster examples of hydrocarbon binding should be seriously considered as test models in the interpretation of spectroscopic and diffraction data for chemisorbed states of hydrocarbons on extended metal surfaces.

There has been no consideration of reaction dynamics in this analysis of the cluster-surface analogy simply because the comparative data are not available. The issue of reaction mechanism in stoichiometric and catalytic reactions will rep-resent the most stringent test of the analogy or better the most revealing comparison since divergent behavior is most apt to appear in this type of comparison. Because of the relatively low metal-metal bond energies and because most known metal clusters are coordinately saturated, clusters may partially fragment or wholly fragment into mononuclear complexes throughout or at some reaction step in a reaction sequence. However, the chemistry of coordinately unsaturated metal clusters should more closely conform to those of metal sur-faces.[295]

to publication: Stig Anderson, Chris Allyn, Robert Bau, Jack Blakely, Michael Boudart, Gert Brodén, Paulo Chini, Joseph Demuth, Gert Ehrlich, Gerhard Ertl, Gregory Geoffrey, Tom Grimley, Robert Gomer, Torgny Gustafsson, Michael Van Hove, H. Ibach, Franco Jona, B.F.G. Johnson, Herbert Kaesz, Joseph Lauber, Jack Lewis Bengt Lundqvist, Robert Messmer, G. A. Ozin, Ward Plummer, Roy Pruett, Robert Merrill, W.R. Salaneck, Dave Shirley, John Sinfelt, Gabor Somorjai, William Spicer, Dave S.Y. Tong, R. Willis, and M.L. Ziegler.

VI. References and Notes

(1) (a) R. Ugo, *Catal. Rev.*, **11**, 225 (1975); (b) R. L. Burwell, Jr., *Chem. Eng. News*, **44** (34), 56 (1966).
(2) E. L. Muetterties, *Bull. Soc. Chim. Belg.*, **84**, 959 (1975); **85**, 451 (1976).
(3) E. L. Muetterties, *Science*, **196**, 839 (1977).
(4) E. L. Muetterties, *Angew. Chem., Int. Ed. Engl.*, **17**, 545 (1978).
(5) (a) T. N. Rhodin and G. Ertl, Ed., "The Nature of the Surface Chemical Bond", North Holland Press, Amsterdam, 1979; (b) T. Rhodin and D. Adams, "Adsorption of Gases on Solids", N. B. Hannay, Ed., "Treatise on Solid State Chemistry. Surfaces I and II, Vol. 6A and 6B, Pergamon Press, New York, 1976.
(6) A. J. Deeming, S. Hasso, M. Underhill, A. J. Canty, B. F. G. Johnson, W. Jackson, J. Lewis, and T. W. Matheson, *J. Chem. Soc., Chem. Commun.*, 807 (1974).
(7) A. J. Deeming and M. Underhill, *J. Chem. Soc., Dalton Trans.*, 1415 (1974).
(8) J. Lewis and B. F. G. Johnson, *Pure Appl. Chem.*, **44**, 43 (1975).
(9) M. G. Thomas, W. R. Pretzer, B. F. Beier, F. J. Hirsekorn, and E. L. Muetterties, *J. Am. Chem. Soc.*, **99**, 743 (1977).
(10) E. L. Muetterties, W. R. Pretzer, M. G. Thomas, B. F. Beier, D. L. Thorn, V. W. Day, and A. D. Anderson, *J. Am. Chem. Soc.*, **100**, 2090 (1978).
(11) E. L. Muetterties, *Pure Appl. Chem.*, **50**, 941 (1978).
(12) A nearly comprehensive review of the literature to ~1976 is given by A. K. Smith and J. M. Basset, *J. Mol. Catal.*, **2**, 229 (1977).
(13) J. L. Vidal, L. A. Cosby, R. A. Fiato, W. E. Walker, and R. L. Pruett, 175th National Meeting of the American Chemical Society, Anaheim, Calif., March 13–17, 1978, No. INOR-005; J. L. Vidal, personal communication.
(14) J. B. Keister and J. R. Shapley, *J. Am. Chem. Soc.*, **98**, 1056 (1976).
(15) R. M. Laine, R. G. Rinker, and P. C. Ford, *J. Am. Chem. Soc.*, **99**, 252 (1977).
(16) R. C. Ryan, C. U. Pittman, Jr., and J. P. O'Connor, *J. Am. Chem. Soc.*, **99**, 1986 (1977).
(17) E. Band, W. R. Pretzer, M. G. Thomas, and E. L. Muetterties, *J. Am. Chem. Soc.*, **99**, 7380 (1977).
(18) G. C. Demitras and E. L. Muetterties, *J. Am. Chem. Soc.*, **99**, 2796 (1977).
(19) M. A. Andrews and H. D. Kaesz, *J. Am. Chem. Soc.*, **99**, 6474 (1977).
(20) There is no up-to-date comprehensive review on metal clusters. For an enumeration of cluster literature through ca. 1971, see R. B. King, *Prog. Inorg. Chem.*, **15**, 287 (1972).
(21) A review of large cluster ions has been presented by P. Chini, G. Longoni, and V. G. Albano, *Adv. Organomet. Chem.*, **14**, 285 (1976); and a definitive analysis of naked cluster ion chemistry has been made by J. D. Corbett, *Prog. Inorg. Chem.*, **21**, 129 (1976).
(22) V. G. Albano, A. Ceriotti, P. Chini, G. Ciani, S. Martinengo, and W. N. Anker, *J. Chem. Soc., Chem. Commun.*, 859 (1975).
(23) S. Martinengo, G. Ciani, A. Sironi, and P. Chini, ref 13, No. INOR-073.
(24) P. Longoni and P. Chini, *J. Am. Chem. Soc.*, **98**, 7225 (1976).
(25) J. C. Calabrese, L. F. Dahl, P. Chini, G. Longoni, and S. Martinengo, *J. Am. Chem. Soc.*, **96**, 2614 (1974).
(26) N. K. Adams, "Physics and Chemistry of Surfaces", Oxford Press, Oxford, 1938, Chapter 5.
(27) A. L. Ruoff, "Introduction to Materials Science", Prentice-Hall, New York, 1972, Chapter 5.
(28) A. D. Crowell in "The Solid-Gas Interface", Vol. I, E. Flood, Ed., Marcel Dekker, New York, 1967, Chapter 7.
(29) J. Kittel, "Introduction to Solid State Physics", Wiley, New York, 1970.
(30) C. S. Barrett, "Structure of Metals", McGraw-Hill, New York, 1943, Chapter XI.
(31) L. Darken and R. Gurry, "Physical Chemistry of Metals", McGraw-Hill, New York, 1953, Chapter 12.
(32) A. W. Adamson, "Physical Chemistry of Surfaces", Interscience, New York, 1960, Chapter 5.
(33) E. G. Derouane and A. A. Lucas, "Electronic Structure and Reactivity of Metal Surfaces", Vol. B16, NATO Advanced Study Institutes Series, Plenum, New York, 1976.
(34) J. F. Nicholas, "An Atlas of Models of Crystal Surfaces", Gordon and Breach, New York, 1956.
(35) J. M. Blakely, "Introduction to the Properties of Crystal Surfaces", Pergamon Press, New York, 1973, Chapter 7.
(36) T. B. Grimley in "Electronic Structure and Reactivity of Metal Surfaces", Vol. B16, E. Derouane and A. Lucas, Eds., Plenum, New York, 1970, p 35.
(37) R. Messmer in "Nature of the Surface Chemical Bond", T. Rhodin and G. Ertl, Eds., North Holland Press, Amsterdam, 1979, Chapter 2.
(38) C. Herring in "Physics of Powder Metallurgy", W. Kingston, Ed., McGraw-Hill, New York, 1951, Chapter 8.

(39) G. Ertl and J. Küppers, "Low Energy Electrons and Surface Chemistry", Verlag Chemie, Weinheim, 1974.
(40) P. F. Kane and G. B. Larabee, "Characterization of Solid Surfaces", Plenum, New York, 1974.
(41) R. Gomer in "Topics in Applied Physics", Vol. 4, Springer, New York, 1976.
(42) R. Baetzold, *Adv. Catal.*, **25**, 1 (1976).
(43) N. Rösch, "Electrons in Finite and Infinite Systems", P. Paharisean, Ed., Plenum Press, New York, 1977.
(44) J. C. Robertson and C. W. Wilmsen, *J. Vac. Sci. Technol.*, **9**, 901 (1972).
(45) W. A. Goddard III, S. P. Walch, A. K. Rappe, T. H. Upton, and C. F. Melius, *J. Vac. Sci. Technol.*, **14**, 416 (1977).
(46) H. Huber, G. A. Ozin, and W. J. Power, *J. Am. Chem. Soc.*, **98**, 6508 (1976).
(47) G. A. Ozin, H. Huber, and D. McIntosh, *Inorg. Chem.*, **16**, 3078 (1977).
(48) W. E. Kotzbucher and G. A. Ozin, *J. Am. Chem. Soc.*, **100**, 2262 (1978).
(49) D. M. P. Mingos, *J. Chem. Soc., Dalton Trans.*, 133 (1977).
(50) Trinh-Toan, B. K. Teo, J. A. Ferguson, T. J. Meyer, and L. F. Dahl, *J. Am. Chem. Soc.*, **99**, 408 (1977).
(51) M. B. Hall and R. F. Fenske, *Inorg. Chem.*, **11**, 768 (1972).
(52) B. K. Teo, M. B. Hall, R. F. Fenske, and L. F. Dahl, *Inorg. Chem.*, **14**, 3103 (1975).
(53) J. P. Lauher, *J. Am. Chem. Soc.*, **100**, 5305 (1978).
(54) The use of the boranes as models for clusters has been suggested by Wade[55] and Mingos.[56] Direct relationship of framework electrons in B_nH_n species with those in a metal cluster, M_nL_m, would seem the simplest and most effective format in this kind of analogy. This follows more or less the Mingos analogy rather than the more complicated, closo, nido and arachno subclassifications used by Wade.
(55) K. Wade, *Chem. Commun.*, 792 (1971); "Electron Deficient Compounds", Nelson, London, 1971.
(56) D. M. P. Mingos, *Nature, Phys. Sci.*, **236**, 99 (1972).
(57) R. Hoffmann and W. N. Lipscomb, *J. Chem. Phys.*, **36**, 2179 (1962).
(58) J. D. Corbett, ref 21.
(59) L. Que, Jr., M. A. Bobrik, J. A. Ibers, and R. H. Holm, *J. Am. Chem. Soc.*, **96**, 4168 (1974), and references therein.
(60) L. J. Guggenberger and A. W. Sleight, *Inorg. Chem.*, **8**, 2041 (1969).
(61) F. A. Cotton and T. E. Haas, *Inorg. Chem.*, **3**, 10 (1964).
(62) M. J. Buerger, "X-ray Crystallography", Wiley, New York, 1942.
(63) G. H. Stout and L. H. Jensen, "X-ray Structure Determination", Macmillan, New York, 1968.
(64) W. C. Hamilton and J. A. Ibers, "Hydrogen Bonding in Solids", W. A. Benjamin, New York, 1968, Chapter 2.
(65) R. Bau, *Acc. Chem. Res.*, to be published.
(66) J. W. Emsley, J. Feeney, and L. H. Sutcliffe, "High Resolution Nuclear Magnetic Resonance Spectroscopy", Vol. 1 and 2, Pergamon Press, New York, 1965.
(67) L. N. Jackman and F. A. Cotton, Eds., "Dynamic Nuclear Magnetic Resonance Spectroscopy", Academic Press, New York, 1975.
(68) J. E. Demuth, D. W. Jepson, and P. M. Marcus, *Phys. Rev. Lett.*, **31**, 540 (1973).
(69) M. Van Hove and S. Y. Tong, *J. Vac. Sci. Technol.*, **12**, 230 (1975).
(70) See ref 39, pp 128–129.
(71) (a) A. Liebsch in ref 84, p 167; (b) J. W. Gadzuk, *Solid State Commun.*, **15**, 1011 (1974); *Phys. Rev. B*, **10**, 5030 (1974).
(72) H. Froitzheim, "Electron Spectroscopy for Surface Analysis", H. Ibach, Ed., Springer, New York, 1977, p 205.
(73) M. Van Hove, "The Nature of the Surface Chemical Bond", T. Rhodin, and G. Ertl, Ed., North-Holland, Amsterdam, 1979, Chapter 4.
(74) J. Pendry, "Low Energy Electron Diffraction", Academic Press, New York, 1974.
(75) M. G. LaGally, T. C. Ngoc, and M. B. Webb, *Solid State Phys.*, **28**, 302, Ehrenreich, Seitz, and Turnbull, Eds., Academic Press, New York, 1973.
(76) D. Adams and U. Landman, *Phys. Rev. Lett.*, **33**, 585 (1974); *Surf. Sci.*, **51**, 149 (1975).
(77) S. L. Cunningham, C. M. Chan, M. A. Van Hove, S. P. Withraw, and W. H. Weinberg, *Surf. Sci.*, **66**, 394 (1977).
(78) S. Y. Tong, Proceedings of the 50th Anniversary Conference on Electron Diffraction, London, Sept 1977 (Institute of Physics).
(79) C. B. Duke, *J. Vac. Sci. Technol.*, **15**, 157 (1978).
(80) E. Zanazzi and F. Jona, *Surf. Sci.*, **62**, 61 (1977).
(81) T. N. Rhodin and S. Y. Tong, *Phys. Today*, **28**, (10)23 (1975).
(82) S. P. Walch and W. A. Goddard III, *Solid State Commun.*, **23**, 907 (1977).
(83) A. B. Anderson, *J. Chem. Phys.*, **62**, 1187 (1975).
(84) B. Feuerbacher, B. Fitton, and R. F. Willis, Eds., "Photoemission and the Electronic Properties of Surfaces", Wiley, New York, 1978.
(85) C. Kunz in ref 84, p 501.
(86) G. Ertl and J. Küppers in ref 39, p 67.
(87) C. H. Li and S. Y. Tong, *Phys. Rev. Lett.*, **40**, 46 (1978).
(88) (a) T. N. Rhodin and C. Brucker, "Characterization of Metal and Polymer Surfaces", L. H. Lee, Ed., Academic Press, New York, 1977, p 431; (b) G. Brodén, T. N. Rhodin, C. Brucker, R. Benbow, and Z. Hurych, *Surf. Sci.*, **59**, 593 (1976); (c) L. S. Cederbaum, W. Domike, W. Von Nilsson, and W. Brenig, *Z. Phys. B*, **21**, 381 (1975); (d) O. Gunnarsson, J. Harris, and R. O. Jones, *J. Chem. Phys.*, **67**, 3970 (1977); (e) C. Brucker and T. Rhodin, Proceedings of the Conference on Thin Films and Surfaces, Tokyo, July 1979; *Surf. Sci.*, in press.
(89) H. Ibach, H. Hopster, and B. Sexton, *Appl. Surf. Sci.*, **1**, 1 (1977).
(90) M. J. Chester, J. Pritchard, and M. L. Sims, "Adsorption—Desorption Phenomena", F. Ricca, Ed., Academic Press, New York, 1972.
(91) F. M. Propst and T. C. Piper, *J. Vac. Sci. Technol.*, **4**, 53 (1967).
(92) S. Andersson, *Solid State Commun.*, **20**, 229 (1976); **21**, 75 (1977).
(93) J. Lambe and R. C. Jaklevic, *Phys. Rev.*, **165**, 821 (1968).

(94) P. K. Hansina, D. A. Hickson, and J. A. Schwarz, *J. Catal.*, **48**, 237 (1977).
(95) W. H. Weinberg, "Proceedings of Symposium on Inelastic Electron Tunneling", 1978; *Bull. Am. Phys. Soc.*, **22**, 256 (1977) (abstract).
(96) E. A. Stern, *Phys. Rev. B*, **10**, 3027 (1974).
(97) G. Somorjai, "Principles of Surface Chemistry", Prentice-Hall, Englewood Cliffs, N.J., 1972, p 18.
(98) R. L. Park and H. H. Madden, *Surf. Sci.*, **11**, 188 (1968).
(99) See ref 39, p 140.
(100) K. O. Legg, F. Jona, D. W. Jepson, and P. M. Marcus, *J. Phys. C*, **8**, L492 (1975).
(101) E. A. Wood, *J. Appl. Phys.*, **35**, 1306 (1964).
(102) H. D. Shih, F. Jona, D. W. Jepsen, and P. M. Marcus, *J. Phys. C*, **9**, 1405 (1976).
(103) H. D. Shih, F. Jona, D. W. Jepsen, and P. M. Marcus, *Phys. Rev. Lett.*, **36**, 798 (1976).
(104) P. M. Marcus, J. E. Demuth, and D. W. Jepsen, *Surf. Sci.*, **53**, 501 (1975).
(105) M. G. LaGally, J. C. Bucholz, and G. C. Wang, *J. Vac. Sci. Technol.*, **12**, 213 (1975).
(106) M. A. Van Hove and S. Y. Tong, *Phys. Rev. Lett.*, **35**, 1092 (1975).
(107) See Demuth, Jepsen, and Marcus, ref 127c.
(108) S. Andersson and J. Pendry, *Surf. Sci.*, **71**, 75 (1978).
(109) L. L. Kesmodel, P. C. Stair, R. C. Baetzold, and G. A. Somorjai, *Phys. Rev. Lett.*, **36**, 1316 (1976).
(110) T. Gustaffson and E. Plummer in ref 84, p 371.
(111) R. Loubriel, T. Gustafsson, and E. Plummer, private communication.
(112) T. Rhodin and J. Kanski, *Surf. Sci.*, **65**, 63 (1977).
(113) R. Colton, C. J. Common, and B. F. Haskins, *J. Chem. Soc., Chem. Commun.*, 363, (1975).
(114) S. Y. Tong, C. H. Li, and A. R. Lubinsky, *Phys. Rev. Lett.*, **39**, 498 (1977).
(115) C. H. Li and S. Y. Tong, *Phys. Rev. Lett.*, **40**, 46 (1978).
(116) C. L. Allyn, T. Gustafsson, and E. W. Plummer, *Chem. Phys. Lett.*, **47**, 127 (1977).
(117) G. Apai, P. S. Williams, J. Stöhr, and D. A. Shirley, *Phys. Rev. Lett.*, **37**, 1497 (1976).
(118) C. Seabury, C. Brucker, and T. Rhodin, to be published.
(119) H. J. Krebs and H. Luth, *Appl. Phys.*, **14**, 337 (1977).
(120) H. Froitzheim, H. Ibach, and S. Lehwald, *Phys. Rev. B*, **14**, 1362 (1976).
(121) M. Neuman, G. Ertl, and K. M. Streit, *Surf. Sci.*, **64**, 393 (1977).
(122) J. E. Demuth, *Surf. Sci.*, in press.
(123) (a) C. Brucker and T. Rhodin, *J. Catal.*, **47**, 214 (1977); (b) J. E. Demuth and H. Ibach, *Surf. Sci.*, in press; (c) J. E. Demuth, *ibid.*, **69**, 365 (1977).
(124) D. J. C. Yates et al., *Nature (London)* **234**, 345 (1971).
(125) P. W. Palmberg and T. N. Rhodin, *J. Chem. Phys.*, **49**, 134 (1968).
(126) (a) T. E. Felter, R. A. Barker, and P. J. Estrup, *Phys. Rev. Lett.*, **38**, 1138 (1977); (b) R. A. Barker, P. J. Estrup, F. Jona, and P. M. Marcus, *Solid State Commun.*, **25**, 375 (1978).
(127) (a) A. Ignatiev, A. V. Jones, and T. N. Rhodin, *Surf. Sci.*, **30**, 573 (1971); (b) T. N. Rhodin and G. Brodén, *ibid.*, **60**, 466 (1976); (c) J. E. Demuth, D. W. Jepsen, and P. M. Marcus, *Phys. Rev. Lett.*, **31**, 540 (1973); (d) *ibid.*, **32**, 1182 (1974); (e) J. A. Van Vechten and J. C. Phillips, *Phys. Rev. B*, **2**, 2160 (1970); (f) S. Andersson and J. B. Pendry, *Solid State Commun.*, **16**, 563 (1975); J. E. Demuth, D. W. Jepsen, and P. M. Marcus, *J. Phys. C*, **8**, 8 (1975); (g) B. A. Hutchins, T. N. Rhodin, and J. E. Demuth, *Surf. Sci.*, **54**, 419 (1976).
(128) F. A. Cotton and B. M. Foxman, *Inorg. Chem.*, **7**, 1563 (1968).
(129) J. A. Bertrand, F. A. Cotton, and W. A. Dollase, *Inorg. Chem.*, **2**, 1166 (1963).
(130) J. E. Fergusson, *Coord. Chem. Rev.*, **1**, 459 (1966).
(131) P. A. Vaughn, *Proc. Natl. Acad. Sci., U.S.A.*, **36**, 461 (1950); C. Brosset, *Ark. Kemi, Mineral. Geol.*, A20 (7), 1 (1945).
(132) H. Schäfer, H. G. Schnering, J. Tillack, F. Kuhnen, H. Wöhrle, and H. Baumann, *Z. Anorg. Allgem. Chem.*, **353**, 281 (1967).
(133) L. J. Guggenberger and A. W. Sleight, *Inorg. Chem.*, **8**, 2041 (1969).
(134) L. R. Bateman, J. F. Blount, and L. F. Dahl, *J. Am. Chem. Soc.*, **88**, 1082 (1966).
(135) P. A. Vaughn, J. H. Sturdivant, and L. Pauling, *J. Am. Chem. Soc.*, **72**, 5477 (1950).
(136) (a) J. D. Corbett, R. L. Doake, K. R. Poeppelmeier, and D. H. Guthrie, *J. Am. Chem. Soc.*, **100**, 652 (1978); (b) M. Manassero, M. Sansoni, and G. Longoini, *J. Chem. Soc., Chem. Commun.*, 919 (1976).
(137) A. F. Wells, "Structural Inorganic Chemistry", 3rd ed, Oxford University Press, London, 1962, p 984.
(138) L. Pauling, "The Nature of the Chemical Bond", 3rd ed, Cornell University Press, Ithaca, N.Y., 1960.
(139) C. H. Wei, G. R. Wilkes, and L. F. Dahl, *J. Am. Chem. Soc.*, **89**, 4792 (1967).
(140) V. G. Albano, G. Ciani, A. Fumagalli, S. Martinengo, and W. M. Anker, *J. Organomet. Chem.*, **116**, 343 (1976).
(141) R. Mason, K. M. Thomas, and D. M. P. Mingos, *J. Am. Chem. Soc.*, **95**, 3802 (1973), and references therein.
(142) V. G. Albano, P. Chini, and V. Scattuis, *Chem. Commun.*, 163 (1968).
(143) [Co₆(CO)₁₅]²⁻, ref 2; *Adv. Organomet. Chem.*, **14**, 341 (1976).
(144) [Co₆(CO)₁₄]⁴⁻, ref 3.
(145) [Rh₇(CO)₁₆]²⁻, ref 11.
(146) [Rh₇(CO)₁₆]³⁻, ref 2.
(147) Rh₆(CO)₁₆, ref 53.
(148) [Rh₆(CO)₁₅I]⁻, ref 6.
(149) R. C. Elder, F. A. Cotton, and R. A. Schunn, *J. Am. Chem. Soc.*, **89**, 3645 (1967).
(150) J. R. Norton, J. P. Collman, G. Dolcetti, and W. T. Robinson, *Inorg. Chem.*, **11**, 382 (1972).

(151) R. Mason and A. I. B. Rae, *J. Chem. Soc. A*, 778 (1968).
(152) V. W. Day, R. O. Day, J. S.Kristoff, F. J. Hirsekorn, and E. L. Muetterties, *J. Am. Chem. Soc.*, **97**, 2571 (1975).
(153) M. Green, J. A. K. Howard, M. Murray, J. L. Spencer, and F. G. A. Stone, *J. Chem. Soc., Dalton Trans.*, 1509 (1977).
(154) A. L. Balch, J. R. Boehm, H. Hope, and M. M. Olmstead, *J. Am. Chem. Soc.*, **98**, 7431 (1976).
(155) J. C. Hemminger, E. L. Muetterties, and G. A. Somorjai, *J. Am. Chem. Soc.*, **101**, 62 (1979).
(156) R. S. Gall, C. Tang-Wah Chu, and L. F. Dahl, *J. Am. Chem. Soc.*, **96**, 4019 (1974).
(157) M. Laing, P. M. Kiernan, and W. P. Griffeth, *J. Chem. Soc., Chem. Commun.*, 221 (1977).
(158) M. R. Churchill and B. G. DeBoer, *Inorg. Chem.*, **16**, 2397 (1977).
(159) G. Ciani, M. Manassero, V. G. Albano, F. Canziani, G. Giordano, S. Martinengo, and P. Chini, *J. Organomet. Chem.*, **150**, C17 (1978).
(160) R. D. Wilson and R. Bau, *J. Am. Chem. Soc.*, **98**, 4687 (1976).
(161) B. T. Huie, C. B. Knobler, and H. D. Kaesz, *J. Chem. Soc., Chem. Commun.*, 684 (1975).
(162) T. F. Koetzle, R. K. McMullan, R. Bau, D. W. Hart, R. G. Teller, P. L. Tipton, and R. D. Wilson, Report 1977, Brookhaven National Laboratory, BNL 22982; *Chem. Abstr.*, **88**, 129333g (1978).
(163) G. Huttner and H. Lorenz, *Chem. Ber.*, **108**, 973 (1975).
(164) R. D. Wilson, S. M. Wu, R. A. Love, and R. Bau, *Inorg. Chem.*, **17**, 1271 (1978).
(165) M. R. Churchill, B. G. DeBoer, and F. J. Rotella, *Inorg. Chem.*, **15**, 1843 (1976).
(166) V. W. Day, M. F. Fredrich, G. A. Reddy, A. J. Sivak, W. R. Pretzer, and E. L. Muetterties, *J. Am. Chem. Soc.*, **99**, 8091 (1977).
(167) G. Gervasio, D. Osella, and M. Valle, *Inorg. Chem.*, **15**, 1221 (1976).
(168) J. R. Shapley, S. I. Richter, M. R. Churchill, and R. A. Lashewycz, *J. Am. Chem. Soc.*, **99**, 7384 (1977).
(169) S. Martinengo, B. T. Heaton, R. J. Goodfellow, and P. Chini, *J. Chem. Soc., Chem. Commun.*, 39 (1977); A. Simon, *Z. Anorg. Allg. Chem.*, **355**, 311 (1967); R. W. Broach, L. F. Dahl, G. Longoni, P. Chini, A. J. Schultz, and J. M. Williams, *Adv. Chem. Ser.*, **167**, 93 (1978).
(170) M. J .S. Dewar, *Bull. Soc. Chim. Fr.*, **18**, C71 (1951).
(171) J. Chatt and L. A. Duncanson, *J. Chem. Soc.*, 2939 (1953).
(172) W. I. Bailey, Jr., D. M. Collins, and F. A. Cotton, to be published.
(173) L. F. Dahl and D. L. Smith, *J. Am. Chem. Soc.*, **84**, 2450 (1962).
(174) B. F. G. Johnson, J. Lewis, B. E. Reichert, K. T. Schropp, and G. Sheldrick, *J. Chem. Soc., Dalton Trans.*, 1417 (1977).
(175) R. Mason and K. M. Thomas, *J. Organomet. Chem.*, **43**, C39 (1972).
(176) C. G. Pierpont, *Inorg. Chem.*, **16**, 636 (1977).
(177) M. Tachikawa, J. R. Shapley, R. C. Haltiwanger, and C. G. Pierpont, *J. Am. Chem. Soc.*, **98**, 4651 (1976).
(178) C. G. Pierpont, G. F. Stuntz, and J. R. Shapley, *J. Am. Chem. Soc.*, **100**, 616 (1978).
(179) J. L. Davidson, M. Green, F. G. A. Stone, and A. J. Welch, *J. Amer. Chem. Soc.*, **97**, 7490 (1975).
(180) (a) M. D. Brice, R. J. Dellaca, B. R. Penfold, and J. L. Spencer, *Chem. Commun.*, 72 (1971); (b) C. R. Eady, J. M. Fernandez, B. F. G. Johnson, J. Lewis, P. R. Raithby, and G. M. Sheldrick, *J. Chem. Soc., Chem. Commun.*, 421 (1978).
(181) M. R. Churchill, K. Gold, and P. H. Bird, *Inorg. Chem.*, **8**, 1956 (1969).
(182) O. S. Mills and E. F. Paulus, *J. Organomet. Chem.*, **11**, 587 (1968).
(183) R. Mason and W. R. Robinson, *Chem. Commun.*, 468 (1968).
(184) R. J. Dellaca and B. R. Penfold, *Inorg. Chem.*, **11**, 1855 (1972).
(185) C. W. Bradford, R. S. Nyholm, G. J. Gainsford, J. M. Guss, P. R. Ireland, and R. Mason, *J. Chem. Soc., Chem. Commun.*, 87 (1972).
(186) G. J. Gainsford, J. M. Guss, P. R. Ireland, R. Mason, C. W. Bradford, and R. S. Nyholm, *J. Organomet. Chem.*, **40**, C70 (1972).
(187) R. Belford, M. I. Bruce, M. A. Cairns, M. Green, H. P. Taylor, and P. Woodward, *Chem. Commun.*, 1159 (1970).
(188) A. Cox and P. Woodward, *J. Chem. Soc. A*, 3599 (1971).
(189) G. Gervasio, D. Osella, and M. Valle, *Inorg. Chem.*, **15**, 1221 (1976).
(190) The description of these molecules in localized terms of σ and π interaction is, in fact, inappropriate in those complexes where multicenter bonding is extant.
(191) M. Evans, M. Hursthouse, E. W. Randall, and E. Rosenberg, *J. Chem. Soc., Chem. Commun.*, 545 (1972).
(192) M. Catti, G. Gervasio, and S. A. Mason, *J. Chem. Soc., Dalton Trans.*, 2260 (1977).
(193) M. G. Thomas, E. L. Muetterties, R. O. Day, and V. W. Day, *J. Am. Chem. Soc.*, **98**, 4645 (1976).
(194) J. J. Guy, B. E. Reichert, and G. M. Sheldraick, *Acta Crystallogr., Sect. B*, 32, 3319 (1976).
(195) A. J. Deeming and M. Underhill, *J. Chem. Soc., Dalton Trans.*, 1415 (1974).
(196) J. A. J. Jarvis, R. Pearce, and M. F. Lappert, *J. Chem. Soc., Dalton, Trans.*, 999 (1977).
(197) T. Greiser and E. Weiss, *Chem. Ber.*, **109**, 3142 (1976).
(198) M. R. Churchill and B. G. DeBoer, *Inorg. Chem.*, **16**, 114 (1977).
(199) R. B. Calvert and J. R. Shapley, *J. Am. Chem. Soc.*, **99**, 5225 (1977).
(200) D. Seyferth, *Adv. Organomet. Chem.*, **14**, 98 (1976).
(201) G. M. Sheldrick and J. P. Yesinowski, *J. Chem. Soc., Dalton Trans.*, 873 (1975).
(202) V. Albano, P. Bellon, and V. Scatturin, *J. Chem. Soc., Chem. Commun.*, 730 (1967).
(203) V. F. Allen, R. Mason, and P. B. Hitchcock, *J. Organomet. Chem.*, **140**, 297 (1977).
(204) See earlier discussion of cubane clusters in section I and in Table V.
(205) Triply bridging atoms or ligand groups are very common in metal clusters.
(206) G. Ciani, A. Sironi, and V. G. Albano, *J. Chem. Soc., Dalton Trans.*, 1667 (1977).

(207) R. Bau, B. Don, R. Greatrex, R. J. Haines, R. A. Love, and R. D. Wilson, *Inorg. Chem.*, **14**, 3021 (1975).

(208) G. Gervasio, R. Rossetti and P. L. Stanghellini, *J. Chem. Soc., Chem. Commun.*, 387 (1977).

(209) R. C. Ryan and L. F. Dahl, *J. Am. Chem. Soc.*, **97**, 6904 (1975).

(210) F. A. Cotton, B. E. Hanson and J. D. Jamerson, *J. Am. Chem. Soc.*, **99**, 6588 (1977).

(211) (a) F. A. Cotton, B. E. Hanson, J. D. Jamerson, and B. R. Stultz, *J. Am. Chem. Soc.*, **99**, 3293 (1977); (b) M. A. Cohen and T. L. Brown, *Inorg. Chem.*, **15**, 1417 (1976); (c) C. H. Langford and H. B. Gray, "Ligand Substitution Processes", W. A. Benjamin, New York, 1965, Chapter 2; (d) K. J. Karel and J. R. Norton, *J. Am. Chem. Soc.*, **96**, 6812 (1974).

(212) R. Gomer, Ed., "Topics in Applied Physics", Vol. 4, Springer, New York, 1976.

(213) R. Messmer, ref 5a, chapter 2.

(214) G. Ertl, ref 5a, Chapter 5.

(215) (a) H. Conrad, G. Ertl, H. Knözinger, J. Küppers, and E. E. Latta, *Chem. Phys. Lett.*, **42**, 115 (1976); (b) E. Plummer, W. R. Salaneck, and J. S. Miller, *Phys. Rev. A*, **18**, 1673 (1978).

(216) G. Ehrlich, *J. Chem. Phys.*, **31**, 1111 (1959).

(217) S. Andersson, *Solid-State Commun.*, **21**, 75 (1977).

(218) H. Ibach, Ed., "Topics in Current Physics", Vol. 4, "Electron Spectroscopy for Surface Analysis", Springer-Verlag, New York, 1977.

(219) L. Brewer, *Science*, **161**, 115 (1968).

(220) Some of these data are revised from the original tabulation (personal communication from Brewer.[219]

(221) D. Menzel, ref 212, Chapter 4.

(222) T. N. Rhodin and D. M. Adams, "Treatise in Solid State Chemistry", N. B. Hannay, Ed., Chapter 6, Plenum Press, New York, 1976.

(223) J. C. Tracy and P. W. Palmberg, *J. Chem. Phys.*, **51**, 4852 (1969).

(224) D. L. S. Brown, J. A. Connor and H. A. Skinner, *J. Chem. Soc., Faraday Trans. 1*, **71**, 669 (1975).

(225) P. F. Kane and G. B. Larrabee, "Characterization of Metal Surfaces", Plenum Press, New York, 1976.

(226) R. A. Van Santen, *Surf. Sci.*, **53**, 35 (1975).

(227) W. M. W. Sachtler, *Le Vide*, **164**, 67 (1973).

(228) K. Y. Yu, D. T. Ling, and W. E. Spicer, *J. Catal.*, **44**, 373 (1976).

(229) J. H. Sinfelt, J. L. Carter, and D. J. C. Yates, *J. Catal.*, **24**, 283 (1972).

(230) J. J. Burton and E. Hyman, *J. Catal.*, **37**, 114 (1975).

(231) W. M. H. Sachtler and R. A. Van Santen, *Adv. Catal.*, **26**, 69 (1977).

(232) H. S. Taylor, *J. Phys. Chem.*, **30**, 145 (1926).

(233) H. S. Taylor, *J. Am. Chem. Soc.*, **53**, 578 (1931).

(234) M. Donke, M. G. Jharing, and M. Drechsler, *Surf. Sci.*, **42**, 389 (1974).

(235) D. L. Adams and L. H. Germer, *Surf. Sci.*, **27**, 21 (1971).

(236) G. A. Somorjai, *Adv. Catal.*, **26**, 2 (1977).

(237) H. Conrad, G. Ertl, and E. E. Latta, *Surf. Sci.*, **41**, 435 (1974).

(238) E. L. Muetterties, B. A. Sosinsky, and K. I. Zamariev, *J. Am. Chem. Soc.*, **97**, 5299 (1975).

(239) J. A. Connor, *Top. Curr. Chem.*, **71**, 71 (1977).

(240) Tabulated values are slightly different from those presented by Connor,[239] but the experimental reference data are the same, and the calculational procedure is essentially the same.

(241) J. W. Emsley, J. Feeney, and C. H. Sutcliffe, "High Resolution Nuclear Magnetic Resonance Spectroscopy", Vol. I and II, Pergamon Press, New York, 1965.

(242) L. M. Jackman, and F. A. Cotton, Eds., "Dynamic Nuclear Magnetic Resonance Spectroscopy", Academic Press, New York, 1975.

(243) W. Klemperer in ref 241, p 23.

(244) J. Evans, B. F. G. Johnson, J. Lewis, J. R. Norton, and F. A. Cotton, *J. Chem. Soc., Chem. Commun.*, 807 (1973).

(245) F. A. Cotton, L. Kruczynski, B. L. Shapiro, and L. F. Johnson, *J. Am. Chem. Soc.*, **94**, 6191 (1972).

(246) L. J. Guggenberger and E. L. Muetterties, *J. Am. Chem. Soc.*, **98**, 7221 (1976).

(247) E. L Muetterties and L. J. Guggenberger, *J. Am. Chem. Soc.*, **96**, 1748 (1974).

(248) E. L. Muetterties, *Tetrahedron*, **30**, 1595 (1974).

(249) H. B. Bürgi, *Inorg. Chem.*, **12**, 2321 (1973).

(250) H. B. Bürgi, J. D. Dunitz, and E. Shefter, *J. Am. Chem. Soc.*, **95**, 5065 (1973).

(251) H. B. Bürgi, J. D. Dunitz, J. M. Lehn, and G. Wipff, *Tetrahedron*, **30**, 1563 (1974).

(252) R. R. Gomer, R. Wertmann, and R. Lundy, *J. Chem. Phys.*, **26**, 1147 (1957).

(253) R. Gomer, *Solid State Phys.*, **30**, 93 (1975).

(254) R. Gomer, *Surf. Sci.*, **38**, 373 (1973).

(255) C. Kleint, *Surf. Sci.*, **25**, 394 (1971).

(256) D. W. Bassett and M. J. Parsley, *J. Phys. D*, **3**, 707 (1970).

(257) G. Ehrlich and F. Hudda, *J. Chem. Phys.*, **44**, 1039 (1966).

(258) G. Ayrault and G. Ehrlich, *J. Chem. Phys.*, **60**, 281 (1974).

(259) R. Lewis and R. Gomer, *Surf. Sci.* **17**, 333 (1969).

(260) A. van Oostrom, *Appl. Phys. Lett.*, **17**, 206 (1970).

(261) R. Gomer, see ref 253.

(262) F. Delamare and G. E. Rhead, *Surf. Sci.*, **28**, 267 (1971).

(263) O. S. Mills, *Acta Crystallogr.*, **11**, 620 (1958).

(264) (a) R. D. Adams and F. A. Cotton, *J. Am. Chem. Soc.*, **95**, 6589 (1973); (b) O. A. Gansow, A. R. Burke, and W. D. Vernon, *J. Am. Chem. Soc.*, **94**,

(265) J. Evans, B. F. G. Johnson, J. Lewis, and J. R. Norton, *Chem. Commun.*, **79**, (1973).

(266) (a) C. H. Wei and L. F. Dahl, *J. Am. Chem. Soc.*, **91**, 1351 (1969); (b) F. A. Cotton and J. M. Troup, *ibid.*, **96**, 4155 (1974).

(267) F. A. Cotton and D. L. Hunter, *Inorg. Chim. Acta*, **11**, 29 (1974).

(268) E. R. Corey and L. F. Dahl, *Inorg. Chem.*, **1**, 521 (1962).

(269) (a) S. Aime, O. Gambino, L. Milone, E. Sappa, and E. Rosenberg, *Inorg. Chim. Acta*, **15**, 53 (1975); (b) A. Forster, B. F. G. Johnson, J. Lewis, T. W. Matheson, B. H. Robinson, and W. G. Jackson, *Chem. Commun.*, 1042 (1974).

(270) F. A. Cotton, ref 242, Chapter 12, p 520.

(271) J. R. Shapley, private communication.

(272) G. F. Stuntz and J. R. Shapley, *J. Am. Chem. Soc.*, **99**, 607 (1977).

(273) O. S. Mills and E. F. Paulus, *J. Organomet. Chem.*, **10**, 331 (1967).

(274) R. J. Lawson and J. R. Shapley, *J. Am. Chem. Soc.*, **98**, 7433 (1976).

(275) V. G. Albano, A. Ceriotti, P. Chini, G. Ciani, S. Martinengo, and W. M. Anker, *Chem. Commun.* 859 (1975).

(276) F. A. Cotton, *Inorg. Chem.*, **5**, 1083 (1966).

(277) B. T. Heaton, A. D. C. Towl, P. Chini, A. Fumagalli, D. J. A. McCaffrey and S. Martinengo, *Chem. Commun.*, 253 (1975).

(278) The structure is by analogy to the cobalt derivative.

(279) V. G. Albano, M. Sansoni, P. Chini, and S. Martinengo, *J. Chem. Soc., Dalton Trans.* 651 (1973).

(280) V. G. Albano, P. Chini, S. Martinengo, D. J. A. McCafrey, and D. Strumulo, *J. Am. Chem. Soc.*, **96**, 8106 (1974).

(281) G. L. Goeffrey and W. L. Gladfelter, *J. Am. Chem. Soc.*, **99**, 6675 (1977).

(282) J. R. Wilkinson and L. J. Todd, *J. Organomet. Chem.* **118**, 199 (1976).

(283) L. F. Dahl and J. F. Blount, *Inorg. Chem.* **4**, 1373 (1965).

(284) (a) S. A. R. Knox and H. D. Kaesz, *J. Am. Chem. Soc.*, **93**, 4595 (1971); (b) H. D. Kaesz, Chem. Brit., **9**, 344 (1973).

(285) P. Chini, private communication.

(286) A. J. Campbell, C. E. Cottrell, C. A. Fyte and K. R. Jeffrey, *Inorg. Chem.*, **15**, 1321 (1976).

(287) J. R. Shapley, S. I. Richter, M. Tachikawa, and J. B. Keister, *J. Organomet. Chem.*, **94**, C43 (1975).

(288) P. Chini, private communication.

(289) A special notation is used to designate (1) the crystallographic direction using Miller indices of the metal plane constituting the underlying phase and (2) the orientation and spacing of the atoms in the overlying lattice with reference to that of the metal plane. In this case the former is composed of oxygen atoms arranged in a simple (primitive) square at points each spaced at one lattice vector apart at right angles to each other along symmetry directions parallel to the metal plane. This notation, originated by Wood,[101] is described in detail by Ertl and Kuppers.[99]

(290) It is significant in this sense that the two-dimensional ordering of the overlayer lattice depends more on the surface coverage than the nature of the chemical bonding characteristic of the adsorbate atom. Although exceptions occur, trends in adsorption-site character *appear* to be relatively insensitive to the ionicity and metallic or electronegative character of the adsorbate.

(291) For the hypothetical MCO molecule, a linear array is expected. Mononuclear metal carbonyl complexes have in the crystalline state an M–C–O angle that is close to 180°. Nevertheless, even in this simple class, the angle falls to values as low as 160° because the energy required for bending is relatively low and the ideal or theoretical linearity can be lost in the solid state because of packing forces. For bridging CO ligands in molecular polynuclear carbonyls, the CO ligand is generally normal to MM vectors or M_3 planes. There are, however, a few examples of carbonyl ligands in dinuclear complexes in which a substantial tilt is present. An
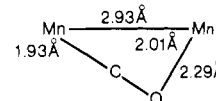
especially notable complex is $Mn_2(CO)_5[(C_6H_5)_2PCH_2CH_2P(C_6H_5)_2]$, in which one CO ligand is bridging but so unsymmetric in form as to allow a strong Mn–O(CO) interaction.[113] In the case of metal surfaces, variances in M–C–O angles may be more common than in molecular metal carbonyl complexes. Since dissociative chemisorption of carbon monoxide prevails at room temperature for the more electropositive transition metals, e.g., iron, intermediate chemisorption states with a substantially "tilted" carbonyl ligand may be found for some metal surfaces. If there is a significant metal–oxygen interaction in such tilted states, this may more than compensate for loss of overlap in the conventional σ–π linear MCO type of interaction.

(292) C. Choo Yin and A. J. Deeming, *J. Chem. Soc., Dalton Trans.*, 2091 (1975).

(293) B. A. Morrow, I. A. Cody, L. E. Moran, and R. Palepu, *J. Catal.*, **44**, 467 (1976).

(294) E. Band and E. L. Muetterties, *Chem. Rev.*, **78**, 639 (1978).

(295) A. J. Sivak and E. L. Muetterties, submitted for publication; (b) R. K. Brown, J. M. Williams, M. F. Fredrich, V. W. Day, A. J. Sivak, and E. L. Muetterties, submitted for publication.